

**UCLA**

**UCLA Electronic Theses and Dissertations**

**Title**

Assessing Urban Ecosystem Alternatives for Changing Land Use Dynamics in the Los Angeles Region

**Permalink**

<https://escholarship.org/uc/item/39p33214>

**Author**

Engel, Ruth Aliza

**Publication Date**

2022

Peer reviewed|Thesis/dissertation

UNIVERSITY OF CALIFORNIA

Los Angeles

Assessing Urban Ecosystem Alternatives for  
Changing Land Use Dynamics in the  
Los Angeles Region

A dissertation submitted in partial satisfaction of the  
requirements for the degree Doctor of Philosophy  
in Geography

by

Ruth Aliza Engel

2022

© Copyright by

Ruth Aliza Engel

2022

## ABSTRACT OF THE DISSERTATION

Assessing Urban Ecosystem Alternatives for  
Changing Land Use Dynamics in the  
Los Angeles Region

by

Ruth Aliza Engel

Doctor of Philosophy in Geography

University of California, Los Angeles, 2022

Professor Thomas Welch Gillespie, Co-Chair

Professor Dennis P. Lettenmaier, Co-Chair

As the world has grown increasingly urbanized over the last half-century, management of regional metropolitan landscapes has become more complex. Planning and research efforts alike require an understanding of local conditions and variability within cities. In this study, I examine changing land cover, urban hydrology, and surface temperature within the Los Angeles region. Using a deep convolutional neural network, I disaggregated mixed Landsat pixels to track land cover change over a continuous 35-year record. I found relatively constant urban area but a higher abundance of irrigated tree cover than is commonly detected in long-term remote sensing data. I used the Distributed Hydrology Soil Vegetation Model to examine hydrology in two distinct neighborhoods within Los Angeles, and observed that new urban vegetation is primarily

impervious areas reduced precipitation-event runoff but universally increased evapotranspiration more substantially than it did in vegetated areas. Both the hydrologic baseline and the responses to land use change varied substantially across different localities. I assessed the contributions of streets to land surface temperature (LST), and found that localized urban morphology and vegetation, rather than road surface, determine LST. In many cases, large impervious or irrigated pockets dominated neighborhood-scale LST signatures. Together, these analyses demonstrate that disparate vegetation, irrigation strategies, and building footprints across an urban area have unique interactions that can make regional approaches impractical and ineffective. Rather, urban ecosystem services can be strengthened by local consideration and an understanding of scale.

The dissertation of Ruth Aliza Engel is approved.

Yongwei Sheng

Erica Natasha Stavros

Stephanie S. Pincetl

Thomas Welch Gillespie, Committee Co-Chair

Dennis P. Lettenmaier, Committee Co-Chair

University of California, Los Angeles

2022

## TABLE OF CONTENTS

LIST OF FIGURES .....	viii
LIST OF TABLES.....	x
ACKNOWLEDGEMENTS.....	xi
VITA.....	xiii
Chapter 1. Introduction.....	1
References.....	6
Chapter 2. Examining urban land cover change using a deep encoder-decoder convolutional neural network .....	12
Abstract.....	12
2.1 Introduction.....	13
2.2 Materials and Methods.....	15
2.2.1 Study Area .....	15
2.2.2 Data .....	18
2.2.3 Data Preprocessing.....	18
2.2.4 Network Architecture.....	20
2.2.5 Model Training .....	22
2.2.6 Validation and Classification.....	23
2.3 Results.....	25
2.3.1 Land Cover Composition in the LAB, 1984-Present.....	25
2.3.2 Comparison to Lower-Resolution Datasets .....	26
2.3.3 Comparison to High-Resolution Data.....	27
2.4 Discussion.....	28
2.4.1 Land Use Trends in the LAB.....	28
2.4.2 Accuracy and Interpretation of Methods .....	29
2.4.3 Applications on work to other areas .....	30
2.4.4 Limitations and Future Work.....	30
2.5 Conclusions.....	31
References.....	33
Chapter 3. The role of urban vegetation change in the basin-scale hydrology of Los Angeles ...	38
Abstract.....	38
3.1 Introduction.....	38
3.2 Methods.....	41
3.2.1 Study Area .....	41

3.2.2 Sample Neighborhoods.....	43
3.2.3 Model Implementation.....	44
3.2.4 Meteorological Forcing Data.....	45
3.2.5 Spatial Data.....	46
3.2.6 Vegetation Change.....	46
3.2.7 Evapotranspiration.....	47
3.2.8 Model Evaluation Data.....	48
3.2.9 Evaluation Methods.....	49
3.3 Results.....	49
3.3.1 Model Accuracy.....	49
3.3.2 Precipitation and Streamflow.....	50
3.3.3 Drought Events and ET.....	51
3.4 Discussion.....	57
3.4.1 Model Accuracy, Precipitation, and Streamflow.....	57
3.4.2 Drought Events and ET.....	58
3.4.3 Limitations and Areas of Opportunity.....	59
3.5 Conclusions.....	60
References.....	62
Chapter 4. Contributions of roads to surface temperature: evidence from Southern California ..	67
Abstract.....	67
4.1 Introduction.....	67
4.2 Mitigating Urban Heat on Roads: Vegetation, Impervious Surfaces, and Land Morphology ..	69
4.3 Data and Methods.....	74
4.3.1 Study Area and Sample Selection.....	74
4.3.2 Data Sources and Calculations.....	74
4.3.3 Regression.....	76
4.3.4 Samples.....	76
4.4 Results.....	80
4.4.1 Effects of Vegetation.....	80
4.4.2 Effects of roads.....	83
4.4.3 Hotspots.....	85
4.5 Discussion.....	86
4.6 Conclusions.....	89
References.....	90



Chapter 5. Conclusions and recommendations for further work .....	99
References.....	103
Appendix A.....	105
Appendix B.....	112
Appendix C.....	116

## LIST OF FIGURES

**Figure 2.1:** Study area. (a) The Los Angeles Basin covers urban Los Angeles and parts of the Santa Monica, Santa Ana, and San Gabriel mountains. (b) 2016 National Land Cover Database (NLCD) classes for Los Angeles (30 m) (Homer et al. 2007). (c) Location of the LAB within California (left), and compared to LA County (black line), the City of LA (shaded), and the Los Angeles, Santa Monica, and San Gabriel HUC8 watersheds (blue)..... 17

**Figure 2.2:** (a) Network architecture for our application of Segnet [30] showing the data structure: an input image, transforming and pooling layers (blue), unpooling and transforming layers (pink), a fully connected ReLu (orange), a classification softmax layer (light green), an unmixing softmax layer (dark green), and a classified image. Semantic segmentation components of figure and architecture follow Audebert et al. (2018). (b) Graphical description of network process. Training images and labels were input, and 20% of training data were reserved for validation (87% accuracy for our training run). The fully trained network was then applied to an input Landsat image, and produces a classified image with majority land cover types for each pixel as well as percentages of land cover types within each pixel. .... 22

**Figure 2.3:** Los Angeles Basin land cover, 1984 to 2020 showing natural non-irrigated vegetation, impervious surfaces, irrigated low vegetation, and urban trees. While land use has been relatively stable over time, there were noticeable increases in natural (non-irrigated) vegetation during drought years (2004-2006, 2011-2015). Impervious areas have declined over the last decade, as greening measures have taken place throughout the city (Pincetl et al. 2013). ..... 25

**Figure 2.4:** Percent (within urban area) of irrigated low vegetation, urban trees, and impervious surfaces, 1984-2019. .... 29

**Figure 3.1:** Location of the LARB (red) within California and within Los Angeles County, with City of Los Angeles (shaded). .... 42

**Figure 3.2:** Locations of weather stations used for DHSVM meteorological forcing (blue) and stream gauges used for data validation (green)..... 45

**Figure 3.3:** Percentage of LARB pixels with changes to irrigated vegetation. Plot shows years in which changes took effect. Vegetation change data based on sub-pixel classification of Landsat imagery (Engel et al. in review)..... 47

**Figure 3.4:** Streamflow (time-varying vegetation model) and precipitation in the LARB, 1985-2020..... 51

**Figure 3.5:** Comparison of average monthly ET (solid lines) and streamflow (dotted lines) during periods of increasing irrigated vegetation (green) and decreasing irrigated vegetation (black). Results shown for time-varying model (a-b) and static model (c-d)..... 54

**Figure 3.6:** Average monthly ET for Woodland Hills (a) and Long Beach (b) in years with increasing irrigated vegetation (dark colors) and decreasing irrigated vegetation (light colors) that are above the 75<sup>th</sup> percentile for precipitation (blue) or under the 25<sup>th</sup> percentile (purple). Results shown for time-varying model (a-b) and static model (c-d). .... 57

**Figure 4.1:** Spatial distribution of sample neighborhoods (a), LST (b) and selected contributing variables within the study area: Elevation (c), CalEPA Environmentally Disadvantaged Communities (d), Street networks (e), SAVI (f), and LCZs (g). Cooler areas are more mountainous and less developed, and often are coastal. Warmer areas are farther inland, and often are within large lowrise developments. Disadvantaged neighborhoods are, on average, hotter than non-disadvantaged neighborhoods. .... 79

**Figure 4.2:** Temperature; SAVI and streets; and satellite imagery (Google 2021) for three sample neighborhoods. Pacoima is largely impervious and sits inland, in the San Fernando Valley. Highways are the coolest surfaces in the neighborhood. Long Beach is a diverse, coastal area, and generally cooler than other neighborhoods because of the summertime marine layer. Chino Hills is wealthier and more vegetated, though it sits inland, in San Bernardino County. Several large warehouses, technically just outside the neighborhood, show the higher LST commonly visible in heavily industrial areas..... 80

**Figure 4.3:** Most common street width (m) within each pixel and SAVI for each sample neighborhood. Colors represent summertime LST within a given pixel, and dashed lines are mean values for width and SAVI. Points for “all urban area” plot come from a random selection of pixels to show a clear distribution without overcrowding. In both the study area as a whole and individual neighborhoods, SAVI is the primary moderator for LST: temperatures change along a vegetation gradient, but do not substantially differ in areas with narrow or wide streets. Areas with more vegetation (higher SAVI) are cooler, but areas with less vegetation (lower SAVI) are more diverse; low-SAVI areas are not universally warmer. In coastal neighborhoods (e.g. Hidden Hills, Long Beach, Pacific Palisades, and Rolling Hills) LST is lower across the board, a result of the summertime marine layer. .... 82

**Figure 4.4:** Distribution of LST (°C) of pixels with no roads (green), residential streets (yellow), arterials (orange), and highways (red) in each sample neighborhood. Rolling Hills and Watts have no highways. In wealthier neighborhoods with substantial vegetation (e.g. Chino Hills, Hidden Hills, Lancaster, and Pacific Palisades) the residential, high-SAVI areas are cooler than streets, and arterials with tree-lined medians can be especially cool. However, highways are the coolest streets in neighborhoods with diverse ground cover. In particularly impervious areas (e.g. Colton, Pacoima, and Vernon) highways are often the coolest areas overall..... 85

**Figure A1:** Water in the Los Angeles Basin (2019), shown in red (Pekel et al. 2016)..... 106

**Figure A2:** LARIAC land cover data (2017) in East Los Angeles. Data is classified orthogonal LiDAR imagery (10 cm)..... 108

**Figure A3:** Ground truth polygons of land cover classes in the test area. The dataset comprises 165 polygons and was constructed from a combination of field survey and manual categorization of 0.5m October 2019 imagery (ESRI 2021)..... 109

## LIST OF TABLES

<b>Table 2.1:</b> Basin-wide land cover distribution vs. Landsat-based NLCD land cover distribution, 2016. NLCD categories were aggregated as follows. Non-irrigated vegetation included evergreen and mixed forests, wetlands herbaceous, and shrub/scrub. Irrigated low vegetation included pasture and developed open space. Urban trees included deciduous forests and cultivated crops. Impervious surfaces included high-, medium-, and low-intensity development. Our comparison shows that NLCD underestimates non-majority land cover categories, most notably urban trees.	26
<b>Table 2.2:</b> Kappa statistic with producer’s and user’s accuracy across urban areas for NLCD (30 km) vs. our predicted maximum land cover type in each pixel, 2016. While impervious surfaces compare well, majority-tree pixels within urban areas are rare and do not compare well. Most trees in urban areas of the LAB are not dominant within a 30 km pixel.	27
<b>Table 2.3:</b> Accuracy for neural network derived land cover types within urban space compared to LARIAC’s classified 10 cm orthogonal imagery from 2017 (LARIAC 2015). Overall weighted error for the three land cover types combined is 9.01%.	28
<b>Table 3.1:</b> Streamflow in cubic meters per second (cms) and validations statistics. DA is drainage area, and starred gauge is basin outlet. Efficiency statics are monthly. Kling-Gupta Efficiency at basin outlet is 0.23.	50
<b>Table 3.2:</b> Average ET in all years, wet years and dry years; percent of seasonal ET that changes between years of increasing and decreasing vegetation. All data shown for summertime (JJA) and wintertime (DJF) across the time-varying (TV) and static (S) models in Woodland Hills (WH) and Long Beach (LB). Wet years are above the 75 <sup>th</sup> percentile in precipitation; dry years are below the 25 <sup>th</sup> percentile.	52
<b>Table 4.1:</b> Sample neighborhoods.	77
<b>Table 4.2:</b> Scaled regression coefficients for study area and all samples from model including normalized street area, SAVI, albedo, and building footprint as well as bins for elevation and ocean proximity ( $R^2 = 0.767$ ). Variables are normalized so as to be directly comparable with one another. Coefficients between street area and LST tend to be small, and they do not demonstrate a particular pattern. SAVI is the most noticeable predictor of LST, with cooling effects across all areas.	81
<b>Table A1:</b> NDVI values.	107
<b>Table A2:</b> Accuracy for neural network derived land cover types within urban space in two validation areas of one square kilometer each. Each table shows calculated percent of area, actual percent of area, and percent accuracy for impervious surfaces, irrigated low vegetation, and urban trees. (a) Accuracy within a highly impervious commercial area. (b) Accuracy within a mixed-use residential area.	110
<b>Table B1:</b> Processing time and memory demands for various implementations of DHSVM with identical size (~5.8 million pixels) and timespan (01/01/1980-12/31/2020).	112

## ACKNOWLEDGEMENTS

This dissertation was made possible by the work of many collaborators. My advisers, Tom Gillespie and Dennis Lettenmaier, have been a source of support and counsel throughout the research and writing process. The chapters contained here have benefited immensely from Dr. Lettenmaier's conscientious approach to research, high standards, and deep knowledge of the field. Dr. Gillespie, always generous with expertise and encouragement, facilitated and made possible the interdisciplinary collaboration that shaped this work.

I am grateful to Yongwei Sheng, Natasha Stavros, and Stephanie Pincetl, my dissertation committee, for their guidance and input. Kelly Turner and Adam Millard-Ball provided insights and mentorship, as well as offering me the chance to work on a truly collaborative project. Erik Porse shared a wide-ranging, applied approach that substantially benefited both the research and writing of this dissertation. Michael Shin and Sierra Burkhart helped me think deeply about geography and what it means to contribute to the field.

I would like to thank Qian Cao, Zhuoran Duan, and Miriam Marlier for their technical expertise and advice. I am lucky to have worked alongside each of my lab group members: Mu Xiao, Kim Wang, Lu Su, Zhoaxin Ban, Emilie Tarouilly, Jessica Fayne, Solomon Vimal, Xiaoyu Ma, Monica Dimson, Jon Ocon, Morgan Rogers, Erica Gallerani, and Nadia Colombi. Within UCLA Geography, I am grateful to Kasi McMurray and the department staff for their knowledge and generosity.

Sam Meier, Jess Altamira, Sam Kelley, Lincoln Scott, Felicia Yang, Spencer Lee Lenfield, and Adam Lyon offered conversation, perspective, and jokes. The rotating Friday crew always knew what to say and when to laugh. Monday evening conversation with Jon, Steve, and

Rich started each week on the right foot. I am grateful to Dr. Joseph W. Michels for sharing his clear-eyed insights on the evolving nature of the academic world.

Sam Engel was a true collaborator in this process, asking questions and providing advice at the intersection of the technical and theoretical. My deepest thanks to Asa Bush for his unwavering support and keen editorial eye.

Finally, I would like to thank Dina Michels, my first and best adviser, and Peter Engel, who introduced me to geography.

## VITA

### EDUCATION

#### **University of California, Los Angeles**

C.Phil in Geography 2020

M.A. in Geography 2017

Thesis: *On the Causes of the Summer 2015 Eastern Washington Wildfires*

#### **Harvard University, Cambridge MA**

A.B. in Government; Secondary Field in English 2012

Institute for Quantitative Social Science Undergraduate Research Scholar

Independent Study: *Applications of Crowdsourcing in the Nonprofit Sector*

### REFEREED PUBLICATIONS

#### *Published*

Li, D., **Engel, R.A.**, Ma, X., Porse, E., Kaplan, J.D., Margulis, S.A., & D.P. Lettenmaier (2020). Stay-at-home orders during the COVID-19 pandemic reduce urban water use. *Environmental Science & Technology Letters*

**Engel, R.A.**, Marlier, M.E., & D.P. Lettenmaier (2019). On the causes of the summer 2015 Eastern Washington wildfires. *Environmental Research Communications*, 1(1)

Marlier, M. E., Xiao, M., **Engel, R.A.**, Livneh, B., Abatzoglou, J. T., & D.P. Lettenmaier (2017). The 2015 drought in Washington State: a harbinger of things to come?. *Environmental Research Letters*, 12(11)

Mote, P. W., Li, S., Lettenmaier, D. P., Xiao, M., & **R.A. Engel** (2018). Dramatic declines in snowpack in the western US. *NPJ Climate and Atmospheric Science*, 1(1)

#### *Submitted or in preparation*

**Engel, R.A.**, Colombi, N., Gillespie, T.W., and D.P. Lettenmaier. Examining urban land cover change using a deep encoder-decoder convolutional neural network. *Remote Sensing (in revision)*

**Engel, R.A.**, Millard-Ball, A., and V.K. Turner. Contributions of Roads to Surface Temperature: Evidence from Southern California. *Landscape and Urban Planning (in review)*

### SELECTED CONFERENCE PRESENTATIONS

**Engel, R.A.**, Gillespie, T., Colombi, N., and Lettenmaier, D.P. Deep Learning for Urban Watershed Land Use Assessments. American Geophysical Union Annual Meeting, December 2019.

Invited participant, Deep Learning for Science, July 2019. Organized by Lawrence Berkeley National Laboratory, U.S. Department of Energy.

- Engel, R.A.**, Colombi, N., and Lettenmaier, D.P. Implications for Future Ecosystem Management Alternatives in the LA Basin. Water Self-Sufficiency in Los Angeles Conference, May 2019.
- Engel, R.A.**, Colombi, N., and Lettenmaier, D.P. Assessing Urban Land Cover Change for Ecosystem Management in the Los Angeles Basin. UCLA Water Resources Association Conference, February 2019.
- Engel, R.A.**, Colombi, N., and Lettenmaier, D.P. Assessing Urban Ecosystem Management Alternatives for the Water Balance of the Los Angeles Basin. Poster. American Geophysical Union Annual Meeting, December 2018.
- Engel, R.A.**, Marlier, M.E., and Lettenmaier, D.P. On the Causes of the Summer 2015 Eastern Washington Wildfires. Association of American Geographers Annual Meeting, March 2018.
- Engel, R.A.**, Marlier, M.E., and Lettenmaier, D.P. Quantifying the Causes and Propagation of the 2015 Washington Wildfires. American Geophysical Union Annual Meeting, December 2017.
- Engel, R.A.**, Marlier, M.E., and Lettenmaier, D.P. On the Causes of the Summer 2015 Pacific Northwest Fires. American Geophysical Union Annual Meeting, December 2016.
- Engel, R.A.** Baltimore City’s Infrastructure Vulnerability to Climate Change. Poster. Association of American Geographers Annual Meeting, March 2007.

## **TEACHING AND GUEST LECTURES**

**Geospatial Program, UCLA Extension** 2021-2022  
 Instructor: Advanced Geographic Information Systems, Intermediate Geographic Information Systems, Cartography, Introduction to Geographic Information Systems

**Geography Department, UCLA** 2017-2022  
 Instructor: Intermediate Geographic Information Systems (2021)  
 Teaching Assistant: Advanced Geographic Information Systems, Introduction to Geographic Information Systems, People and Earth’s Ecosystems, Urban Geography

“GIS for Ecology and Earth Science” guest seminar, UCLA. In combined graduate and undergraduate “Finding Ecological Solutions to Environmental Problems” (2022)

“Neural Network Implementation” guest seminar, UCLA. In graduate “Regional Climate and Terrestrial Surface Processes” (2019)

“Policy and Earth Science” guest lecture, UCLA. In undergraduate “People and Earth’s Ecosystems” (2019)

“Hydropower in Central Asia” guest seminar, UCLA. In combined graduate and undergraduate “Global Environment and Development: Problems and Issues” (2017; 2018)



## **Chapter 1. Introduction**

Increasingly, people across the world are moving to cities. By 2050, 67% of the global population is projected to live in urban areas (IOM 2015). Within the United States, cities are expanding in terms of both land area and density, leading to shifts in socio-ecological systems (US Census Bureau 2010; Rounsevell et al. 2012). In planning and science, analyses of urban dynamics and ecosystem services are critical in determining both how cities might continue to grow and how they can sustain increasingly large populations (Luederitz et al. 2015).

Contemporary municipal managers strive for sustainable land use planning and resilience in the face of climate change and resource scarcity (Hersperger et al. 2018; Garcetti 2019). Not only are local planners expected to implement city-wide changes, they are reliant on large interconnected systems (e.g. water distribution, transportation networks) that increase the complexity of any discrete consideration (Graham and Marvin 2001). Consequently, plans are frequently created at a city level, applying land or ecosystem management strategies across a large urban area (Luederitz et al. 2015; Middell et al. 2020).

In academic research, urban dynamics studies are often constrained in terms of detail by the availability and scale of data. In order to examine heterogeneity within cities, land use data must be high-resolution (~10 m), as changes can occur at a block-scale (Welch 1982). While such high-resolution datasets exist, they are limited to the last decade (EROS 2017; Planet Team 2017). Urban change analyses, such as modeling studies examining regional hydrology or carbon cycles, rely on long temporal records (>30 years). Remotely sensed land cover data with sufficient time scales usually have moderate spatial resolutions (e.g. 30 m). Consequently, mixed pixels are a pervasive problem in urban analyses: minority-pixel features – such as trees – are masked, and urban areas look more homogeneous than they truly are (Mitraka et al. 2016; Wang

et al. 2019). In both long-term and more recent, short-term studies, large high-resolution datasets have proven unwieldy, requiring substantial processing power to analyze (Perkins et al. 2019). Moderate-resolution, regional studies, however, are practical and can be tailored to a city's ecosystem and climate, and are frequently used to understand physical dynamics (Gould 2000; Imhoff et al. 2004; Myeong et al. 2006).

Because cities vary by race and income as well as physical characteristics (e.g. building density, climate), regional-level studies often obscure differences among neighborhoods in ways that can exacerbate environmental injustices. Imperviousness, air pollution, soil contamination, and urban heat are all correlated with marginalized and historically redlined communities (Wilson 2020; Madrigano et al. 2021; Lane et al. 2022). These trends hold for predominantly Black and Latino neighborhoods, often due at least in part to a lack of vegetation (Schell et al. 2020; Dialesandro 2021). Resource allocation is also distributed unequally; in water-scarce cities, wealthy communities use substantially more water (often for outdoor irrigation) than low-income areas (Clarke et al. 2013; Litvak et al. 2017). Treating a city as an undifferentiated whole implicitly assumes that physical, social, and environmental characteristics are homogeneous enough to support a single set of scientific results or planning outcomes (Deziel et al. 2022). In cities with diverse socio-ecological conditions, these analyses can exclude neighborhoods that are more vulnerable to environmental change (Gallopín 2006; CalEPA 2015). Recent studies have made efforts to quantify environmental disadvantage, understand mechanisms of environmental racism at a local level, and conduct specific ecosystem services assessments in vulnerable neighborhoods (Transformative Climate Communities 2021; Deziel et al. 2022).

Given the environmental and social importance of local context, scientific studies have increasingly sought to examine heterogeneous conditions and processes within cities. In

particular, remote sensing analyses now regularly capture or construct local land cover conditions. Some of these studies rely on traditional machine learning or statistical methods (Zhao et al. 2019; Coleman et al. 2020), while others employ deep learning approaches (Shao et al. 2019; Perikamana et al. 2021). Using combinations of high-resolution aerial photography (Gillespie et al. 2012; LARIAC 2015) and human or field surveys (Pincetl et al. 2013; Yao et al. 2019), scholars are mapping urban forests. These analyses can facilitate both modeling and long-term change scholarship and localized investigations into specific block-scale conditions.

Studies of ecosystem services have begun to parse local interactions between vegetation, urban morphology, and climatology. Urban heat mitigation strategies are being designed to make use of existing local infrastructure, prioritize vulnerable communities, and reflect changes in topography and microclimates across diverse cities (Soudoudi et al. 2014; Wong et al. 2016; Mavrakou et al. 2018). Analyses of water management systems suggest mixing green and grey infrastructure in response to local conditions (McPhearson et al. 2014). Proposals for increasing urban biodiversity account for income and development differences across neighborhoods (Clarke and Jenerette 2015; Lin et al. 2015). These studies contribute to a growing body of literature analyzing diversity in intra-city dynamics.

The goal of this study is to examine heterogeneity in urban space and to understand how urban ecosystem services vary locally within the greater Los Angeles Region. Los Angeles, a megacity with a growing metropolitan area that extends into San Bernardino and Orange Counties, makes an ideal case study for examination of changing urban dynamics. It has high neighborhood-scale heterogeneity, with an impervious downtown, irrigated urban area, chaparral mountains, and inland desert areas (Rashed et al. 2003). Tree cover is highly variable: tree canopy estimates range from 7-31% of land across city council districts (McPhearson et al. 2011).

A coastal marine layer shades and cools most coastal neighborhoods (Edinger 1959). As a result, neighborhoods vary by land use, vegetation, evapotranspiration (ET), and heat on distinct diurnal and seasonal cycles (Hall et al. 2015).

The built environment in the Los Angeles area is equally diverse. Los Angeles County contains 114 neighborhoods and over 10 million people (Rashed et al. 2003). A legacy of redlining and environmental injustice across the urban area is exacerbated by substantial income inequality and racial segregation (Mini et al. 2014; Su et al. 2018). Both the City and the County of Los Angeles have sustainability plans that prioritize reduced dependence on imported water (Garcetti 2019; OurCounty 2019). Accordingly, both governments actively manage water use and have restricted outdoor irrigation during periods of drought, though these restrictions were observed unequally among neighborhoods with different income levels (Litvak et al. 2017; Porse et al. 2017). Both land use and ecosystem services vary across these disparate areas of environment and development.

Here, I assess urban dynamics and their interactions in different parts of the greater Los Angeles area. The science questions I will address are:

1. How have urban land cover and irrigation in Los Angeles changed over the last 35 years (1984-2019)?
2. What are the cumulative effects of small-scale land use changes on evapotranspiration (ET) and water balance, both across Los Angeles and within distinct neighborhoods?
3. Is there a relationship between street area and land surface temperature (LST), either regionally or at a local scale, and is that relationship affected by urban morphology?

In this dissertation, each question guides one of the subsequent three chapters. In Chapter 2,

**Examining urban land cover change using a deep encoder-decoder convolutional neural**

**network**, I disaggregate mixed Landsat pixels (30 m) to understand distributed land cover change across a 35-year record in the Los Angeles Sedimentary Basin, which includes all of the City and most of the County of Los Angeles. In Chapter 3, **The role of urban vegetation change in the basin-scale hydrology of Los Angeles**, I integrate that land cover change data into the Distributed Hydrology Soil Vegetation Model across the Los Angeles River Basin and within two individual neighborhoods in order to examine ways in which irrigation and imperviousness affect ET and runoff in different parts of the city. In Chapter 4, **Contributions of roads to surface temperature: evidence from Southern California**, I use a statistical model to examine the role of street area in determining LST, both across the unified urbanized area of Los Angeles and San Bernardino Counties and within individual neighborhoods of varied morphology.

Each chapter includes analyses encompassing both a regional view of the Los Angeles area and conditions within individual neighborhoods. In assessing changes to land cover, hydrology, and LST, I consider a wide range of physical processes across and within a megacity. Throughout the course of this dissertation, I contextualize results in contemporary urban management strategies and ongoing questions about climate adaptation, with the aim of making this research useful to researchers and planners working in the Los Angeles region and in megacities more generally. Together, these studies explore heterogeneity within the Los Angeles region from the perspectives of land use, hydrology, and surface temperature. They ask how physical systems and ecosystem services are distributed, and how spatial patterns within an urban area might guide locally driven research and planning efforts.

## References

- CalEPA. (2015, November 20). SB 535 Disadvantaged Communities [Text]. OEHHA. <https://oehha.ca.gov/calenviroscreen/sb535>
- Churkina, G. (2008). Modeling the carbon cycle of urban systems. *Ecological Modelling*, 216(2), 107–113. <https://doi.org/10.1016/j.ecolmodel.2008.03.006>
- Clarke, L. W., & Jenerette, G. D. (2015). Biodiversity and direct ecosystem service regulation in the community gardens of Los Angeles, CA. *Landscape Ecology*, 30(4), 637–653. <https://doi.org/10.1007/s10980-014-0143-7>
- Clarke, L. W., Jenerette, G. D., & Davila, A. (2013). The luxury of vegetation and the legacy of tree biodiversity in Los Angeles, CA. *Landscape and Urban Planning*, 116, 48–59. <https://doi.org/10.1016/j.landurbplan.2013.04.006>
- Coleman, R. W., Stavros, E. N., Yadav, V., & Parazoo, N. (2020). A Simplified Framework for High-Resolution Urban Vegetation Classification with Optical Imagery in the Los Angeles Megacity. *Remote Sensing*, 12(15), 2399.
- Deziel, N. C., Warren, J. L., Bravo, M. A., Macalintal, F., Kimbro, R. T., & Bell, M. L. (2022). Assessing community-level exposure to social vulnerability and isolation: Spatial patterning and urban-rural differences. *Journal of Exposure Science & Environmental Epidemiology*, 1–9. <https://doi.org/10.1038/s41370-022-00435-8>
- Dialesandro, J., Brazil, N., Wheeler, S., & Abunnasr, Y. (2021). Dimensions of Thermal Inequity: Neighborhood Social Demographics and Urban Heat in the Southwestern U.S. *International Journal of Environmental Research and Public Health*, 18(3), 941. <https://doi.org/10.3390/ijerph18030941>
- Edinger, J. G. (1959). Changes in the depth of the marine layer over the Los Angeles Basin. *Journal of Meteorology*, 16(3), 219–226.
- EROS. (2017). National Agriculture Imagery Program (NAIP) [Tiff]. U.S. Geological Survey. <https://doi.org/10.5066/F7QN651G>
- Gallopín, G. C. (2006). Linkages between vulnerability, resilience, and adaptive capacity. *Global Environmental Change*, 16(3), 293–303. <https://doi.org/10.1016/j.gloenvcha.2006.02.004>
- Garcetti, E. (2019). LA's Green New Deal (p. 152). LA City. [https://plan.lamayor.org/sites/default/files/pLAn\\_2019\\_final.pdf](https://plan.lamayor.org/sites/default/files/pLAn_2019_final.pdf)
- Gillespie, T. W., Pincetl, S., Brossard, S., Smith, J., Saatchi, S., Pataki, D., & Saphores, J.-D. (2012). A time series of urban forestry in Los Angeles. *Urban Ecosystems*, 15(1), 233–246. <https://doi.org/10.1007/s11252-011-0183-6>

- Giridharan, R., Lau, S. S. Y., Ganesan, S., & Givoni, B. (2007). Urban design factors influencing heat island intensity in high-rise high-density environments of Hong Kong. *Building and Environment*, 42(10), 3669–3684. <https://doi.org/10.1016/j.buildenv.2006.09.011>
- Gould, W. (2000). Remote Sensing of Vegetation, Plant Species Richness, and Regional Biodiversity Hotspots. *Ecological Applications*, 10(6), 1861–1870. JSTOR. <https://doi.org/10.2307/2641244>
- Graham, S., & Marvin, S. (2001). *Splintering Urbanism: Networked Infrastructures, Technological Mobilities and the Urban Condition*. Routledge. <https://doi.org/10.4324/9780203452202>
- Hall, S. J., Learned, J., Ruddell, B., Larson, K. L., Cavender-Bares, J., Bettez, N., Groffman, P. M., Grove, J. M., Heffernan, J. B., Hobbie, S. E., Morse, J. L., Neill, C., Nelson, K. C., O’Neil-Dunne, J. P. M., Ogden, L., Pataki, D. E., Pearse, W. D., Polsky, C., Chowdhury, R. R., ... Trammell, T. L. E. (2016). Convergence of microclimate in residential landscapes across diverse cities in the United States. *Landscape Ecology*, 31(1), 101–117. <https://doi.org/10.1007/s10980-015-0297-y>
- Hersperger, A. M., Oliveira, E., Pagliarin, S., Palka, G., Verburg, P., Bolliger, J., & Grădinaru, S. (2018). Urban land-use change: The role of strategic spatial planning. *Global Environmental Change*, 51, 32–42. <https://doi.org/10.1016/j.gloenvcha.2018.05.001>
- Imhoff, M. L., Bounoua, L., DeFries, R., Lawrence, W. T., Stutzer, D., Tucker, C. J., & Ricketts, T. (2004). The consequences of urban land transformation on net primary productivity in the United States. *Remote Sensing of Environment*, 89(4), 434–443. <https://doi.org/10.1016/j.rse.2003.10.015>
- IOM (Ed.). (2015). *Migrants and cities: New partnerships to manage mobility*. International Organization for Migration (IOM).
- Lane, H. M., Morello-Frosch, R., Marshall, J. D., & Apte, J. S. (2022). Historical Redlining Is Associated with Present-Day Air Pollution Disparities in U.S. Cities. *Environmental Science & Technology Letters*, 9(4), 345–350. <https://doi.org/10.1021/acs.estlett.1c01012>
- LARIAC. (2015). *LARIAC Product Guide*. Los Angeles County. [https://egis2.lacounty.gov/hub/lariac\\_documents/LARIAC4-Product-Guide-1.pdf](https://egis2.lacounty.gov/hub/lariac_documents/LARIAC4-Product-Guide-1.pdf)
- Lin, B. B., Philpott, S. M., & Jha, S. (2015). The future of urban agriculture and biodiversity-ecosystem services: Challenges and next steps. *Basic and Applied Ecology*, 16(3), 189–201. <https://doi.org/10.1016/j.baae.2015.01.005>
- Litvak, E., Manago, K., Hogue, T., & Pataki, D. (2017). Evapotranspiration of urban landscapes in Los Angeles, California at the municipal scale—Litvak—2017—Water Resources Research—Wiley Online Library. *Water Resources Research*, 53(5), 4236–4253.

- Luederitz, C., Brink, E., Gralla, F., Hermelingmeier, V., Meyer, M., Niven, L., Panzer, L., Partelow, S., Rau, A.-L., Sasaki, R., Abson, D. J., Lang, D. J., Wamsler, C., & von Wehrden, H. (2015). A review of urban ecosystem services: Six key challenges for future research. *Ecosystem Services*, 14, 98–112. <https://doi.org/10.1016/j.ecoser.2015.05.001>
- Madrigano, J., Hernandez, C. C., Stephenson, S., Chari, R., Gahlon, G., Huttinger, A., Siddiqi, S. M., & Preston, B. L. (2021). Environmental Racism: The Relationship Between Historical Residential Redlining and Current Environmental Hazards. ISEE Conference Abstracts. <https://doi.org/10.1289/isee.2021.O-LT-061>
- Mavrakou, T., Polydoros, A., Cartalis, C., & Santamouris, M. (2018). Recognition of Thermal Hot and Cold Spots in Urban Areas in Support of Mitigation Plans to Counteract Overheating: Application for Athens. *Climate*, 6(1), 16. <https://doi.org/10.3390/cli6010016>
- McPhearson, T., Hamstead, Z. A., & Kremer, P. (2014). Urban Ecosystem Services for Resilience Planning and Management in New York City. *AMBIO*, 43(4), 502–515. <https://doi.org/10.1007/s13280-014-0509-8>
- McPherson, E. G., Simpson, J. R., Xiao, Q., & Wu, C. (2011). Million trees Los Angeles canopy cover and benefit assessment. *Landscape and Urban Planning*, 99(1), 40–50. <https://doi.org/10.1016/j.landurbplan.2010.08.011>
- Middel, A., Turner, V. K., Schneider, F. A., Zhang, Y., & Stiller, M. (2020). Solar reflective pavements—A policy panacea to heat mitigation? *15(6)*, 064016. <https://doi.org/10.1088/1748-9326/ab87d4>
- Mini, C., Hogue, T. S., & Pincetl, S. (2014). Estimation of residential outdoor water use in Los Angeles, California. *Landscape and Urban Planning*, 127, 124–135. <https://doi.org/10.1016/j.landurbplan.2014.04.007>
- Mitraka, Z., Frate, F. D., & Carbone, F. (2016). Nonlinear Spectral Unmixing of Landsat Imagery for Urban Surface Cover Mapping. *IEEE Journal of Selected Topics in Applied Earth Observations and Remote Sensing*, 9(7), 3340–3350. <https://doi.org/10.1109/JSTARS.2016.2522181>
- Myeong, S., Nowak, D. J., & Duggin, M. J. (2006). A temporal analysis of urban forest carbon storage using remote sensing. *Remote Sensing of Environment*, 6.
- OurCounty. (2019). The Plan. OurCounty. <https://ourcountyla.lacounty.gov/plan>
- Pataki, D. E., McCarthy, H. R., Gillespie, T., Jenerette, G. D., & Pincetl, S. (2013). A trait-based ecology of the Los Angeles urban forest. *Ecosphere*, 4(6), art72. <https://doi.org/10.1890/ES13-00017.1>



- Peng, S., & Maing, M. (2021). Influential factors of age-friendly neighborhood open space under high-density high-rise housing context in hot weather: A case study of public housing in Hong Kong. *Cities*, 115, 103231. <https://doi.org/10.1016/j.cities.2021.103231>
- Perikamana, K. K., Balakrishnan, K., & Tripathy, P. (2021). A CNN based method for Sub-pixel Urban Land Cover Classification using Landsat-5 TM and Resourcesat-1 LISS-IV Imagery. ArXiv:2112.08841 [Cs]. <http://arxiv.org/abs/2112.08841>
- Perkins, W. A., Duan, Z., Sun, N., Wigmosta, M. S., Richmond, M. C., Chen, X., & Leung, L. R. (2019). Parallel Distributed Hydrology Soil Vegetation Model (DHSVM) using global arrays. *Environmental Modelling & Software*, 122, 104533. <https://doi.org/10.1016/j.envsoft.2019.104533>
- Pincetl, S., Gillespie, T., Pataki, D., Saatchi, S., & Saphores, J. (2013). Urban tree planting programs, function or fashion? Los Angeles and urban tree planting campaigns. <https://doi.org/10.1007/S10708-012-9446-X>
- Planet Team. (2017). Planet Application Program Interface: In Space for Life on Earth. San Francisco, CA. <https://api.planet.com>
- Porse, E., Mika, K. B., Litvak, E., Manago, K. F., Naik, K., Glickfeld, M., Hogue, T. S., Gold, M., Pataki, D. E., & Pincetl, S. (2017). Systems Analysis and Optimization of Local Water Supplies in Los Angeles. *Journal of Water Resources Planning and Management*, 143(9), 04017049. [https://doi.org/10.1061/\(ASCE\)WR.1943-5452.0000803](https://doi.org/10.1061/(ASCE)WR.1943-5452.0000803)
- Rashed, T., Weeks, J. R., Roberts, D., Rogan, J., & Powell, R. (2003). Measuring the Physical Composition of Urban Morphology Using Multiple Endmember Spectral Mixture Models. *Photogrammetric Engineering & Remote Sensing*, 69(9), 1011–1020. <https://doi.org/10.14358/PERS.69.9.1011>
- Rounsevell, M. D. A., Pedrolì, B., Erb, K.-H., Gramberger, M., Busck, A. G., Haberl, H., Kristensen, S., Kuemmerle, T., Lavorel, S., Lindner, M., Lotze-Campen, H., Metzger, M. J., Murray-Rust, D., Popp, A., Pérez-Soba, M., Reenberg, A., Vadineanu, A., Verburg, P. H., & Wolfslehner, B. (2012). Challenges for land system science. *Land Use Policy*, 29(4), 899–910. <https://doi.org/10.1016/j.landusepol.2012.01.007>
- Schell, C. J., Dyson, K., Fuentes, T. L., Des Roches, S., Harris, N. C., Miller, D. S., Woelfle-Erskine, C. A., & Lambert, M. R. (2020). The ecological and evolutionary consequences of systemic racism in urban environments. *Science*, 369(6510), eaay4497. <https://doi.org/10.1126/science.aay4497>
- Shao, Z., Cai, J., Fu, P., Hu, L., & Liu, T. (2019). Deep learning-based fusion of Landsat-8 and Sentinel-2 images for a harmonized surface reflectance product. *Remote Sensing of Environment*, 235, 111425. <https://doi.org/10.1016/j.rse.2019.111425>

- Sodoudi, S., Shahmohamadi, P., Vollack, K., Cubasch, U., & Che-Ani, A. I. (2014). Mitigating the Urban Heat Island Effect in Megacity Tehran. *Advances in Meteorology*, 2014, e547974. <https://doi.org/10.1155/2014/547974>
- Su, J. G., Morello-Frosch, R., Jesdale, B. M., Kyle, A. D., Shamasunder, B., & Jerrett, M. (2009). An Index for Assessing Demographic Inequalities in Cumulative Environmental Hazards with Application to Los Angeles, California. *Environmental Science & Technology*, 43(20), 7626–7634. <https://doi.org/10.1021/es901041p>
- Sultana, F., Sufian, A., & Dutta, P. (2020). Evolution of Image Segmentation using Deep Convolutional Neural Network: A Survey. *Knowledge-Based Systems*, 201–202, 106062. <https://doi.org/10.1016/j.knosys.2020.106062>
- Thanapakpawin, P., Richey, J., Thomas, D., Rodda, S., Campbell, B., & Logsdon, M. (2007). Effects of land use change on the hydrologic regime of the Mae Chaem river basin, NW Thailand. *Journal of Hydrology*, 334(1), 215–230. <https://doi.org/10.1016/j.jhydrol.2006.10.012>
- Transformative Climate Communities. (2021). Transformative Climate Communities. <https://greenlining.org/our-work/environmental-equity/transformative-climate-communities-2/>
- US Census Bureau. (2010). 2010 Census Urban and Rural Classification and Urban Area Criteria. The United States Census Bureau. <https://www.census.gov/programs-surveys/geography/guidance/geo-areas/urban-rural/2010-urban-rural.html>
- Wang, W., Liu, K., Tang, R., & Wang, S. (2019). Remote sensing image-based analysis of the urban heat island effect in Shenzhen, China. *Physics and Chemistry of the Earth, Parts A/B/C*, 110, 168–175. <https://doi.org/10.1016/j.pce.2019.01.002>
- Welch, R. (1982). Spatial resolution requirements for urban studies. *International Journal of Remote Sensing*, 3(2), 139–146. <https://doi.org/10.1080/01431168208948387>
- Wilson, B. (2020). Urban Heat Management and the Legacy of Redlining. *Journal of the American Planning Association*, 86(4), 443–457. <https://doi.org/10.1080/01944363.2020.1759127>
- Wong, M. S., Peng, F., Zou, B., Shi, W. Z., & Wilson, G. J. (2016). Spatially Analyzing the Inequity of the Hong Kong Urban Heat Island by Socio-Demographic Characteristics. *International Journal of Environmental Research and Public Health*, 13(3), E317. <https://doi.org/10.3390/ijerph13030317>
- Yao, N., Konijnendijk van den Bosch, C. C., Yang, J., Devisscher, T., Wirtz, Z., Jia, L., Duan, J., & Ma, L. (2019). Beijing's 50 million new urban trees: Strategic governance for large-scale urban afforestation. *Urban Forestry & Urban Greening*, 44, 126392. <https://doi.org/10.1016/j.ufug.2019.126392>

Zhao, Y., Zhong, K., Xu, J., Sun, C., & Wang, Y. (2019). Directional Analysis of Urban Expansion Based on Sub-pixel and Regional Scale: A Case Study of Main Districts in Guangzhou, China. *Chinese Geographical Science*, 29(4), 652–666.  
<https://doi.org/10.1007/s11769-019-1048-9>

## **Chapter 2. Examining urban land cover change using a deep encoder-decoder convolutional neural network**

This chapter has been submitted in its current form to *Remote Sensing* and is now in revision as Engel, R.A., Colombia, N., Gillespie, T.W., and D.P. Lettenmaier, 2022: Examining urban land cover change using a deep encoder-decoder convolutional neural network, *Remote Sensing* (in revision). The supplementary materials for this chapter are provided in Appendix A.

### **Abstract**

As the world continues to urbanize, studies of coupled human-environmental systems increasingly require access to heterogeneous, high-resolution land cover data. Currently, high-resolution satellite imagery exists only for recent years, and often is difficult to acquire. Moderate-resolution (~30 m) images (e.g. Landsat) and pixel-based classifications are more readily available over a multidecadal period suitable for hydrologic modeling and change analyses, but lack the spatial resolution necessary to identify parcel-level features. We resolved these broad classifications using an application of Segnet, an encoder-decoder convolutional neural network, to produce a single 35-year land cover time series for the Los Angeles Sedimentary and Hydrologic Basin (LAB). In doing so, we disaggregated urban mixed pixels to understand changing distributions of non-irrigated vegetation, impervious surfaces, irrigated low vegetation, and urban trees over the period 1984-2019, achieving an overall accuracy of 90.9% compared to contemporary high-resolution (10 cm) data from 2017. We find that while the urban area within the Los Angeles has remained relatively constant over the last 30 years, drought-driven vegetation changes are visible. We also find that commonly used moderate resolution (e.g., Landsat-derived) datasets significantly underestimate tree cover across the dense urban domain within the LAB. Because our methodology requires only freely available training data, a

digital elevation model, globally-available water cover information, and medium resolution (e.g., Landsat) imagery, the analysis can be reproduced anywhere.

## **2.1 Introduction**

As the global population has rapidly urbanized over the last half-century, analyses of land cover change for growing urban centers have become more critical. Currently, 54% of the world's population lives in cities (vs. 30% in 1950) and 67% of the world's population is projected to live in cities by 2050 (IOM 2015). In the United States, urban areas grew over 10% (from ~234,000 km<sup>2</sup> to ~275,000 km<sup>2</sup>) from 2000 to 2010 (US Census Bureau 2010). As urban areas expand and population density increases, land use and resource availability are changing.

The Los Angeles region is an ideal case study for examinations of changing urban resource dynamics. Both the City and County of Los Angeles carefully plan for, legislate, and monitor land use and water consumption (Wiersema 2018). For instance, Los Angeles City water use restrictions during times of drought (most recently 2014-2017) have decreased irrigation unequally across the city, by anywhere from 6-35%, and water savings are often correlated strongly with median neighborhood income (Mini et al. 2014; Lund et al. 2018). Because processes like these are heterogeneously distributed across urban areas (e.g. specific to lawns or parks), long-term, high-resolution land cover data are needed for change detection and planning purposes.

Our domain is the Los Angeles Basin (LAB), a hydrologic and sedimentary region encompassing most of Los Angeles County (and home to > 9.7 million people). The diverse topography, development, and ecology of the LAB make it a uniquely complex case study for examinations of urban land cover change (see 2.2.1). Within the LAB, the urban area is undergoing substantial land use change, but regional land cover analyses show little variation

(Homer et al. 2007; LA County 2015; Coleman et al. 2020). To evaluate the cumulative effects of small, local changes within our domain, high-resolution (< 10 m), long-term land cover data are essential.

Currently, no such domain-wide high-resolution time series land cover data exist; land cover data that are available are limited to either approximately the last decade or to moderate resolution (Porse et al. 2017; Gallo et al. 2020). Recent high-resolution products include National Agriculture Imagery Program (NAIP) imagery (based on aerial imagery) every 5 years from 2003-2008 and every 3 years from 2009 at 1 m resolution, and Planet satellite imagery at 3 m resolution from 2015 to present (EROS 2017; Planet Team 2017). However, these products do not have a long enough record to support hydrologic modeling or multidecadal change detection. More established moderate resolution datasets (e.g. Landsat) do not provide sufficient spatial detail to capture local land use changes. Furthermore, broad categories are insufficient; because of difference in their runoff generation and evapotranspiration characteristics, urban hydrologic models must distinguish among tree, grass, water, and impervious surfaces as well as land use (irrigated vs. non-irrigated).

Mixed pixels are a pervasive problem in remote sensing, masking features and their spatial distribution (Wang et al. 2019). In urban environments, this problem is exacerbated, both because individual features exist at fine scales and because varied land cover types can exist in close proximity (Mitraka et al. 2016). Medium-resolution datasets, such as the Landsat-derived National Land Cover Database (NLCD; released in 1992, 2001, 2006, 2011, and 2016 at 30 m resolution), assign diverse landscapes – such as golf courses, parks, and tree-lined streets – to categories such as “Developed – Open Space” or “Low Intensity Development”. In Los Angeles County, NLCD groups over 60% of land area into one of these two categories (Fry et al. 2011).

Conventional resolution enhancement often has too low a signal-to-noise ratio or lacks sufficient spectral dimension to yield accurate disaggregation of these categories (Miao et al. 2007; Arun et al. 2018).

We resolve these broad categories by disaggregating mixed pixels to understand distributed land cover changes across the Los Angeles Basin. We test a deep encoder-decoder convolutional neural network to examine multispectral imagery to produce a breakdown of each mixed pixel among four land cover types: non-irrigated vegetation, impervious surfaces, irrigated low vegetation, and urban trees. Specifically, we examine:

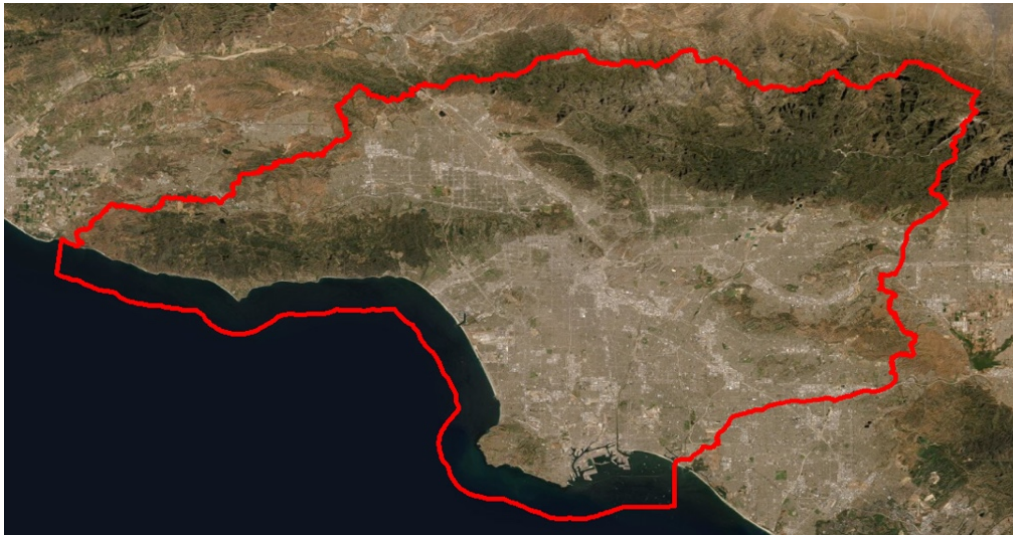
1. What is the current land cover composition of the Los Angeles Basin (2020) and how has that composition changed over the last 35 years?
2. How does the dataset we derive compare to contemporary, lower-resolution sources and cumulative totals for our domain?
3. How accurate is the dataset we produce in comparison to independent high-resolution (10 cm from 2017) and manually-collected ground truth data?

## **2.2 Materials and Methods**

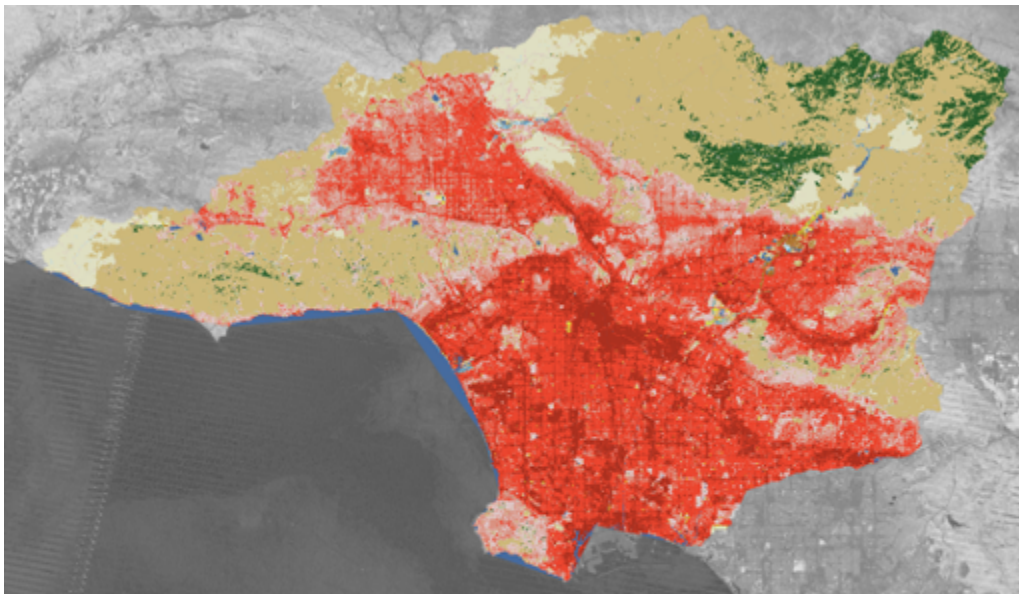
### *2.2.1 Study Area*

Our study is the Los Angeles Sedimentary Basin (LAB), a region between the San Gabriel, Santa Monica, and Santa Ana mountains (Jahns 1973) encompassing three Hydrologic Unit Codes 8 (HUC8) basins that drain into the Pacific (Figure 2.1; Jahns 1973). It excludes inland parts of LA County that do not sit within these watersheds. We examine changes to land use in the LAB between 1984 and 2020, the period covered by Landsat data (Homer et al. 2007). The 34-year record we produce is long enough period to support hydrologic modeling or change analysis studies.









(a)



(b)



NCLD Classes

- |   |  |
|---|--|
|  Developed, Open Space       |  Grassland/Herbaceous |
|  Developed, Low Intensity    |  Shrub/Scrub          |
|  Developed, Medium Intensity |  Evergreen Forest     |
|  Developed, High Intensity   |  Open Water           |



(c)

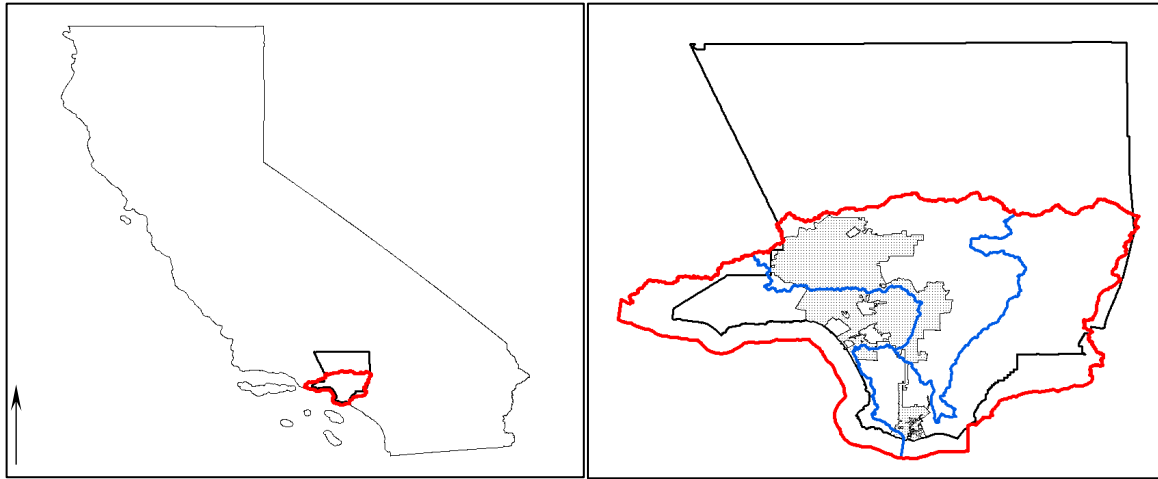


**Figure 2.1:** Study area. (a) The Los Angeles Basin covers urban Los Angeles and parts of the Santa Monica, Santa Ana, and San Gabriel mountains. (b) 2016 National Land Cover Database (NLCD) classes for Los Angeles (30 m) (Homer et al. 2007). (c) Location of the LAB within California (left), and compared to LA County (black line), the City of LA (shaded), and the Los Angeles, Santa Monica, and San Gabriel HUC8 watersheds (blue).

The LAB includes 3.5 million housing units in  $> 5,600 \text{ km}^2$  with elevations ranging from sea level to  $> 3,000 \text{ m}$  (LA County 2015; US Census Bureau 2019). It includes national forest land, local and state beaches and parks, and a dense urban core (LA County Planning 2010). The LAB includes multiple administrative areas, among which the City of Los Angeles, with 114 distinct neighborhoods and a population of  $\sim 4$  million, is the largest (LA County Planning 2010).

Los Angeles County, which covers 92% of the LAB, developed the first county-wide sustainability plan, with sections that address both water and landscape issues (OurCounty 2019). The City of Los Angeles also has a sustainability plan, which provides for the planting of 90,000 new trees by 2021 and recycling 100% of wastewater by 2035 (Garcetti 2019). Its previous sustainability efforts included 400,000 new trees planted between 2006 and 2013 (McPherson et al. 2011). Given the explicit focus on land use and associated processes (i.e. irrigation, runoff recapture), we examine current land use as well as long-term changes and their distribution across the LAB.

### *2.2.2 Data*

We used Landsat data (30 m) from 1984-2020 as our moderate resolution data source (Homer et al. 2007). Landsat images are collected every 16 days globally. Our analysis combined Red, Green, Blue, and Near Infrared (R, G, B, NIR) Surface Reflectance data from Landsat 5 for the period 1984-2011, corrected Landsat 7 from 2012-2013, and Landsat 8 for 2014-2020, with inter-sensor calibration from Google Earth Engine. We employed a neural network in conjunction with water and irrigation masking to estimate the fraction of each pixel that is made up of each component class.

To train the neural network, we used the International Society for Photogrammetry and Remote Sensing Semantic Labeling Potsdam Dataset (Cramer 2010), which was intended to train networks to identify features in high-resolution data (Audebert et al. 2018). The Potsdam dataset consists of 38 scenes of 5 cm RGB urban imagery from aerial photography with corresponding categorized, labeled ground truth images. The data are divided into six categories: impervious surfaces, buildings, low vegetation, trees, cars, and clutter.

### *2.2.3 Data Preprocessing*

We preprocessed the Landsat data for integration into the neural network by masking out natural (non-irrigated) vegetation and water using Google Earth Engine. For water, we used the Pekel et al. data set (2016), which contains individual pixels classified as water or non-water, 1984-2019 (Figure A1). We found that this dataset, which covers our period of study, is consistent with other water datasets, Normalized Difference Water Index (NDWI) analyses, and a supervised classification, but notably contains fewer false positive values (Appendix A.1). The water polygons across the LAB (21 km<sup>2</sup> in total) did not noticeably change over our study period.

We stitched together greenest pixel composites of all cloud-free Landsat scenes for each summer (June, July, August; JJA) and winter (December, January, February; DJF) to cover the entire domain with Landsat scenes for each year for the two seasons. To align our vegetation to the irrigated training data vegetation, we filtered out non-irrigated vegetation examining summer and winter Normalized Difference Vegetation Index (NDVI) for each year's imagery. Based on a survey of summer/winter NDVI differences across non-irrigated vegetation and irrigated low vegetation, we used a binary threshold to mask areas where the seasonal difference is  $> 0.069$ , which was the midpoint between median irrigated and non-irrigated summer/winter differences (Appendix A.2). Following Gillespie et al. (2018), we further masked summer NDVI between 0.3 and 0.6, the range for chaparral and coastal sage scrub in the LAB.

We also masked undeveloped high-elevation areas. In doing so, we eliminated heavily coniferous areas that might not show seasonal NDVI changes to further mask out non-irrigated vegetation. Because the pixel sizes are 30 m, they are unlikely to be influenced unduly by conifers except in the higher mountains of the San Gabriel range (Mini et al. 2014). We applied an elevation mask of 1000 m to account for heavily forested areas, and considered any high-elevation vegetation to be non-irrigated. For each year, we masked out fire perimeters to account for burned area that could otherwise register as impervious. We used the California Fire and Resource Assessment Program (FRAP) perimeters, coded annually (FRAP 2021). For input into the neural network, we applied all four masks (water, NDVI, elevation, fire) and then filtered for cloud cover and found the composite greenest pixel value for each time period, so as to provide the highest level of visual contrast to the network. We completed all preprocessing work in Google Earth Engine. Landsat, water, NDVI, and elevation data are free and open-source on the

platform, and we manually uploaded FRAP perimeters. We used the native JavaScript environment to mask and clean the data for integration into the neural network.

#### *2.2.4 Network Architecture*

To create the classified maps, we employed a semi-supervised spectral unmixing of mixed Landsat pixels. Following Arun et al. (2018), we employed deep learning to approach unmixing as a soft classification problem. Rather than increasing image resolution, we produced fractional abundance statistics for each mixed pixel. Traditional convolutional neural networks (CNNs) as well as other deep learning methods (e.g. convolutional long short-term memory networks, semantic segmentation networks) have demonstrated increasingly accurate results in unmixing, often performing better than traditional methods (e.g. Markov, Random Forest Classifiers) (Zhao and Du 2016; Badinarayanan et al. 2017; Liu et al. 2018; Yoo et al. 2019).

We employed an application of Segnet, a deep convolutional encoder-decoder semantic segmentation neural network primarily used to discern objects in a field of view (Badrinarayanan et al. 2017; Audebert et al. 2018). A CNN is ideal for image analysis because it examines groups of data at once; rather than connecting each neuron in one layer to each neuron in another, it examines an  $n \times n$  set of pixels to examine each pixel in the context of its neighbors (Sultana et al. 2020). Deep CNNs are therefore often employed for semantic segmentation, a process by which an image is divided into its components (Chen et al. 2016). Segnet, an encoder-decoder network, is a CNN that works in two phases. First it convolves and pools data, grouping clusters of pixels and taking the maximum value from each cluster into the next layer, resulting in a smaller layer. Then it unpools the data back to its original resolution and distribution, allowing for final predictive analysis at the original resolution (Chen et al. 2016). Between each pooling step is a batch normalization, to increase predictive stability and processing speed (Ioffe and

Szegedy 2015). Following Audebert et al. (2018), we used 5 convolutional blocks with first 2, then 3, layers of kernel 3 x 3 with a padding of 1. We then applied a rectified linear unit (ReLU) optimizer and a batch normalizer to each hidden layer, which returned a linear result for values  $> 0$  and 0 for values  $< 0$  (Figure 2.2). Following encoding, our image had a width and height at  $1/32$  its original value; the decoder restored its dimensions. Our last layer performed a logarithmic softmax categorization to predict the likelihood that each pixel is a given land cover type. We applied a softmax normalization to our output data to obtain normalized categorical probabilities for each pixel and each land cover type; these probabilities can be interpreted as categorical percentages for land cover type distribution within a pixel (Arun et al. 2018).

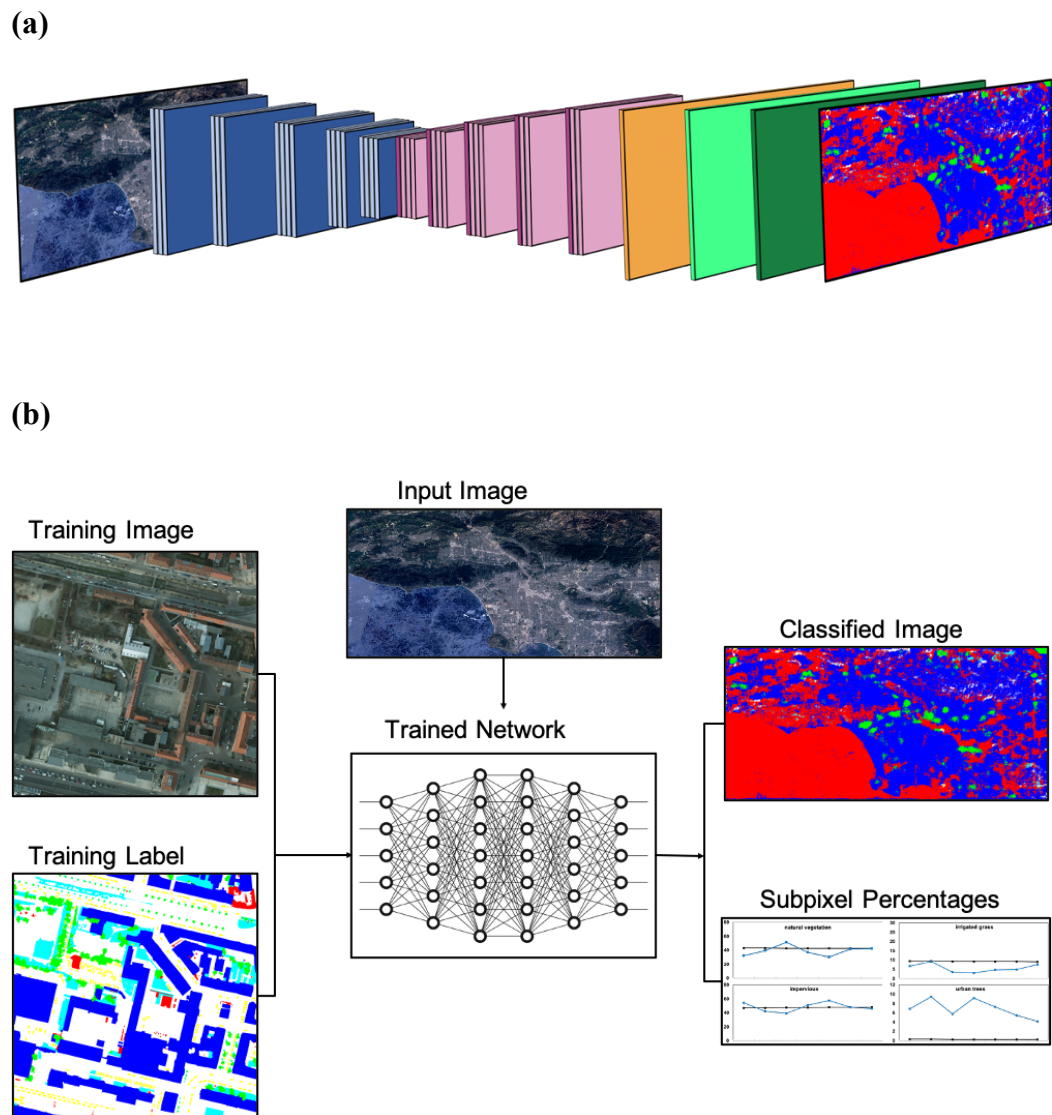


**Figure 2.2:** (a) Network architecture for our application of Segnet [30] showing the data structure: an input image, transforming and pooling layers (blue), unpooling and transforming layers (pink), a fully connected ReLu (orange), a classification softmax layer (light green), an unmixing softmax layer (dark green), and a classified image. Semantic segmentation components of figure and architecture follow Audebert et al. (2018). (b) Graphical description of network process. Training images and labels were input, and 20% of training data were reserved for validation (87% accuracy for our training run). The fully trained network was then applied to an input Landsat image, and produces a classified image with majority land cover types for each pixel as well as percentages of land cover types within each pixel.

### 2.2.5 Model Training

We trained our application of Segnet with 80% of images from the ISPRS Potsdam dataset, reserving 20% for validation. The Potsdam dataset, which covers only irrigated urban

spaces, equipped the network to analyze images of irrigated urban spaces within the LAB. To account for the change in resolution, we condensed their six categories into three (as non-irrigated vegetation was masked): impervious surfaces (including cars), buildings, and vegetation.

We then applied the trained network to Landsat data across the LAB to examine land cover type across and within pixels. Between the preprocessing and the neural network, we categorized land cover among four types: irrigated low vegetation (e.g. grass, shrubs), non-irrigated vegetation, urban trees, and impervious surfaces (see 2.2.6). We trained and ran the neural network on a GPU server through Google Colaboratory, storing both training and Landsat data in Google Drive for ease of access. All Colaboratory code for this project was written in Python 3.

### *2.2.6 Validation and Classification*

We validated the neural network by reserving and testing 20% of the training images. The validation process assessed the pixel-level accuracy of the network, before the final calculation of categorical percentages. Our network classifies land cover types at 87% accuracy. The accuracy metric is based on a combined value of the six raw ISPRS training dataset categories designed for high-resolution analysis (trees, low vegetation [irrigated], buildings, roads, cars, and clutter). We validated the network in Google Colaboratory after training but before running the Landsat data.

We aggregated the ISPRS as follows because our mixed pixel classification is at a lower spatial resolution than the ISPRS data. We included cars, buildings, and roads in an “impervious” class, as cars are not distinguishable enough at 30 m to make the class relevant and buildings and roads are not spectrally distinct from one another. In our study area, the ISPRS

“clutter” is almost exclusively mixed landscaping, with a densely arrayed variety of trees, shrubs, and grass. Accordingly, reflecting a visual analysis of 200 majority-clutter pixels, we divided this category between grass, low vegetation, and trees, which aggregated to ~66% low vegetation and 33% trees. Therefore, we ultimately used four land cover classes: non-irrigated vegetation, urban trees, irrigated low vegetation, and impervious surfaces.

To understand how our data compare to existing land cover datasets, we used three validation methods. First, we assessed correspondence between our 2016 basin-wide totals and the 2016 NLCD (Homer et al. 2007). NLCD maps are produced from Landsat data every 5 years between 2001 and 2016 at 30 m, and reflect 20 possible land cover types across the United States. Relevant to our study are Low-, Medium-, and High-Intensity development, which comprise the urban part of our domain; shrub/scrub and mixed forest, which reflect the natural hillsides; and deciduous and evergreen forest and barren land, which cover much of the higher mountainous areas. We computed kappa statistics with producer’s and consumer’s accuracy using ArcMap 10.6 (Smits et al. 1999).

We derived our primary accuracy measurement by comparing our urban area totals to 2017 Los Angeles Image Acquisition Consortium (LARIAC) 10 cm composite orthogonal imagery categorized across 218 individual city areas (Appendix A.3; LARIAC 2015). We clipped this dataset to reflect the area almost fully encompassed by the urban part of our domain. Within urban areas (omitting non-irrigated vegetation), we directly compared our trees, irrigated low vegetation, and impervious surfaces categories to LARIAC trees; grass and low vegetation; and buildings, roads, and other impervious surfaces in ArcMap 10.6.

To assess the ground-truth accuracy of individual mixed pixel classifications at a granular level, we compared our categorical percentages to manually collected data over two areas of one



square kilometer each within the LAB reflecting (a) a dense, highly-developed region in East LA with no green space, and (b) a mixed-use residential area in the San Fernando Valley with a park. We used no selection criteria other than level of development, and selected a 1 km<sup>2</sup> at random from within a relatively homogeneous area of the LAB. Across each study area, we manually digitized polygons using the ESRI collector app and a 0.5 m DigitalGlobe basemap (ESRI 2021).

## 2.3 Results

### 2.3.1 Land Cover Composition in the LAB, 1984-Present

Our analyses show that the LAB was approximately half non-irrigated vegetation, including forested areas, bare ground, and non-irrigated vegetation in 2020 (Figure 2.3). Of developed areas, 36% of space was impervious, ~6% was irrigated low vegetation, and ~6% was urban trees.

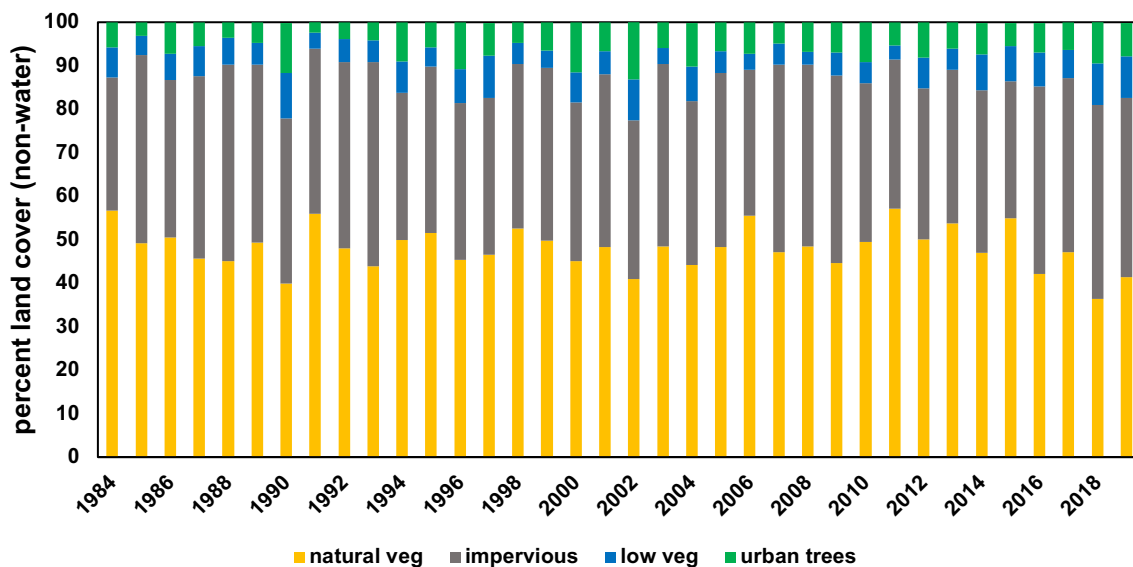


**Figure 2.3:** Los Angeles Basin land cover, 1984 to 2020 showing natural non-irrigated vegetation, impervious surfaces, irrigated low vegetation, and urban trees. While land use has been relatively stable over time, there were noticeable increases in natural (non-irrigated) vegetation during drought years (2004-2006, 2011-2015). Impervious areas have declined over the last decade, as greening measures have taken place throughout the city (Pincetl et al. 2013).

The composition of the LAB over the last 35 years has been relatively stable (Figure 2.3). We provide here a time series of annual land cover data for the LAB, 1984-2019. These land cover distributions reflect the heterogeneity of the LAB, including isolated landscaping features that otherwise would be elided due to focus on more dominant features.

### 2.3.2 Comparison to Lower-Resolution Datasets

To understand the land cover predictions for each 30 m pixel, we compared 2016 basin-wide totals to 2016 NLCD totals (Table 2.1). While both datasets were derived from Landsat data, their classification schemes differ. We aggregated their categories across the LAB to compare totals, and found that our data demonstrate slightly more non-irrigated vegetation and less impervious and irrigated area (Table 2.1). Our produced data aggregated land cover percentages within pixels; however, rough agreement between the datasets across the LAB was important. We found more non-irrigated vegetation and urban trees than in the NLCD data, perhaps because of parsing composition within the NLCD “open space” category.

**Table 2.1:** Basin-wide land cover distribution vs. Landsat-based NLCD land cover distribution, 2016. NLCD categories were aggregated as follows. Non-irrigated vegetation included evergreen and mixed forests, wetlands herbaceous, and shrub/scrub. Irrigated low vegetation included pasture and developed open space. Urban trees included deciduous forests and cultivated crops. Impervious surfaces included high-, medium-, and low-intensity development. Our comparison shows that NLCD underestimates non-majority land cover categories, most notably urban trees.

Land Cover	Produced Data (%)	NLCD (%)
Non-Irr Veg.	42.3	42.6
Irr Low Veg.	7.9	10.4
Urban Trees	6.8	0.26
Impervious	43.1	48.1

We also computed a kappa statistic with producer’s and consumer’s accuracy between NLCD and our majority pixel predictions, which show the primary land use categories in each pixel, throughout urban areas in 2016 (Table 2.2). The overall accuracy is 0.80 across 500

randomly selected points within classified pixels, which demonstrates a general spatial agreement between our predictions and NLCD. Our majority pixel predictions show strong agreement with NLCD in impervious areas (user’s accuracy is 0.95, producer’s accuracy is 0.83). However, urban trees were more difficult to identify: only 3 of 500 random points within classified pixels were in areas where the majority area of pixels were trees, and those points had no agreement with our classified majority-tree pixels.

**Table 2.2:** Kappa statistic with producer’s and user’s accuracy across urban areas for NLCD (30 km) vs. our predicted maximum land cover type in each pixel, 2016. While impervious surfaces compare well, majority-tree pixels within urban areas are rare and do not compare well. Most trees in urban areas of the LAB are not dominant within a 30 km pixel.

	NLCD Impervious	NLCD Irr. Low Veg	NLCD Trees	Total	U_Accuracy
<b>Impervious</b>	393	16	3	412	0.9539
<b>Irr. Low Veg</b>	79	9	0	88	0.1023
<b>Trees</b>	0	0	0	0	0
<b>Total</b>	472	25	3	500	0
<b>P_Accuracy</b>	0.8326	0.36	0	0	0.804

### 2.3.3 Comparison to High-Resolution Data

We compared our categorical percentages to classified 2017 10 cm LARIAC orthogonal imagery, aggregated across 69,201 ha of urban area (Table 2.3). The overall average percent error, weighted by land cover type, was 9.01%, demonstrating strong agreement between our calculated land cover and the high-resolution dataset. Our estimates of impervious surfaces were highly accurate, with an error of 4.75% (68% of calculated land cover vs 72% of LARIAC data). For vegetation, we achieved 29.08% error for low vegetation (calculated at 19% of land cover vs 14% in the LARIAC dataset) and 9.36% error for tree distribution (12% calculated land cover vs 13%).

**Table 2.3:** Accuracy for neural network derived land cover types within urban space compared to LARIAC’s classified 10 cm orthogonal imagery from 2017 (LARIAC 2015). Overall weighted error for the three land cover types combined is 9.01%.

Land Cover	Calculated % Land Cover	LARIAC % Land Cover	Percent Error
Impervious	75.58	69.31	9.05
Grass/Shrub	12.46	14.44	13.71
Urban Trees	11.90	12.66	6.00

We compared our classified mixed pixel data to two areas 1 km<sup>2</sup> to examine how errors were distributed within different types of landscape. We masked the classified data using the test polygons and calculate totals for each land cover type within the small area (Appendix A.4). Our pixel breakdowns were extremely accurate with respect to impervious surfaces (0.21 and 0.06 percent error). They overestimated tree cover (62.88 percent error), but within an extremely small area (0.54% vs 0.33% of the test region).

## 2.4 Discussion

### 2.4.1 Land Use Trends in the LAB

Over the last 35 years, the developed region of the LAB has been relatively stable (Figure 2.3). This stability reflects the abundance of redevelopment, lack of available land zoned for new development, and price of land in urban areas (Thomas 2009; LADRP 2021). Within the city, redevelopment, new housing, and increased green spaces were visible as both a greater density within the urban core of the city and increasing sprawl in the suburban parts of LA County. These trends are in line with LA’s development goals (Garcetti 2019).

We also see a decrease in irrigated area and an increase in non-irrigated vegetation during drought years (e.g. 2006-2007, 2013-2016) (Keeley et al. 2009; Lund et al. 2018). During some of these years, non-irrigated vegetation was seen within urban areas as water restrictions discourage people from watering. Since 2016, irrigated grass has grown in area again as watering

has resumed (Figure 2.4). Though different years contain different error values because of variability among composite images, the overall trends were aligned with major drought events.

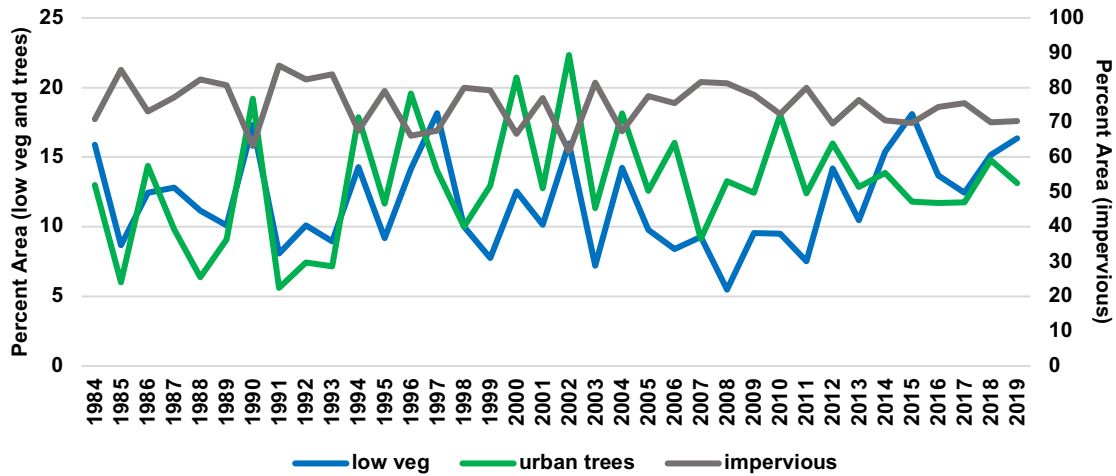


**Figure 2.4:** Percent (within urban area) of irrigated low vegetation, urban trees, and impervious surfaces, 1984-2019.

#### 2.4.2 Accuracy and Interpretation of Methods

Overall, our land cover data gave a more detailed depiction of the LAB than did traditional 30 m classifications. While we agreed with NLCD trends with respect to impervious surfaces, we found more irrigated low vegetation and many more urban trees than the NLCD datasets. These results were logical, considering the large number of Low-Medium Intensity Development NLCD pixels that we parsed for vegetation.

Our calculated land cover distributions were highly accurate across heterogeneous urban areas: compared to the current best-available dataset, LARIAC’s 10 cm classified imagery from 2017, we found an overall 91% agreement in developed regions. In comparison to traditional supervised classifications (e.g. CART, Random Forest) our approach required much less individual training and produced at least as accurate results in comparison to ground truth data (Zhu et al. 2012; Yoo et al. 2019).

Our work is lacking in its categorization within the impervious surface class because road surfaces tend to be comprised of diverse materials (asphalt, concrete, etc.) and we have found difficulty training the network to distinguish between buildings and roads (Lee et al. 2005). We therefore created a single category for impervious surfaces, which can combine in most distributed physical models with a road network. We also accounted for fine-scale mixed vegetation distribution with an estimate based on local observations that in studies encompassed other regions. This distribution might be different and should certainly be recalibrated. Some individual variability among annual results can be explained by these classification errors.

#### *2.4.3 Applications on work to other areas*

The efficacy of deep learning semantic segmentation in peri-urban and rural areas has been established (Grinias et al. 2016; Mortensen et al. 2016). Using infrared data and these established segmentation methods, our approach could be applied to classify mixed crop pixels or to distinguish among vegetation types within a pixel (Beninde et al. 2015; Chu et al. 2020). Distinguishing biodiversity in urban or agricultural regions could provide detailed forcing data for urban heat analyses, carbon cycling studies, and urban planning work (Pincetl et al 2013; Van Oijen et al. 2014; Vahmani and Ban-Weiss 2016).

#### *2.4.4 Limitations and Future Work*

Certain features were necessarily erased because the input data for the network was at 30 m resolution. Machine learning analyses usually mask out water (Powell et al. 2007; Coleman et al. 2020). We chose to do so because natural bodies of water are extremely stable throughout our study period (Pekel et al. 2016) and because, spectrally, water can be diverse enough to confound an algorithmic learning process. Similarly, we masked non-irrigated vegetation so as to isolate irrigated areas. However, these preprocessing steps limited our ability to discern mixed pixels

with, for instance, swimming pools, which our data grouped with impervious surfaces. We believe that, for many modeling assessments, this grouping will be sufficient (with regard to hydrologic models, for instance, there is no aquifer recharge from swimming pools) but future or more high-resolution efforts might address this issue.

Our application of Segnet demonstrates a foundational capacity for deep encoder-decoder semantic segmentation of mixed pixels. As more (and increasingly sophisticated) training data become available, including classified high-resolution data at larger scales, we expect future work to improve both the accuracy and the localized categorizations of our approach (Planet Team 2017).

## **2.5 Conclusions**

We present here a subpixel land cover classification of the LAB, covering  $>5,600 \text{ km}^2$  across the megacity of Los Angeles and its surrounding mountain ranges. Our approach demonstrates the efficacy of a sub-pixel land cover classification approach over a 30 year period at a regional spatial scale. The data produced can be easily assimilated into spatially distributed hydrological models (so long as they provide for specification of mixed pixel information), with sufficient historical record to support long-term analyses. We find little change in net urban area within the LAB: much of the development over the last 34 years has been redevelopment, rather than new building in previously mountainous areas. We do see fluctuations in irrigated vs. non-irrigated vegetation with drought periods, a trend that can be investigated further in future modeling studies. In comparisons to medium-resolution datasets, notably NLCD, we find that our approach was able to identify minority-pixel features. When comparing our data to NLCD, we find  $\sim 356 \text{ km}^2$  (6.6% of the LAB) more urban areas than were shown in the 30 m pixels. We

conclude that NLCD underestimates the number of trees in urban spaces due to majority estimates for mixed pixels (e.g. parks with grass and trees are classified as grass).

Our sub-pixel classification was 91% accurate when compared to contemporary 10 cm composite imagery from 2017 across the urban portions of the LAB. In particular, our application of Segnet was able to identify small urban green spaces and landscape features that were missed by medium resolution data sets over a long record, rather than exclusively in recent years. Because our methodology requires only freely available training data, a Digital Elevation Model, globally-available water cover information, and medium resolution (e.g., Landsat) imagery, the analysis can be reproduced anywhere. Adjustment of the training data would allow for tailoring to local vegetation or particular features.

**Acknowledgments:** We thank E. Natasha Stavros for discussions on utility and applications of the work.



## References

- Arun, P. V., Buddhiraju, K. M., & Porwal, A. (2018). CNN based sub-pixel mapping for hyperspectral images. *Neurocomputing*, 311, 51–64. <https://doi.org/10.1016/j.neucom.2018.05.051>
- Audebert, N., Le Saux, B., & Lefèvre, S. (2018). Beyond RGB: Very high resolution urban remote sensing with multimodal deep networks. *ISPRS Journal of Photogrammetry and Remote Sensing*, 140, 20–32. <https://doi.org/10.1016/j.isprsjprs.2017.11.011>
- Badrinarayanan, V., Kendall, A., & Cipolla, R. (2017). SegNet: A Deep Convolutional Encoder-Decoder Architecture for Image Segmentation. *IEEE Transactions on Pattern Analysis and Machine Intelligence*, 39(12), 2481–2495. <https://doi.org/10.1109/TPAMI.2016.2644615>
- Beninde, J., Veith, M., & Hochkirch, A. (2015). Biodiversity in cities needs space: A meta-analysis of factors determining intra-urban biodiversity variation. *Ecology Letters*, 18(6), 581–592. <https://doi.org/10.1111/ele.12427>
- Chen, J., Yang, L., Zhang, Y., Alber, M., & Chen, D. Z. (2016). Combining Fully Convolutional and Recurrent Neural Networks for 3D Biomedical Image Segmentation. ArXiv:1609.01006 [Cs]. <http://arxiv.org/abs/1609.01006>
- Chu, P., Li, Z., Lammers, K., Lu, R., & Liu, X. (2020). DeepApple: Deep Learning-based Apple Detection using a Suppression Mask R-CNN. ArXiv:2010.09870 [Cs]. <http://arxiv.org/abs/2010.09870>
- Coleman, R. W., Stavros, E. N., Yadav, V., & Parazoo, N. (2020). A Simplified Framework for High-Resolution Urban Vegetation Classification with Optical Imagery in the Los Angeles Megacity. *Remote Sensing*, 12(15), 2399.
- Cramer, M. (2010). The DGPF-Test on Digital Airborne Camera Evaluation Overview and Test Design. *Photogrammetrie - Fernerkundung - Geoinformation*, 73–82. <https://doi.org/10.1127/1432-8364/2010/0041>
- EROS. (2017). National Agriculture Imagery Program (NAIP) [Tiff]. U.S. Geological Survey. <https://doi.org/10.5066/F7QN651G>
- ESRI. (2021). World Imagery. <https://www.arcgis.com/home/item.html?id=10df2279f9684e4a9f6a7f08febac2a9>
- Fry, J. A., Xian, G., Jin, S. M., Dewitz, J. A., Homer, C. G., Yang, L. M., Barnes, C. A., Herold, N. D., & Wickham, J. D. (2011). Completion of the 2006 National Land Cover Database for the conterminous United States. *Photogrammetric Engineering & Remote Sensing*, 77(9), 858–864.

- Gallo, E. M., Bell, C. D., Panos, C. L., Smith, S. M., & Hogue, T. S. (2020). Investigating Tradeoffs of Green to Grey Stormwater Infrastructure Using a Planning-Level Decision Support Tool. *Water*, 12(7), 2005. <https://doi.org/10.3390/w12072005>
- Garcetti, E. (2019). LA's Green New Deal (p. 152). LA City. [https://plan.lamayor.org/sites/default/files/pLAn\\_2019\\_final.pdf](https://plan.lamayor.org/sites/default/files/pLAn_2019_final.pdf)
- Gillespie, T. W., Ostermann-Kelm, S., Dong, C., Willis, K. S., Okin, G. S., & MacDonald, G. M. (2018). Monitoring changes of NDVI in protected areas of southern California. *Ecological Indicators*, 88, 485–494. <https://doi.org/10.1016/j.ecolind.2018.01.031>
- Grinias, I., Panagiotakis, C., & Tziritas, G. (2016). MRF-based segmentation and unsupervised classification for building and road detection in peri-urban areas of high-resolution satellite images. *ISPRS Journal of Photogrammetry and Remote Sensing*, 122, 145–166. <https://doi.org/10.1016/j.isprsjprs.2016.10.010>
- Homer, C., Dewitz, J., Fry, J., Coan, M., Hossain, N., Larson, C., Herold, N., McKerrow, A., VanDriel, J. N., & Wickham, J. (2007). Completion of the 2001 National Land Cover Database for the Conterminous United States. *PHOTOGRAMMETRIC ENGINEERING*, 5.
- Ioffe, S., & Szegedy, C. (2015). Batch Normalization: Accelerating Deep Network Training by Reducing Internal Covariate Shift. *International Conference on Machine Learning*, 448–456. <http://proceedings.mlr.press/v37/ioffe15.html>
- IOM (Ed.). (2015). *Migrants and cities: New partnerships to manage mobility*. International Organization for Migration (IOM).
- Jahns, R. H. (1973). *A Profile of Southern California Geology and Seismicity of Los Angeles Basin*. Pacific Section of AAPG. [http://archives.datapages.com/data/pacific/data/041/041001/i\\_ps041i.htm](http://archives.datapages.com/data/pacific/data/041/041001/i_ps041i.htm)
- Keeley, J. E., Safford, H., Fotheringham, C. J., Franklin, J., & Moritz, M. (2009). The 2007 Southern California Wildfires: Lessons in Complexity. *Journal of Forestry*, 107(6), 287–296. <https://doi.org/10.1093/jof/107.6.287>
- LA County. (2015). *Enriched LA County Census Tracts*. esri. [https://geohub.lacounty.org/datasets/152f90d3a34a43ef998448281505d45e\\_0](https://geohub.lacounty.org/datasets/152f90d3a34a43ef998448281505d45e_0)
- LA County Planning. (2010). *Estimated Population of the 88 Cities in the County of Los Angeles* (p. 1). [http://file.lacounty.gov/SDSInter/lac/1043532\\_PopulationPg\\_Color.pdf](http://file.lacounty.gov/SDSInter/lac/1043532_PopulationPg_Color.pdf)
- LADRP. (2021). *Zoning Maps & GIS*. <https://planning.lacounty.gov/gis/interactive>
- LARIAC. (2015). *LARIAC Product Guide*. Los Angeles County. [https://egis2.lacounty.gov/hub/lariac\\_documents/LARIAC4-Product-Guide-1.pdf](https://egis2.lacounty.gov/hub/lariac_documents/LARIAC4-Product-Guide-1.pdf)

- Lee, E.-B., Ibbs, C. W., & Thomas, D. (2005). Minimizing Total Cost for Urban Freeway Reconstruction with Integrated Construction/Traffic Analysis. *Journal of Infrastructure Systems*, 11(4), 250–257. [https://doi.org/10.1061/\(ASCE\)1076-0342\(2005\)11:4\(250\)](https://doi.org/10.1061/(ASCE)1076-0342(2005)11:4(250))
- Liu, Z., Li, X., Luo, P., Loy, C. C., & Tang, X. (2018). Deep Learning Markov Random Field for Semantic Segmentation. *IEEE Transactions on Pattern Analysis and Machine Intelligence*, 40(8), 1814–1828. <https://doi.org/10.1109/TPAMI.2017.2737535>
- Lund, J., Medellin-Azuara, J., Durand, J., & Stone, K. (2018). Lessons from California's 2012–2016 Drought. *Journal of Water Resources Planning and Management*, 144(10). [https://doi.org/10.1061/\(ASCE\)WR.1943-5452.0000984](https://doi.org/10.1061/(ASCE)WR.1943-5452.0000984)
- McPherson, E. G., Simpson, J. R., Xiao, Q., & Wu, C. (2011). Million trees Los Angeles canopy cover and benefit assessment. *Landscape and Urban Planning*, 99(1), 40–50. <https://doi.org/10.1016/j.landurbplan.2010.08.011>
- Miao, L., Qi, H., & Szu, H. (2007). A Maximum Entropy Approach to Unsupervised Mixed-Pixel Decomposition. *IEEE Transactions on Image Processing*, 16(4), 1008–1021. <https://doi.org/10.1109/TIP.2006.891350>
- Mini, C., Hogue, T. S., & Pincetl, S. (2014). Estimation of residential outdoor water use in Los Angeles, California. *Landscape and Urban Planning*, 127, 124–135. <https://doi.org/10.1016/j.landurbplan.2014.04.007>
- Mitraka, Z., Frate, F. D., & Carbone, F. (2016). Nonlinear Spectral Unmixing of Landsat Imagery for Urban Surface Cover Mapping. *IEEE Journal of Selected Topics in Applied Earth Observations and Remote Sensing*, 9(7), 3340–3350. <https://doi.org/10.1109/JSTARS.2016.2522181>
- Mortensen, A. K., Dyrmann, M., Karstoft, H., Jørgensen, N., & Gislum, R. (2016). Semantic segmentation of mixed crops using deep convolutional neural network. 1–6. <https://www.cabdirect.org/cabdirect/abstract/20183376904>
- OurCounty. (2019). The Plan. OurCounty. <https://ourcountyla.lacounty.gov/plan>
- Pekel, J.-F., Cottam, A., Gorelick, N., & Belward, A. S. (2016). High-resolution mapping of global surface water and its long-term changes. *Nature*, 540(7633), 418–422. <https://doi.org/10.1038/nature20584>
- Pincetl, S., Prabhu, S. S., Gillespie, T. W., Jenerette, G. D., & Pataki, D. E. (2013). The evolution of tree nursery offerings in Los Angeles County over the last 110 years. *Landscape and Urban Planning*, 118, 10–17. <https://doi.org/10.1016/j.landurbplan.2013.05.002>

- Planet Team. (2017). Planet Application Program Interface: In Space for Life on Earth. San Francisco, CA. <https://api.planet.com>
- Porse, E., Mika, K. B., Litvak, E., Manago, K. F., Naik, K., Glickfeld, M., Hogue, T. S., Gold, M., Pataki, D. E., & Pincetl, S. (2017). Systems Analysis and Optimization of Local Water Supplies in Los Angeles. *Journal of Water Resources Planning and Management*, 143(9), 04017049. [https://doi.org/10.1061/\(ASCE\)WR.1943-5452.0000803](https://doi.org/10.1061/(ASCE)WR.1943-5452.0000803)
- Powell, R. L., Roberts, D. A., Dennison, P. E., & Hess, L. L. (2007). Sub-pixel mapping of urban land cover using multiple endmember spectral mixture analysis: Manaus, Brazil. *Remote Sensing of Environment*, 106(2), 253–267. <https://doi.org/10.1016/j.rse.2006.09.005>
- Smits, P. C., Dellepiane, S. G., & Schowengerdt, R. A. (1999). Quality assessment of image classification algorithms for land-cover mapping: A review and a proposal for a cost-based approach. *International Journal of Remote Sensing*, 20(8), 1461–1486. <https://doi.org/10.1080/014311699212560>
- Sultana, F., Sufian, A., & Dutta, P. (2020). Evolution of Image Segmentation using Deep Convolutional Neural Network: A Survey. *Knowledge-Based Systems*, 201–202, 106062. <https://doi.org/10.1016/j.knosys.2020.106062>
- Thomas, J. V. (2009). Residential Construction Trends in America’s Metropolitan Regions. EPA.
- US Census Bureau. (2010). 2010 Census Urban and Rural Classification and Urban Area Criteria. The United States Census Bureau. <https://www.census.gov/programs-surveys/geography/guidance/geo-areas/urban-rural/2010-urban-rural.html>
- US Census Bureau. (2019). Los Angeles County, California; California. US Census Quick Facts. <https://www.census.gov/quickfacts/fact/table/losangelescountycalifornia,CA/PST045219>
- Vahmani, P., & Ban-Weiss, G. A. (2016). Impact of remotely sensed albedo and vegetation fraction on simulation of urban climate in WRF-urban canopy model: A case study of the urban heat island in Los Angeles—Vahmani—2016—*Journal of Geophysical Research: Atmospheres*—Wiley Online Library. *Journal of Geophysical Research: Atmospheres*, 121(4), 1511–1531. <https://doi.org/10.1002/2015JD023718>
- Van Oijen, M., Balkovi, J., Beer, C., Cameron, D. R., Ciais, P., Cramer, W., Kato, T., Kuhnert, M., Martin, R., Myneni, R., Rammig, A., Rolinski, S., Soussana, J.-F., Thonicke, K., Van der Velde, M., & Xu, L. (2014). Impact of droughts on the carbon cycle in European vegetation: A probabilistic risk analysis using six vegetation models. *Biogeosciences*, 11(22), 6357–6375. <https://doi.org/10.5194/bg-11-6357-2014>
- Wang, W., Liu, K., Tang, R., & Wang, S. (2019). Remote sensing image-based analysis of the urban heat island effect in Shenzhen, China. *Physics and Chemistry of the Earth, Parts A/B/C*, 110, 168–175. <https://doi.org/10.1016/j.pce.2019.01.002>

- Wiersema, I. (2018). One Water LA Plan. City of Los Angeles.  
[https://www.lacitysan.org/cs/groups/sg\\_owla/documents/document/y250/mdmx/~edisp/cont031540.pdf](https://www.lacitysan.org/cs/groups/sg_owla/documents/document/y250/mdmx/~edisp/cont031540.pdf)
- Xiao, M., Nijssen, B., & Lettenmaier, D. P. (2016). Drought in the Pacific Northwest, 1920–2013. *Journal of Hydrometeorology*, 17(9), 2391–2404. <https://doi.org/10.1175/JHM-D-15-0142.1>
- Yoo, C., Han, D., Im, J., & Bechtel, B. (2019). Comparison between convolutional neural networks and random forest for local climate zone classification in mega urban areas using Landsat images. *ISPRS Journal of Photogrammetry and Remote Sensing*, 157, 155–170. <https://doi.org/10.1016/j.isprsjprs.2019.09.009>
- Zhao, W., & Du, S. (2016). Spectral–Spatial Feature Extraction for Hyperspectral Image Classification: A Dimension Reduction and Deep Learning Approach. *IEEE Transactions on Geoscience and Remote Sensing*, 54(8), 4544–4554.  
<https://doi.org/10.1109/TGRS.2016.2543748>
- Zhu, Z., Woodcock, C. E., Rogan, J., & Kelndorfer, J. (2012). Assessment of spectral, polarimetric, temporal, and spatial dimensions for urban and peri-urban land cover classification using Landsat and SAR data. *Remote Sensing of Environment*, 117, 72–82.  
<https://doi.org/10.1016/j.rse.2011.07.020>

## **Chapter 3. The role of urban vegetation change in the basin-scale hydrology of Los Angeles**

The supplementary materials for this chapter are provided in Appendix B.

### **Abstract**

As development has matured in Los Angeles over the last 35 years, management of the urban landscape has become increasingly scrutinized. While imperviousness has increased, city managers have planted over 400,000 new trees and sought to increase urban green space. We use a novel implementation of the Distributed Hydrology Soil Vegetation Model (DHSVM), using time-varying land cover data to evaluate the cumulative effects of these land use changes on basin storage, streamflow, and evapotranspiration (ET) in the Los Angeles River Basin (LARB) and two different sample neighborhoods. We find that small-scale, discrete increases in urban green space reduce runoff in over 90% of modeled days overall and during 98% of days during non-drought years. However, increases in non-native urban vegetation increases ET substantially year-round, and especially during drought periods. Basin- and neighborhood-scale hydrology shows the effects of isolated, pixel-level (30 m) land use changes, indicating that local efforts to reduce imperviousness and cultivate drought-resistant vegetation could lead to long-term water savings.

### **3.1 Introduction**

As the global population has rapidly urbanized over the last half-century, analyses of urban hydrology have increasingly hinged on accurate, detailed land use data. Currently, 54% of the world's population lives in cities, and that figure is projected to grow to 67% by 2050 (IOM 2015). Within the United States (US), urban area grew over 10% between 2000 and 2010 (US Census 2010). In these expanding cities, land cover is more heterogeneously distributed than in suburban or rural areas, and changes occur at a finer scale, often block-to-block (Welch 1982).

For examination of urban dynamics, particularly hydrologic studies, granular and time-varying land cover data provide information on infiltration, evapotranspiration (ET), and runoff that can be invisible in medium-resolution analyses (Litvak and Pataki 2016; Usery et al. 2014). These challenges are particularly evident in Los Angeles, where suburban sprawl, undeveloped upland areas, and a dense urban core are mingled. Prolonged drought and income inequality have led to highly concentrated, unequal water use and landscape changes at the neighborhood level (Mini et al. 2014).

While high-resolution (< 30 m) land cover data is available in recent years, it is not readily available for long enough time periods to support multidecadal hydrologic modeling. For instance, the National Land Cover Database (NLCD), at 30 m, is only available in 8 epochs between 2001 and 2019 (Fry et al. 2011, Litvak and Pataki 2016). More detailed datasets, such as the National Agriculture Imagery Program (NAIP, available at 1 m resolution at 5-year intervals 2003-2008 and 3-year intervals 2009-2019), are more labor-intensive to produce and have shorter record lengths (EROS 2017). In order to examine regional hydrologic effects of land use changes, we integrate a 34-year record of annual fractional land cover change (1985-2019) into the Distributed Hydrology Soil Vegetation Model (DHSVM), an offline physically-based model (Engel et al. in review; Wigmosta et al. 1994).

We take as our study area the Los Angeles River Basin (LARB), which drains ~2,110 km<sup>2</sup> from the San Gabriel Mountains through the urban core of Los Angeles to the port of Long Beach. The basin has been subject to extreme drought events during the period of study, notably during 2014-2018 (Porse et al. 2016). Overall water use has been slowly decreasing over the last half century, but only 14% of LA County's water is sourced locally (LADWP 2018). Both the City and County of Los Angeles actively manage water use and have restricted outdoor irrigation

during droughts (Porse et al. 2017). Within the LARB, we further examine two neighborhoods that underwent substantial development during our study period: Long Beach, which grew with expansion of the aerospace industry in the 1980s-1990s and a more recent housing expansion in the 2010s (Addison 2017; Sabau 2020), and Woodland Hills, which saw residential and economic growth during the years since 1990 (ALFRED 2022).

Throughout the LARB, land cover is highly variable: tree canopy coverage estimates range from 7-31% across city council districts, with an average density of ~100 trees per hectare (McPherson et al. 2011; Gillespie et al. 2012). Historical records show an overall decline in urban tree cover across the LARB between 2005 and 2009 and an increase in impervious surfaces, but city efforts resulted in a reported 400,000 new trees planted between 2006 and 2013 (Nowack and Greenfield 2012; Mini et al. 2014). This number is relatively small when averaged across the whole basin, and trees were often planted in already-irrigated neighborhoods (Litvak and Pataki 2016). We therefore examine the effects of these relatively minimal land cover changes in two distinct neighborhoods – one highly green, the other primarily impervious – within the LARB. We specifically answer the following questions:

1. What are the cumulative effects of small-scale (30m) land use changes across the LARB on local hydrology, and how are those effects distributed among heavily irrigated and primarily impervious neighborhoods?
2. How do small-scale land cover changes affect summertime ET in irrigated and impervious neighborhoods?



## **3.2 Methods**

### *3.2.1 Study Area*

Our study area is the Los Angeles River Basin, a region between the San Gabriel, Santa Monica, and Santa Ana mountains that drains into the Pacific Ocean at the Port of Long Beach (Read et al. 2019). It excludes inland parts of LA County that do not flow to the Pacific Ocean (Figure 3.1). The LARB ranges in elevation from sea level to >3000 m, and includes national forests, state beaches, and local parks. It includes multiple administrative areas, notably the majority of the City of Los Angeles, which has a population of ~4 million (City of LA 2012). The LARB has a Mediterranean climate, with mild winter-dominant precipitation. Though the San Gabriel Mountains in the north of the Basin experience wintertime snowfall, spring runoff is minimal compared to runoff in winter from isolated precipitation events (Kesseli et al. 1942). The basin contains five reservoirs in the upstream, mountainous regions (Read et al. 2019).

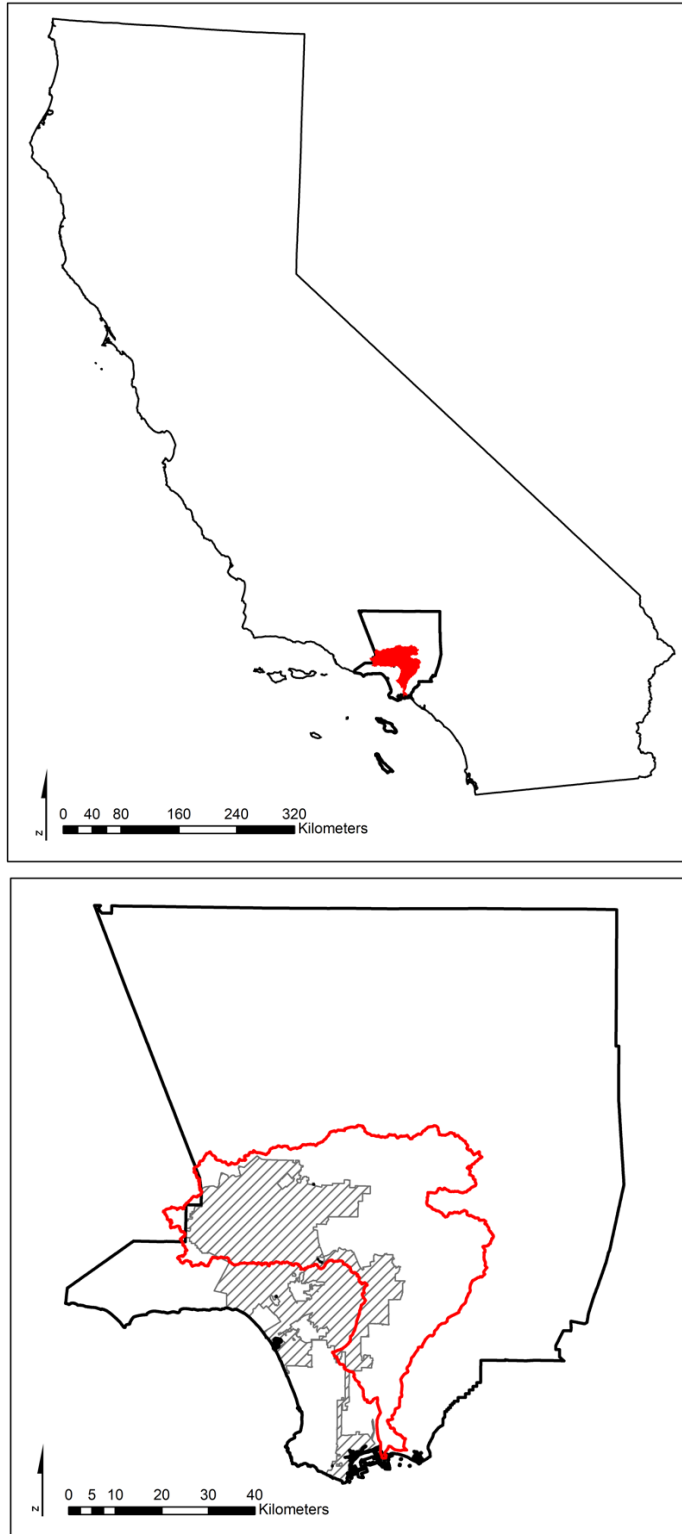


**Figure 3.1:** Location of the LARB (red) within California and within Los Angeles County, with City of Los Angeles (shaded).

Both the City and the County of Los Angeles (which covers 98% of the LARB) actively manage water consumption. LA City residential water restrictions during droughts have reached 35%, though both the restrictions and associated water savings are distributed unequally across the city and show strong correlations with median income (Mini et al. 2014). Uneven urban irrigation cutbacks have resulted from different pre-restriction water use, predominant land cover types, and ability to pay fines (Mini et al. 2014). Both the City and the County also have independent sustainability plans that address coupled land and water use (Garcetti 2019; OurCounty 2019). The City of Los Angeles in particular has focused on planting trees to lower surface temperature and increase shade, and historical records show increased tree presence on private lands since 2000 (McPherson et al. 2011; Gillespie et al. 2012). In light of the strong and overt focus on land and water use in regional planning, we examine the cumulative effects of local land cover changes on regional hydrology.

### *3.2.2 Sample Neighborhoods*

We selected two sample neighborhoods for which we examine land use and ET: Woodland Hills and Long Beach. These neighborhoods developed substantially during the study period: Woodland Hills has experienced significant residential growth since the 1990s, and Long Beach saw a boom through the late 1980s due to growth in the aerospace industry and then a redevelopment of its downtown in the 2010s (Sabau 2020; ALFRED 2022). While both neighborhoods saw development, neither experienced large-scale land use change: like the majority of the LARB, redevelopment was common and new projects were rare (Sabau 2020). Therefore, changes to irrigated vegetation were comparable between the neighborhoods.

The two neighborhoods are dissimilar in region and character. Woodland Hills, a part of the City of Los Angeles within the San Fernando Valley, abuts the Santa Monica Mountains. It is

affluent and green, with an NDVI in the top 20% of Los Angeles neighborhoods, four LA parks, and a large golf course (Bartholomew 2020; LA Parks 2021). Its climate is more variable than that of Long Beach, with summertime average daily air temperature at  $\sim 35^{\circ}$  C. Because of its high income level and park area, Woodland Hills has a reputation as a heavy water consumer, even during times of drought (Mini et al. 2014). Long Beach is the seventh most populous city in California, and has an airport, port, and large commercial sector (US Census 2022). It is coastal, with a summertime marine layer (Edinger 1959). While it has residential areas, the landscape is dominated by large impervious areas, including an airport, a shipping port, a downtown, warehouses and supply chain management facilities, and oil refineries (Sabau 2020; Engel et al. in review). Long Beach per capita water use is consistently lower than both LA City and LA County values (2013-2020; CA DWR via Pacific Institute 2022). Long Beach also imports less water than surrounding areas due to a large aquifer that provides 60% of the city's needs (LB Water 2022).

### *3.2.3 Model Implementation*

To assess water use, we implemented DHSVM3.2 across the LARB, Woodland Hills, and Long Beach (Wigmosta et al. 1994; Perkins et al. 2011). We compared results using time-varying vegetation cover (hereafter called the time-varying model) and constant vegetation cover based on 2016 NLCD categorization (hereafter called the static model; Homer et al. 2007). For the time-varying model, we incorporated annual vegetation updates (Engel et al. in review). We ran both models at a 12-hour time step at a 30 m spatial resolution (5.8 million pixels) to assess the long-term hydrologic effects of local land cover changes.

### 3.2.4 Meteorological Forcing Data

DHSVM requires six meteorological inputs: precipitation (m), wind speed (m/s), temperature ( $^{\circ}\text{C}$ ), relative humidity (%), downward longwave radiation ( $\text{W}/\text{m}^2$ ), and downward shortwave radiation ( $\text{W}/\text{m}^2$ ). In order to format the station data for DHSVM, we first filled missing daily observation values using observations from the nearest reporting station. We then used MTCLIM algorithms to obtain relative humidity and incoming short/longwave radiation (Bohn et al. 2013).

We assembled daily observations of precipitation, wind speed, and max/min temperature from 73 stations in and around the LARB (Figure 3.2). Our weather data were obtained from the Iowa State Environmental Mesonet collection (25 from the ASOS automated airport weather observations network and 50 from the NCEI Cooperative Observer Network). We used data from 2 Mesonet stations with long ( $>30$  year) records to assess the model's accuracy against precipitation.

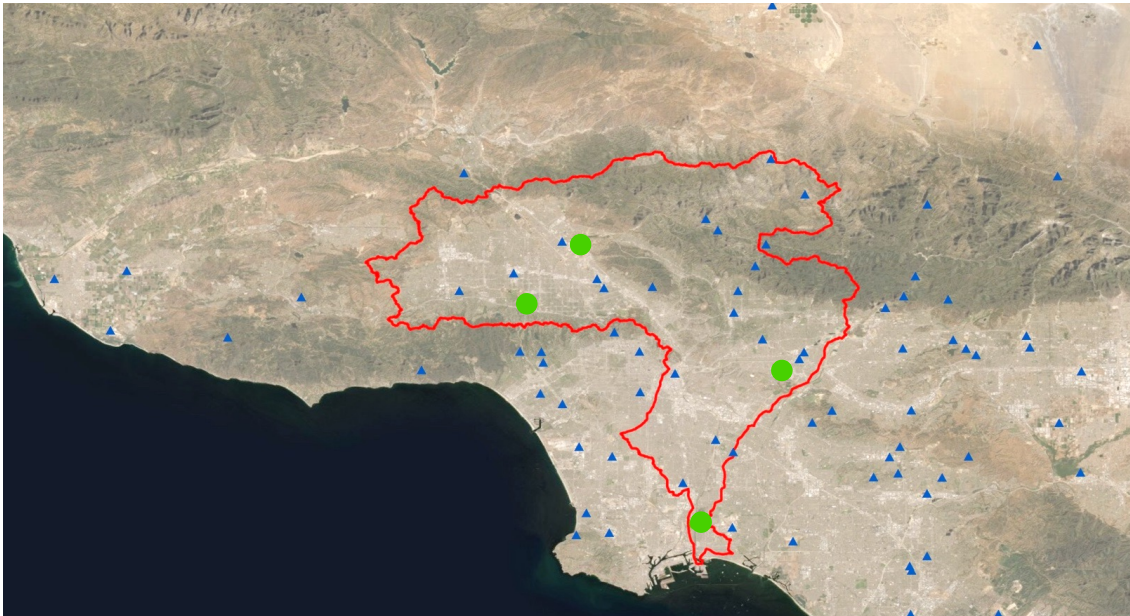


**Figure 3.2:** Locations of weather stations used for DHSVM meteorological forcing (blue) and stream gauges used for data validation (green).

### *3.2.5 Spatial Data*

We incorporated both static (NLCD) and time-varying (prescribed) vegetation changes into DHSVM 3.2 (Wigmosta et al. 1994; Fry et al. 2006; Engel et al. in revision).

We used the U.S. Geological Survey 3D Elevation Program's 10 meter (1/3 arc-second) digital elevation model for our topography (US Geological Survey 2020). Elevation data is a direct input for DHSVM, and also serves as the basis for modeled flow routing and stream network calculations.

We merged two soil datasets to provide urban and wilderness inputs to DHSVM. For mountainous regions, we relied on the comprehensive 2018 U.S. Department of Agriculture National Resources Conservation Service (NRCS) Soil Survey (SSURGO), formatted as polygons throughout >95% of counties in the conterminous United States (Soil Survey Staff 2018). However, comparisons of the NRCS data to samples of urban soils show a lack of comprehensive data in urban areas, particularly with respect to hydrologic properties (Effland and Pouyat 1997; Schifman and Shuster 2019). We therefore used 2018 Los Angeles County soil type polygons for all of LA County, which includes the urban section of the LARB (Public Works, LA County 2018). The polygons were derived from scanned soil maps created by the Water Resources Division. We rasterized the polygons at 30 m resolution.

### *3.2.6 Vegetation Change*

We spatially reclassified annual categorical percentages of impervious surfaces, irrigated trees, irrigated low vegetation, and non-irrigated vegetation within Landsat pixels from categorical percentages across our study areas (30 m). Our data were produced using a deep semantic segmentation neural network to decompose mixed pixels within the LARB and demonstrated 91% accuracy in comparison to contemporary classifications derived from 10cm

LiDAR data (Engel et al. in review). For the static vegetation model we used land cover classifications derived from the 2016 NLCD land cover dataset (30 m; Fry et al. 2006).

Due to model processing constraints, we applied minimal land cover changes: between 1985 and 2020, there was an average annual change of 3.86% of total pixels within the LARB (Figure 3.3; Appendix B). Annual land cover change varied between 0.2% of pixels (2016-2017) and 14% of pixels (1990-1991). Changes were smallest after 2013, when drought conditions reduced the effect of irrigation across the LARB. Overall, the time-varying vegetation model contained more urban vegetated area than the static vegetation model.

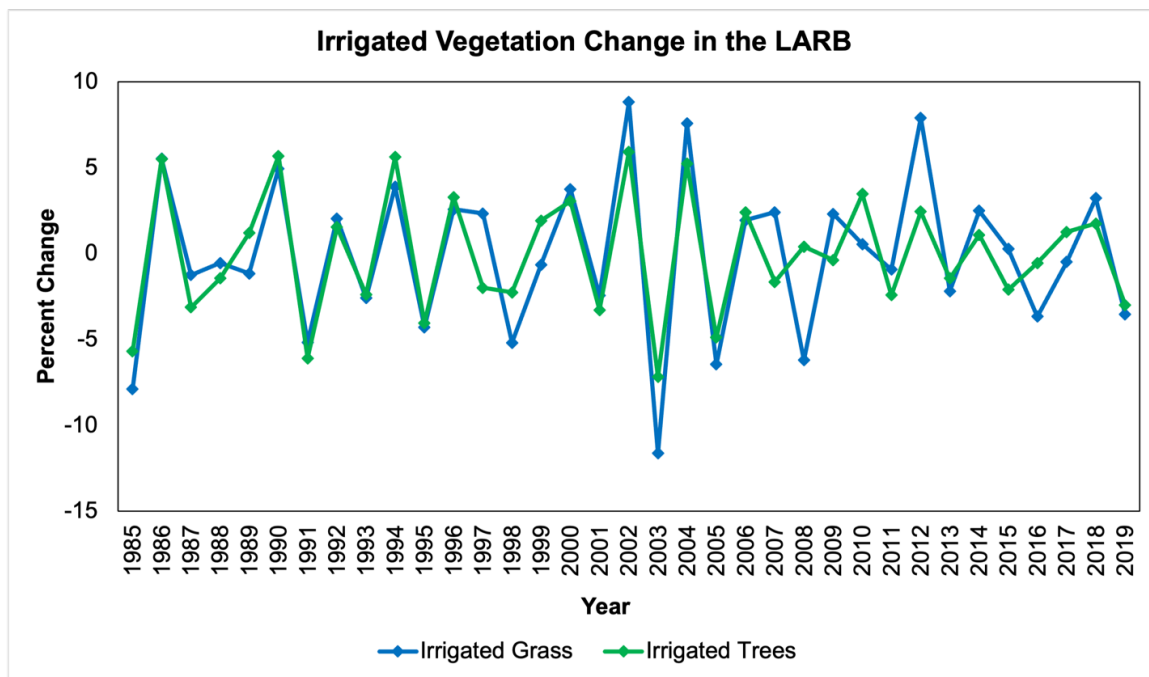


**Figure 3.3:** Percentage of LARB pixels with changes to irrigated vegetation. Plot shows years in which changes took effect. Vegetation change data based on sub-pixel classification of Landsat imagery (Engel et al. in review).

### 3.2.7 Evapotranspiration

We modeled urban irrigation independently of the DHSVM implementation (Thanapakpawin et al. 2007; Perkins et al. 2022) to assess the role of anthropogenic watering. We used a combination of empirical models for turfgrass and trees (angiosperm, gymnosperm,

and palm) across Los Angeles to calculate neighborhood ET from irrigation (Litvak et al. 2017). We proportionally added the irrigated vegetation ET values for irrigated land area and DHSVM-produced ET values for non-irrigated land area (Litvak et al. 2017; Engel et al. in review).

### *3.2.8 Model Evaluation Data*

To evaluate modeled streamflow, we used observed streamflow data from four stream gauges within the LARB (Figure 3.2). Our primary evaluation point was the basin outlet (LA Department of Public Works F319-R), which is managed by the Army Corps of Engineers (Cummings 2016; Public Works 2021b). The data were available daily between October 1988 and October 1992, and annually between 1985-1996 and 2000-2012. During 1997-1999, no observations were available. The site is within the concretized channel of the lower Los Angeles River.

In times of high streamflow, 20 cubic feet per second from the river can be diverted to the nearby Dominguez Gap Spreading Grounds, a ~15 ha wetland that also recharges the 1,088 km<sup>2</sup> aquifer (Johnson et al. 2001; Public Works 2021a). The spreading grounds first opened in 1957, but were converted into a multi-use wetland and indigenous species habitat in 2008 (LA County 2021). Uncontrolled stormwater runoff from nearby impervious areas within the LARB also flow into the Dominguez Gap Spreading Grounds.

We also evaluated streamflow with observations from three other gauges within the LARB, including the most upstream gauge and the easternmost and westernmost gauges. Two gauges (USGS 11097000 and USGS 11101250) recorded streamflow at 15-minute intervals beginning in 10/1988, resulting in an evaluation period of 32 years (USGS 2021). The third (USGS 11092450) had 15-minute data beginning in 10/2002, resulting in an evaluation period of 18 years (USGS 2021).



### 3.2.9 Evaluation Methods

To assess model accuracy, we compared static and time-varying modeled streamflow to observed monthly streamflow at the basin outlet using Kling-Gupta Efficiency (KGE), a metric designed for assessment of accuracy of hydrologic models. The KGE is a single number reflecting correlation, bias, and ratios of variance (Liu 2020). Mathematically, the KGE indicates a reasonable model at  $> (1 - \sqrt{2})$ , but most literature uses 0 as a benchmark of adequate performance (Knoben et al. 2019).

We compared root mean square error (RMSE) and relative bias for daily streamflow from each model and our four reference gauges throughout the LARB. These indicators show mismatches between the two datasets and can be useful in comparing magnitudes of flow over time (Moriassi et al. 2015). In examining basin-scale performance, we expect to find more accurate results at the pour point than at gauges with small drainage areas (Cao et al. 2019).

## 3.3 Results

### 3.3.1 Model Accuracy

We assessed model accuracy using KGE at the basin outlet (LA Department of Public Works F319-R) and found a value of 0.23 for both the time-varying and static vegetation models at an annual time step.

We also compared RMSE and relative bias in cubic meters per second (cms) between each model and four stream gauges. We discuss here results for the time-varying model; there was only a negligible difference between accuracy assessments for the two models. Values for RMSE varied from 19.08-35.29 cms, and values for bias varied from 4.29-17.17 (Table 3.1). Values were lowest at the basin outlet.

**Table 3.1:** Streamflow in cubic meters per second (cms) and validations statistics. DA is drainage area, and starred gauge is basin outlet. Efficiency statistics are monthly. Kling-Gupta Efficiency at basin outlet is 0.23.

Gauge	Manager	Period of Record	DA (mi <sup>2</sup> )	Average Observed Streamflow (cms)	Time-Varying Vegetation	
					RMSE (cms)	Bias
F319-R*	US ACE	10/88-10/92	815	346.14	19.08	4.29
11092450	USGS	10/02-12/20	158	121.29	35.01	16.98
11097000	USGS	10/88-12/20	153	27.64	35.29	17.17
11101250	USGS	10/88-12/20	91.2	49.92	34.37	16.54

### 3.3.2 Precipitation and Streamflow

The time-varying and static vegetation models showed very similar streamflow values; the effects of vegetation changes were primarily visible in ET values. The static vegetation model had slightly higher streamflow values in >90% of days; 80% instances of the time-varying vegetation model producing higher streamflow values in years of heavy drought (2007; 2013-2018). In times without an active precipitation event, ET volumes were greater than streamflow: 4 times greater during non-drought periods and over 11 times greater during periods of drought. Summertime streamflow is negligible due to lack of precipitation (Figure 3.4).

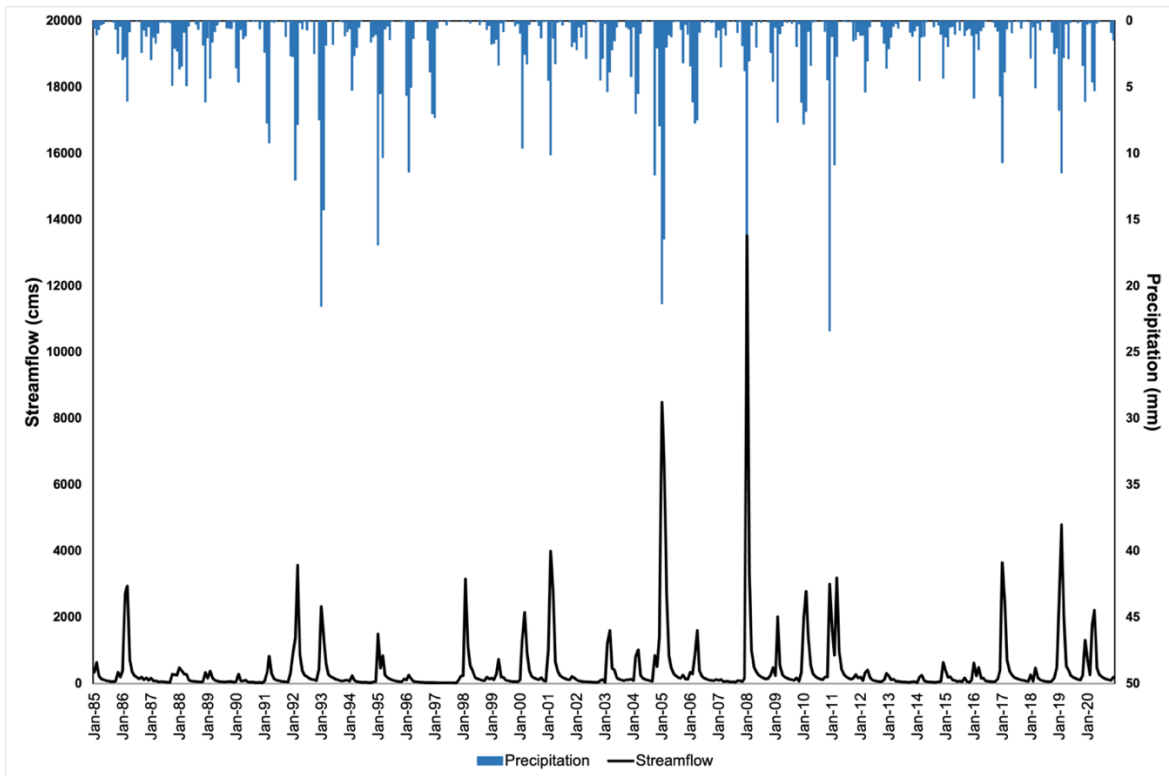


**Figure 3.4:** Streamflow (time-varying vegetation model) and precipitation in the LARB, 1985-2020.

Both the static and time-varying models showed differences between wintertime streamflow in increased- or decreased-vegetation years (Figure 3.5). Streamflow in the LARB is dominated by large wintertime events (Figure 3.4), and these differences are the effect of particular storms occurring in years with increasing or decreasing vegetation. There was no difference in streamflow driven by land use change. However, both overall streamflow and the total range of monthly wintertime streamflow were larger in Long Beach, which is primarily impervious, than in Woodland Hills, which is highly vegetated.

### 3.3.3 Drought Events and ET

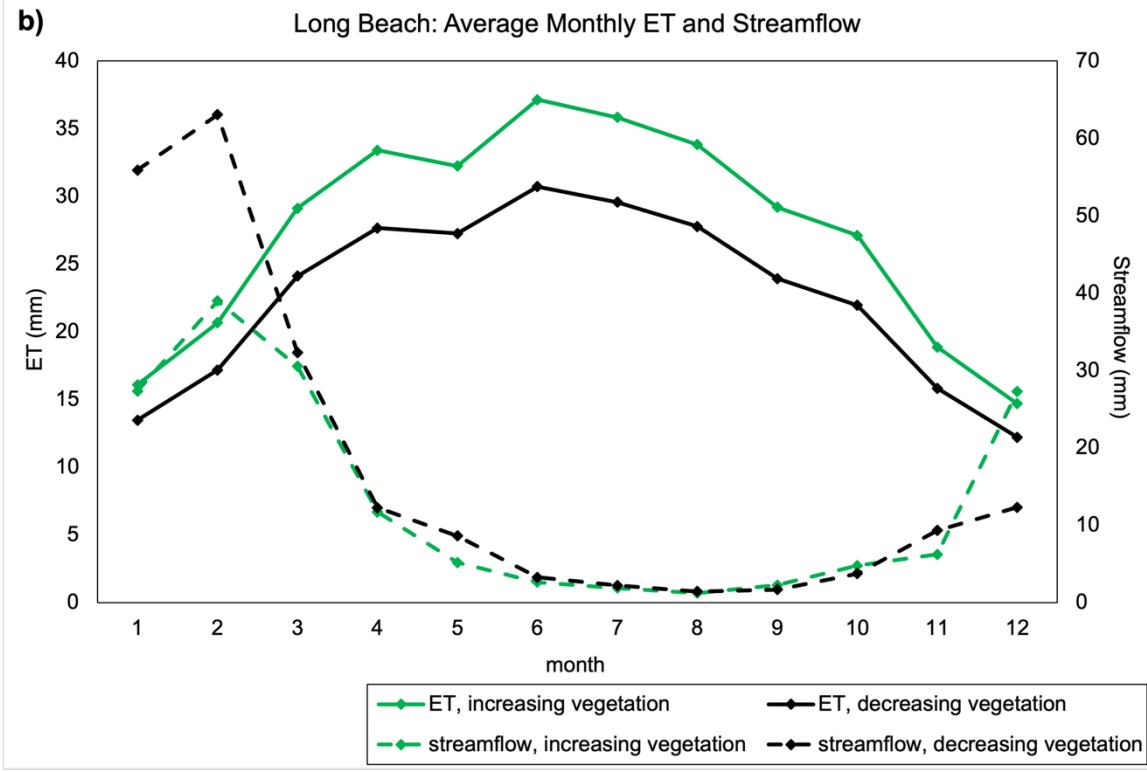
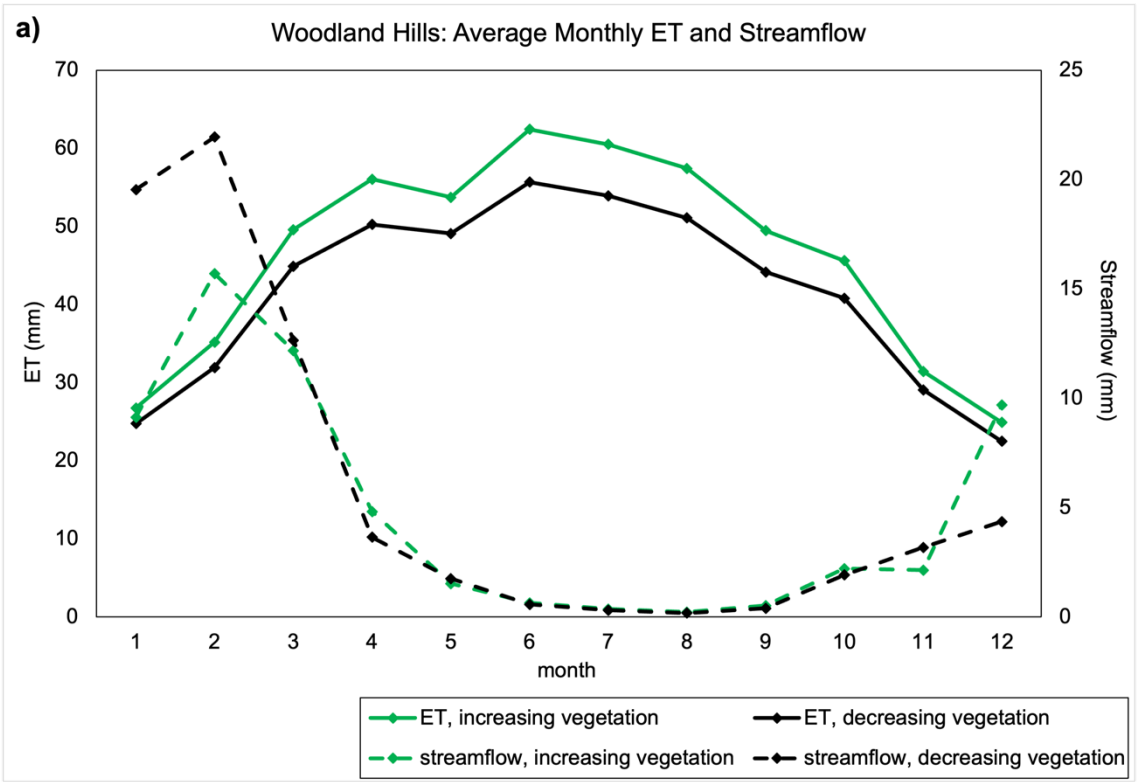
Land cover changes played a role in determining ET, which is primarily influenced by urban irrigation (Table 3.2). Woodland Hills, which has abundant irrigated vegetation, has higher ET across all seasons and conditions than Long Beach, which is primarily impervious.

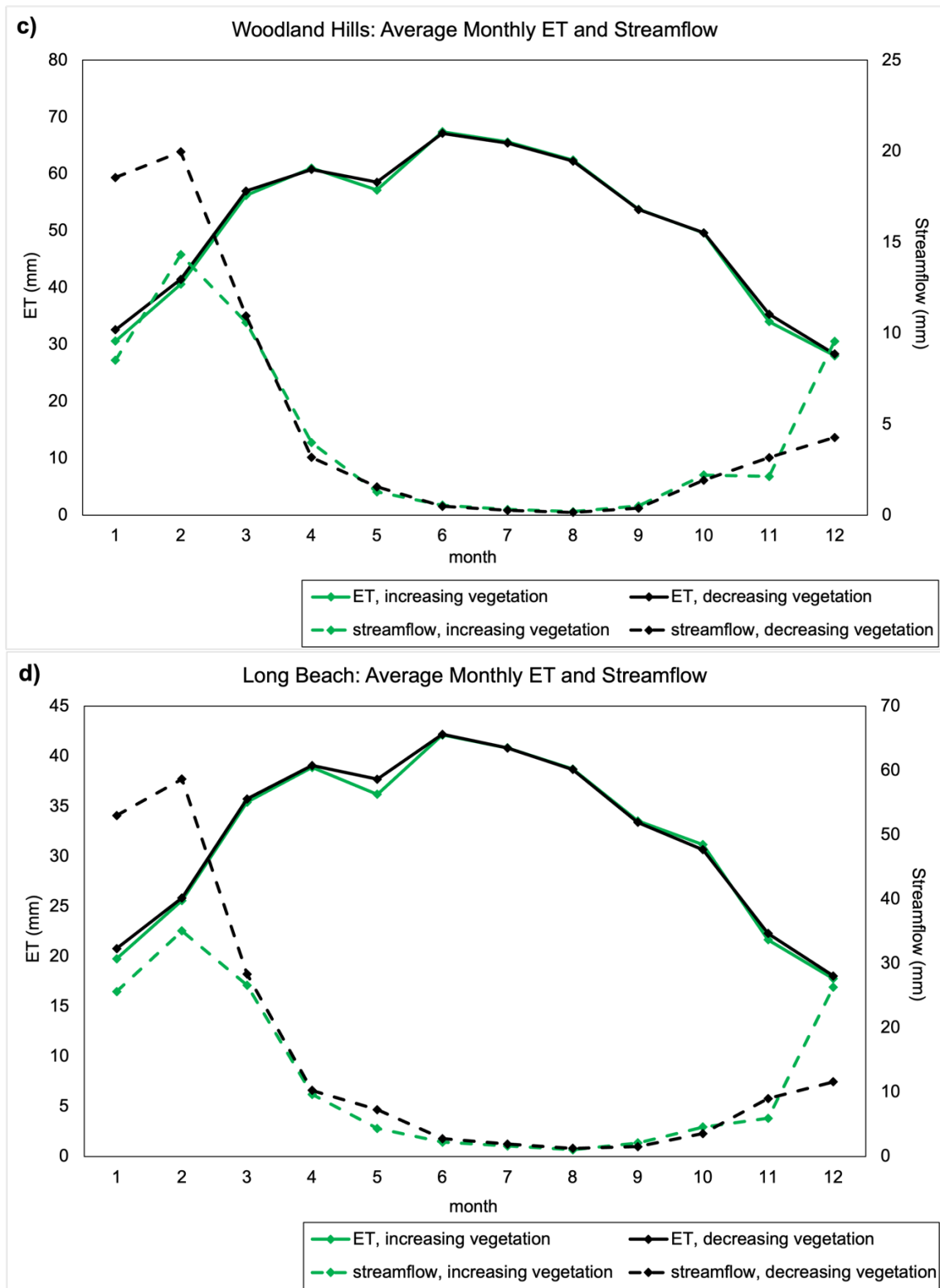
Differences between ET in years of increasing and decreasing vegetation were greater in Long Beach than in Woodland Hills. In the static model, which had no change due to vegetation, differences in precipitation patterns were visible, particularly during winter months.

**Table 3.2:** Average ET in all years, wet years and dry years; percent of seasonal ET that changes between years of increasing and decreasing vegetation. All data shown for summertime (JJA) and wintertime (DJF) across the time-varying (TV) and static (S) models in Woodland Hills (WH) and Long Beach (LB). Wet years are above the 75<sup>th</sup> percentile in precipitation; dry years are below the 25<sup>th</sup> percentile.

Model	Average Summertime ET			Average Wintertime ET			Summer % ET change (inc. vs. dec. vegetation)		Winter % ET change (inc. vs. dec. vegetation)	
	all years	wet years	dry years	all years	wet years	dry years	wet years	dry years	wet years	dry years
WH (TV)	56.8	57.6	56.5	27.7	29.3	26.7	12.6	11.6	11.5	1.1
LB (TV)	32.5	33.1	32.2	15.7	16.1	15.7	20.2	20.0	20.8	5.9
WH (S)	65.0	65.7	64.8	33.6	37.0	30.2	0.9	0.1	0.5	-5.3
LB (S)	40.6	41.2	40.3	21.3	22.8	19.6	-0.3	0.2	2.4	-7.1

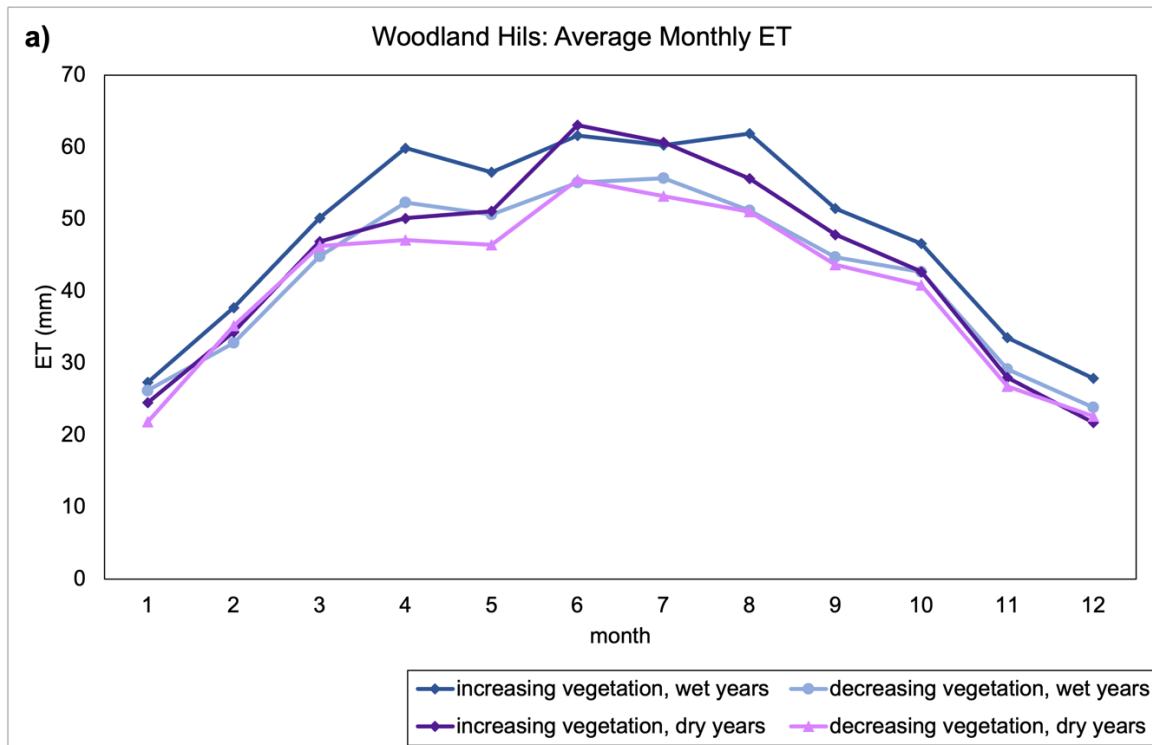
In Woodland Hills, which is greener, irrigation-driven ET was substantially higher than in Long Beach (Figure 3.5a-b). However, in Long Beach, the difference between ET in years with decreasing and increasing irrigated vegetation and was larger than in Woodland Hills. This difference was highest during summer months in Long Beach, where the increases in vegetation created new irrigated areas in a predominantly impervious neighborhood. In Woodland Hills, where much of the area is already irrigated, the difference between ET in years with increasing and decreasing irrigated vegetation was smaller. The static model showed the same annual pattern, but no difference between ET in years with increasing or decreasing vegetation. In monthly ET, the precipitation signal was negligible compared to the effect of urban irrigation (Figure 3.5c-d).

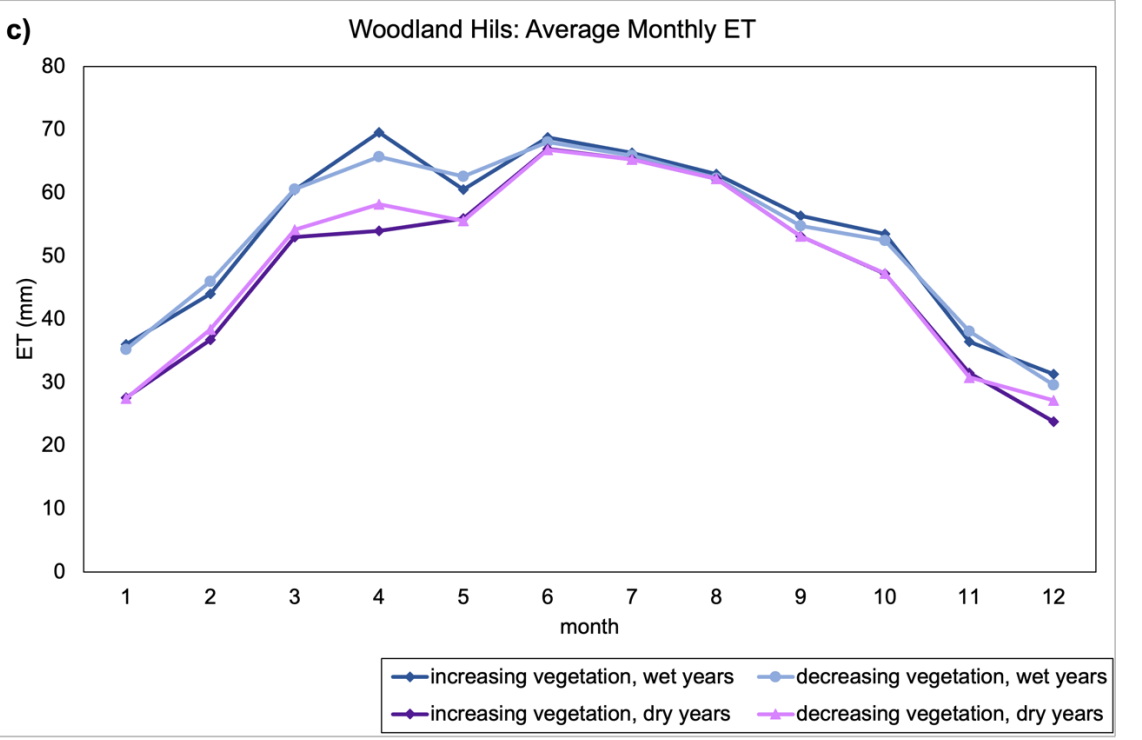
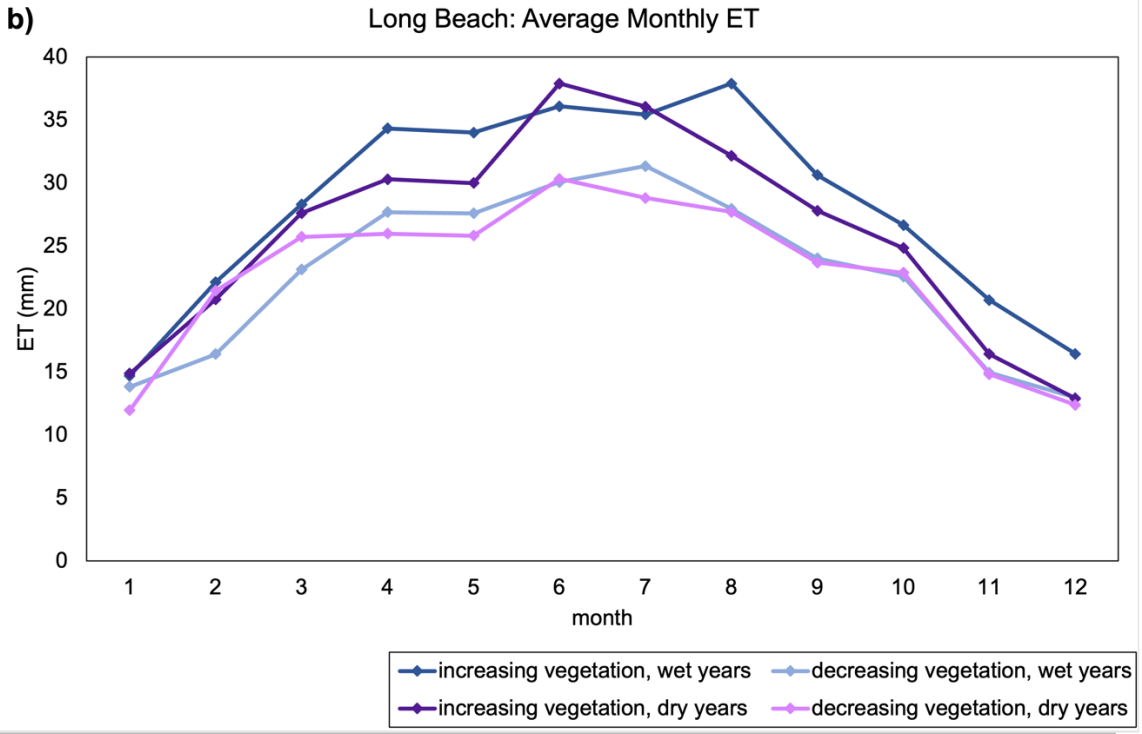




**Figure 3.5:** Comparison of average monthly ET (solid lines) and streamflow (dotted lines) during periods of increasing irrigated vegetation (green) and decreasing irrigated vegetation (black). Results shown for time-varying model (a-b) and static model (c-d).

In the time-varying model results, we did not observe differences between wet and dry year summertime ET in either Woodland Hills or Long Beach. Urban irrigation was the primary contributor to ET, and summertime precipitation is negligible (Figure 3.6a-b). However, the static models for both regions showed slightly higher ET in wet years than in dry, demonstrating a minor precipitation signal (Figure 3.6c-d). In winter months, when precipitation occurs, Woodland Hills ET from the time-varying model was highest in wet years with increasing vegetation; wintertime ET was very similar for years with decreasing vegetation and dry years with increasing vegetation (Figure 3.6a). In Long Beach, however, wintertime ET was similar for years with increasing vegetation and dry years with decreasing vegetation (Figure 3.6b). Wet years with increasing vegetation had lower ET, likely due to runoff from impervious surfaces during precipitation events.







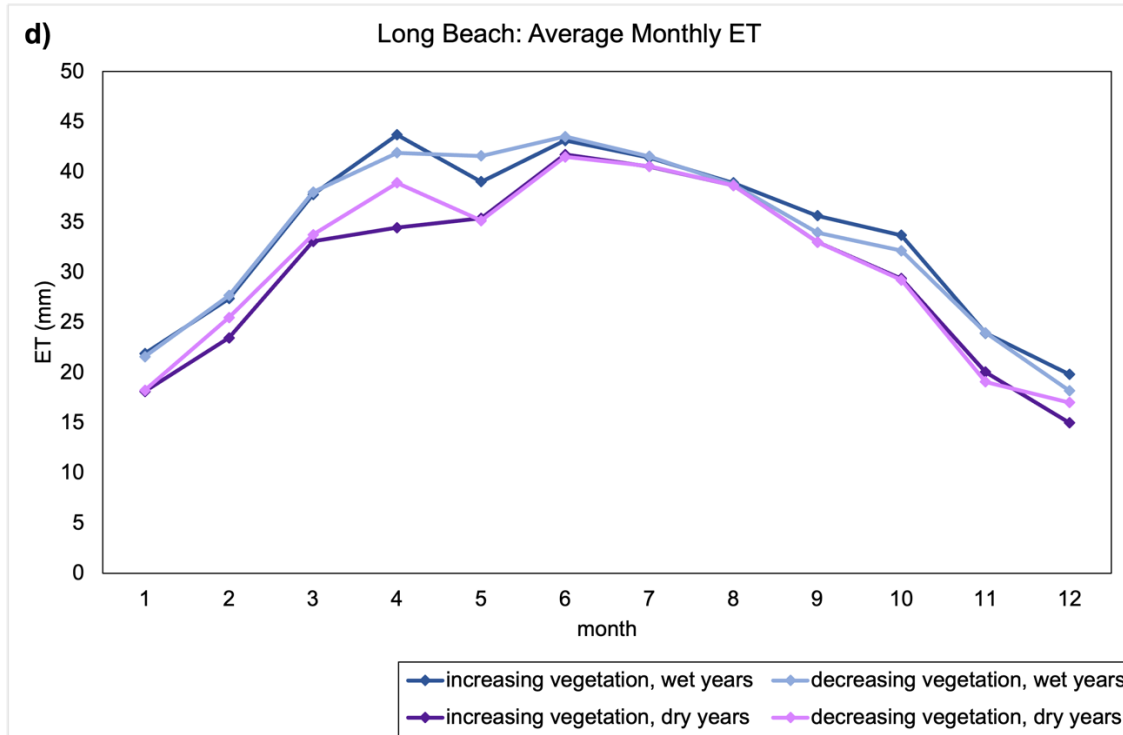


**Figure 3.6:** Average monthly ET for Woodland Hills (a) and Long Beach (b) in years with increasing irrigated vegetation (dark colors) and decreasing irrigated vegetation (light colors) that are above the 75<sup>th</sup> percentile for precipitation (blue) or under the 25<sup>th</sup> percentile (purple). Results shown for time-varying model (a-b) and static model (c-d).

### 3.4 Discussion

#### 3.4.1 Model Accuracy, Precipitation, and Streamflow

Incorporation of land cover changes into a DHSVM improved interactions between urban vegetation and hydrologic fluxes. Time-varying vegetation results showed lower streamflow peaks in accordance with the overall higher proportion of urban vegetation, which can result in increased infiltration and ET (Litvak et al. 2017; Read et al. 2019). However, monthly streamflow was dominated by precipitation events rather than land cover change. While this model shows lower overall accuracy than lower-resolution regional applications (Zhao et al. 2016; Cao et al. 2021), it is within the realm of accuracy enough to sufficiently support a study regarding local and regional ET.

### *3.4.2 Drought Events and ET*

In both the LARB and individual neighborhoods, the effects of minority-pixel urban vegetation are visible. Across both Woodland Hills and Long Beach, the time-varying vegetation model showed that periods with increased urban vegetation experienced higher ET than periods with decreased urban vegetation, a result that supports studies associating increased urban landscaping with higher ET during drought periods in dry climates (Litvak and Pataki 2016; Nouri et al. 2016). The static vegetation models did not show this effect. Rather, ET in all months looked nearly identical to the time-varying model's ET during periods of increased imperviousness (Figure 3.5). While ET from the static model was highest in wetter years, showing a small precipitation signal, ET from the time-varying model was highest in years with increasing urban vegetation, demonstrating that irrigation is the dominant force in driving ET, even during winter months (Figure 3.6). These relationships suggest that the static model, based on NLCD land cover, is failing to capture increases in minority-pixel irrigated vegetation within largely impervious areas. Those increases to irrigated vegetation, visible in the time-varying model, are driving the drought-period increase in ET.

The differences between the two homogeneous neighborhood-scale analyses support the idea that urban irrigation is the dominant factor in ET and associated water loss. In Woodland Hills, where vegetation is abundant enough to become a majority pixel feature and large areas are parks and golf courses, both the static and time-varying models showed higher ET values than in Long Beach, where large impervious surfaces (e.g. the Long Beach Airport, supply chain facilities, oil refineries) dominate the landscape and a coastal marine layer reduces summertime heat (Edinger 1959; Bartholomew 2014; Sabau et al. 2020; LA Parks 2021; Morguita 2022). However, the differences between increased-vegetation and increased-impervious ET were

highest in Long Beach, where new sources of irrigation stood out in a more impervious area. These results accord with studies showing that residential water use is unequally distributed across Los Angeles, with abundant landscaping irrigation in wealthy areas (Mini et al. 2014; Litvak and Pataki 2016).

In looking toward water savings, the LARB results show that minority-pixel green spaces should not be discounted. While the effects of irrigation on ET were most visible in Long Beach, they were also visible in Woodland Hills. Long Beach is in the 35<sup>th</sup> percentile for NDVI among urban Los Angeles neighborhoods: it is impervious, but not without vegetation. The larger differences between increased-vegetation and increased-impervious ET in Long Beach than in Woodland Hills shows that small changes, applied in targeted or vulnerable neighborhoods, can produce more noticeable differences than small changes applied equally across an urban area or in neighborhoods where the changes will further increase majority land use.

### *3.4.3 Limitations and Areas of Opportunity*

We acknowledge several limitations of the study. Most notably, we do not account for reservoir storage and release within the LARB, a real shortcoming in such a heavily managed basin. With access to sufficient reservoir storage data from the LA Department of Public Works, future work could incorporate parts of DHSVM-res to evaluate the impacts of reservoirs in the LARB (Zhao et al. 2016).

Our model also includes some error propagation from the time-varying land cover data. The land cover classification process achieved a 91% overall accuracy, but error varies among years and land use classes (Engel et al. in review). All input vegetation maps necessitate some error, and we find that the time-varying land cover data is a better approximation of ground truth conditions than a single static image.

Our results were modest due in part to small land cover changes across the LARB (Appendix B). Future studies might also examine areas with more radical land cover changes to deepen our findings and understand more granular interactions between land use and hydrologic processes.

### **3.5 Conclusions**

Changing land use in Los Angeles does impact the overall water balance of the LARB. However, our results were most visible at a neighborhood scale, and land use changes primarily affected impervious areas. Across the LARB, increased urban green spaces modestly reduced surface runoff in >90% of modeled days, with larger reductions during precipitation events. Currently, LA City and County planners are striving to increase low-impact development and allocate resources toward spreading grounds and other infiltration mechanisms (Read et al. 2019; LA County 2021). In this context, our results are promising: flood mitigation and aquifer recharge are visible even through disparate, small-scale land use changes. Even small investments in flood control could be effective at a neighborhood scale. In particular, impervious areas, which are almost exclusively low-income, could see flood control and infiltration benefits from increased urban green space (Ladochy et al. 2021).

Throughout the LARB, urban landscaping increased irrigation-related ET, leading to more water loss during summer months and periods of drought. Coupled with data showing that >50% of residential water use is landscaping-related, these results confirm that irrigated, non-native plants lead to water loss across a large urban area (Mini et al. 2014). In areas like Long Beach, where new green spaces amid a mostly impervious neighborhood stood out, a combination of green and grey stormwater management techniques could reduce runoff without increasing ET. In neighborhoods like Woodland Hills, with existing vegetation, more systemic

approaches to turf-replacement or water reduction could prove beneficial. Across the LARB, a combination of techniques for managing local hydrology within individual neighborhoods could combine to form a regional strategy.

## References

- Abatzoglou, J. T. (2013). Development of gridded surface meteorological data for ecological applications and modelling—Abatzoglou—2013—International Journal of Climatology—Wiley Online Library. *International Journal of Climatology*, 33(1), 121–131. <https://doi.org/10.1002>
- Addison, B. (2017, September 13). A History of Housing Practices in Long Beach. KCET. <https://www.kcet.org/shows/city-rising/a-history-of-housing-practices-in-long-beach>
- ALFRED. (2022). Archival FRED | ALFRED | St. Louis Fed. <https://alfred.stlouisfed.org/>
- Bartholomew, D. (2014, August 2). Woodland Hills Country Club beats par for water conservation. *Los Angeles Daily News*. <https://www.dailynews.com/environment-and-nature/20140802/woodland-hills-country-club-beats-par-for-water-conservation>
- Bohn, T., Livneh, B., Oyler, J., Running, S., Nijssen, B., & Lettenmaier, D. (2013). Global evaluation of MTCLIM and related algorithms for forcing of ecological and hydrological models. *Agricultural and Forest Meteorology*, 176, 38–49. <http://dx.doi.org/10.1016/j.agrformet.2013.03.003>
- CA DWR via Pacific Institute. (2022). California Urban Water Use Data. <https://pacinst.org/gpcd/table/#>
- Cao, Q., Mehran, A., Ralph, F. M., & Lettenmaier, D. P. (2019). The Role of Hydrological Initial Conditions on Atmospheric River Floods in the Russian River Basin in: *Journal of Hydrometeorology* Volume 20 Issue 8 (2019). *Journal of Hydrometeorology*, 20(8), 1667–1686.
- Cao, Q., Shukla, S., DeFlorio, M. J., Ralph, F. M., & Lettenmaier, D. P. (2021). Evaluation of the Subseasonal Forecast Skill of Floods Associated with Atmospheric Rivers in Coastal Western U.S. Watersheds. *Journal of Hydrometeorology*, 22(6), 1535–1552. <https://doi.org/10.1175/JHM-D-20-0219.1>
- City of LA. (2012). Los Angeles River. Council for Watershed Health. <https://www.lacitysan.org/cs/groups/public/documents/document/y250/mda4/~edisp/cnt008746.pdf>
- Cummings, C. (2016). Analysis and implication of impervious surface change due to urbanization in the Los Angeles River Watershed. <https://doi.org/10.13140/RG.2.2.34591.76966>
- Edinger, J. G. (1959). Changes in the depth of the marine layer over the Los Angeles Basin. *Journal of Meteorology*, 16(3), 219–226.

- Effland, W. R., & Pouyat, R. V. (1997). The genesis, classification, and mapping of soils in urban areas. *Urban Ecosystems*, 1(4), 217–228. <https://doi.org/10.1023/A:1018535813797>
- EROS. (2017). National Agriculture Imagery Program (NAIP) [Tiff]. U.S. Geological Survey. <https://doi.org/10.5066/F7QN651G>
- Fry, J. A., Xian, G., Jin, S. M., Dewitz, J. A., Homer, C. G., Yang, L. M., Barnes, C. A., Herold, N. D., & Wickham, J. D. (2011). Completion of the 2006 National Land Cover Database for the conterminous United States. *PE&RS, Photogrammetric Engineering & Remote Sensing*, 77(9), 858–864.
- Garcetti, E. (2019). LA's Green New Deal (p. 152). LA City. [https://plan.lamayor.org/sites/default/files/pLAn\\_2019\\_final.pdf](https://plan.lamayor.org/sites/default/files/pLAn_2019_final.pdf)
- Gillespie, T. W., Pincetl, S., Brossard, S., Smith, J., Saatchi, S., Pataki, D., & Saphores, J.-D. (2012). A time series of urban forestry in Los Angeles. *Urban Ecosystems*, 15(1), 233–246. <https://doi.org/10.1007/s11252-011-0183-6>
- Gupta, H. V., Kling, H., Yilmaz, K. K., & Martinez, G. F. (2009). Decomposition of the mean squared error and NSE performance criteria: Implications for improving hydrological modelling. *Journal of Hydrology*, 377(1), 80–91. <https://doi.org/10.1016/j.jhydrol.2009.08.003>
- IOM (Ed.). (2015). *Migrants and cities: New partnerships to manage mobility*. International Organization for Migration (IOM).
- Johnson, T., Reichard, E., Land, M., & Crawford, F. (2001, April). *Monitoring, Modeling, and Managing Saltwater Intrusion, Central and West Coast Groundwater Basins, Los Angeles County, California*. First International Conference on Saltwater Intrusion and Coastal Aquifers— Monitoring, Modeling, and Management, Essaouira, Morocco. <https://olemiss.edu/sciencenet/saltnet//swica1/johnson-richard-land-exabs.pdf>
- Kesseli, J. E. (1942). The Climates of California According to the Köppen Classification. *Geographical Review*, 32(3), 476–480. <https://doi.org/10.2307/210390>
- Knoben, W. J. M., Freer, J. E., & Woods, R. A. (2019). Technical note: Inherent benchmark or not? Comparing Nash-Sutcliffe and Kling-Gupta efficiency scores [Preprint]. *Catchment hydrology/Modelling approaches*. <https://doi.org/10.5194/hess-2019-327>
- LA County. (2021). Dominguez Gap Wetlands. <https://dpw.lacounty.gov/swp/dominguezgapwetlands/#about>
- LA Parks. (2021, October 13). Parks. City of Los Angeles Department of Recreation and Parks. <https://www.laparks.org/parks>

- Ladochy, S., Torres, T., & Hsu, Y. (2021). LOS ANGELES' URBAN HEAT ISLAND CONTINUES TO GROW: URBANIZATION, LAND USE CHANGE INFLUENCES. *Journal of Urban and Environmental Engineering*, 15, 103–116. <https://doi.org/10.4090/juee.2021.v15n2.103116>
- LB Water. (2022). Ground And Imported Water. Long Beach Water Department. <https://lbwater.org/water-sources/ground-and-imported-water/>
- Litvak, E., Manago, K., Hogue, T., & Pataki, D. (2017). Evapotranspiration of urban landscapes in Los Angeles, California at the municipal scale—Litvak—2017—Water Resources Research—Wiley Online Library. *Water Resources Research*, 53(5), 4236–4253.
- Litvak, E., & Pataki, D. E. (2016). Evapotranspiration of urban lawns in a semi-arid environment: An in situ evaluation of microclimatic conditions and watering recommendations. *Journal of Arid Environments*, 134, 87–96. <https://doi.org/10.1016/j.jaridenv.2016.06.016>
- Liu, D. (2020). A rational performance criterion for hydrological model. *Journal of Hydrology*, 590, 125488. <https://doi.org/10.1016/j.jhydrol.2020.125488>
- McPherson, E. G., Simpson, J. R., Xiao, Q., & Wu, C. (2011). Million trees Los Angeles canopy cover and benefit assessment. *Landscape and Urban Planning*, 99(1), 40–50. <https://doi.org/10.1016/j.landurbplan.2010.08.011>
- Mini, C., Hogue, T. S., & Pincetl, S. (2014). Estimation of residential outdoor water use in Los Angeles, California. *Landscape and Urban Planning*, 127, 124–135. <https://doi.org/10.1016/j.landurbplan.2014.04.007>
- Moraisi, D., Gitau, M., Pai, N., & Daggupati, P. (2015). Hydrologic and Water Quality Models: Performance Measures and Evaluation Criteria. *Transactions of the ASABE*, 58(6), 1763–1785.
- Morgutia, J. (2022). Beautiful Lawn to Garden. Beautiful Long Beach Lawn to Garden. <https://lblawntogarden.com/>
- Nouri, H., Glenn, E. P., Beecham, S., Chavoshi Boroujeni, S., Sutton, P., Alaghmand, S., Noori, B., & Nagler, P. (2016). Comparing Three Approaches of Evapotranspiration Estimation in Mixed Urban Vegetation: Field-Based, Remote Sensing-Based and Observational-Based Methods. *Remote Sensing*, 8(6), 492. <https://doi.org/10.3390/rs8060492>
- Nowak, D., & Greenfield, E. (2012). Tree and impervious cover change in U.S. cities. *Urban Forestry & Urban Greening*, 11, 21–30. <https://doi.org/10.1016/J.UFUG.2011.11.005>
- OurCounty. (2019). The Plan. OurCounty. <https://ourcountyla.lacounty.gov/plan>



- Perkins, W. A., Duan, Z., Sun, N., Wigmosta, M. S., Richmond, M. C., Chen, X., & Leung, L. R. (2019). Parallel Distributed Hydrology Soil Vegetation Model (DHSVM) using global arrays. *Environmental Modelling & Software*, 122, 104533. <https://doi.org/10.1016/j.envsoft.2019.104533>
- Pincetl, S., Gillespie, T., Pataki, D., Saatchi, S., & Saphores, J. (2013). Urban tree planting programs, function or fashion? Los Angeles and urban tree planting campaigns. <https://doi.org/10.1007/S10708-012-9446-X>
- Porse, E., Mika, K. B., Litvak, E., Manago, K. F., Naik, K., Glickfeld, M., Hogue, T. S., Gold, M., Pataki, D. E., & Pincetl, S. (2017). Systems Analysis and Optimization of Local Water Supplies in Los Angeles. *Journal of Water Resources Planning and Management*, 143(9), 04017049. [https://doi.org/10.1061/\(ASCE\)WR.1943-5452.0000803](https://doi.org/10.1061/(ASCE)WR.1943-5452.0000803)
- Public Works, LA County. (2018). LA County Soil Types. <https://data.lacounty.gov/Shape-Files/LA-County-Soil-Types/sz94-meiu>
- Public Works, LA County. (2021b). Dominguez Gap Spreading Grounds. <http://www.ladpw.org/wrd/spreadingground/information/facdept.cfm?facinit=15>
- Public Works, LA County. (2021a). LOS ANGELES RIVER below Wardlow River Road. <https://dpw.lacounty.gov/wrd/runoff/GeneralInfo.cfm?facinit=F319-R>
- Read, L. K., Hogue, T. S., Edgley, R., Mika, K., & Gold, M. (2019). Evaluating the Impacts of Stormwater Management on Streamflow Regimes in the Los Angeles River. *Journal of Water Resources Planning and Management*, 145(10), 05019016. [https://doi.org/10.1061/\(ASCE\)WR.1943-5452.0001092](https://doi.org/10.1061/(ASCE)WR.1943-5452.0001092)
- Sabau, D. (2020, August 11). A Short History of Los Angeles Real Estate Development. *CommercialCafe*. <https://www.commercialcafe.com/blog/history-los-angeles-real-estate-development/>
- Schifman, L. A., & Shuster, W. D. (2019). Comparison of Measured and Simulated Urban Soil Hydrologic Properties. *Journal of Hydrologic Engineering*, 24(1), 04018056. [https://doi.org/10.1061/\(ASCE\)HE.1943-5584.0001684](https://doi.org/10.1061/(ASCE)HE.1943-5584.0001684)
- Soil Survey Staff. (2018). Web Soil Survey. Natural Resources Conservation Service, United States Department of Agriculture. <https://websoilsurvey.nrcs.usda.gov/>.
- Thanapakpawin, P., Richey, J., Thomas, D., Rodda, S., Campbell, B., & Logsdon, M. (2007). Effects of landuse change on the hydrologic regime of the Mae Chaem river basin, NW Thailand. *Journal of Hydrology*, 334(1), 215–230. <https://doi.org/10.1016/j.jhydrol.2006.10.012>
- US Census Bureau. (2019). Los Angeles County, California; California. US Census Quick Facts. <https://www.census.gov/quickfacts/fact/table/losangelescountycalifornia,CA/PST045219>

- US Census Bureau. (2022). U.S. Census Bureau QuickFacts: Long Beach city, California. <https://www.census.gov/quickfacts/longbeachcitycalifornia>
- U.S. Geological Survey. (2020). 1/3rd arc-second Digital Elevation Models (DEMs). <https://data.usgs.gov/datacatalog/data/USGS:3a81321b-c153-416f-98b7-cc8e5f0e17c3>
- Usery, E. L., Finn, M. P., Scheidt, D. J., Ruhl, S., Beard, T., & Bearden, M. (2004). Geospatial data resampling and resolution effects on watershed modeling: A case study using the agricultural non-point source pollution model. *Journal of Geographical Systems*, 6(3), 289–306. <https://doi.org/10.1007/s10109-004-0138-z>
- USGS. (2021). National Water Dashboard. <https://dashboard.waterdata.usgs.gov>
- Welch, R. (1982). Spatial resolution requirements for urban studies. *International Journal of Remote Sensing*, 3(2), 139–146. <https://doi.org/10.1080/01431168208948387>
- Western Regional Climate Center. (2022). WOODLAND HILLS PIERCE COLLEGE, CALIFORNIA - Climate Summary. <https://wrcc.dri.edu/cgi-bin/cliMAIN.pl?ca1484>
- Wigmosta, M. S., Vail, L. W., & Lettenmaier, D. P. (1994). A distributed hydrology-vegetation model for complex terrain. *Water Resources Research*, 30(6), 1665–1679. <https://doi.org/10.1029/94WR00436>
- Zhao, G., Gao, H., Naz, B. S., Kao, S.-C., & Voisin, N. (2016). Integrating a reservoir regulation scheme into a spatially distributed hydrological model. *Advances in Water Resources*, 98, 16–31. <https://doi.org/10.1016/j.advwatres.2016.10.014>

## **Chapter 4. Contributions of roads to surface temperature: evidence from Southern California**

This chapter was submitted in its current form to *Landscape and Urban Planning* as Engel, R.A., Millard-Ball, A., and V.K. Turner (2022). Contributions of roads to surface temperature: evidence from Southern California. *Landscape and Urban Planning (in review)*. The supplementary materials for this chapter are provided in Appendix C.

### **Abstract**

Planners often regard streets as targets for mitigating urban heat across cities by virtue of being abundant, publicly-owned, low-albedo, low-vegetation surfaces. Few studies, however, have assessed the role streets play in contributing to urban heat, and the scale of their effect relative to the built environment around them. We examine the relationship between road area and land surface temperature across a variety of biophysical regions through the urban areas of Los Angeles and San Bernardino Counties in Southern California. Our results show that wide streets have little effect on urban heat. Rather, vegetation is the primary cooling mechanism for urban areas. In the absence of trees, concrete highways are the coolest surfaces, though particular hot or cool pockets (e.g. airports, industrial centers, parks) can dominate neighborhood temperature signatures. In considering LST mitigation strategies, these hotspots might outweigh the cumulative effects of road surface changes.

### **4.1 Introduction**

Cities are hot in part because of impervious surfaces like buildings, roads, and parking lots. In most regions, urbanization replaces vegetated land with impervious surfaces, which decreases two key cooling factors: albedo and evapotranspiration. Urban heat planning, therefore, focuses on ways to increase albedo and vegetation to mitigate the effects of

impervious surfaces on urban land. Heat produced by urban land cover is typically characterized as the surface urban heat island (SUHI), a regional phenomenon that causes cities to be, on average 1.5° C warmer than surrounding undeveloped areas and is most pronounced at night (Oke 1982, Peng et al. 2012).

The SUHI as conventionally characterized has several limitations for urban planning. One shortcoming is that the direction of the relationship between urban land and surface temperature depends on background land and climate conditions. Arid regions may experience an inverse heat island whereby irrigated vegetation cools land compared to reference undeveloped dryland and the most pronounced temperature differences overnight (Mohammed et al. 2020). Moreover, the relationship between urban land and temperature is heterogeneous within cities. This is problematic because cities must consider the unique morphology and uses of urban land at a sub-city scale when assessing potential heat mitigation strategies.

One potential source of heat in urbanized regions is streets – large-scale, mostly low-albedo impervious surfaces that lack vegetation and shade (Taleghani et al. 2016). The contribution of streets to urban heat is amplified by the large amount of land that they occupy – up to 30% in US cities such as New York (Manvel, 1968, summarized in Meyer & Gomez-Ibañez, 1981; Millard-Ball 2022). At the same time, however, streets offer prime opportunities to mitigate urban heat – they are publicly owned resources upon which cities can site interventions without the need to incentivize private developers or land holders (Pomerantz et al. 2003; Lee et al. 2018; Gago et al. 2013). For this reason, several cities have begun experimenting with cool pavement and urban tree planting programs to leverage streets as a public resource for mitigating the urban heat (Ko et al. 2022; Turner et al. 2021; Maxwell et al. 2018).

This study examines the relationship between street width and Land Surface Temperature (LST) across a variety of urban forms to examine how and where mitigation strategies might be best applied. We focus on communities in Los Angeles and San Bernardino Counties, California, which contain a mix of background biophysical conditions and built forms, and where policymakers have piloted the use of road surfaces to reduce urban heat through changes to vegetation or albedo (US EPA 2012; Garcetti 2021). These proposals follow a global trend of investment in cool pavement: Western Europe is pushing cool pavements, and pilot programs can be found in Tokyo, Athens, and Rome (Santamouris 2013; C40 2017; Moretti et al. 2021). The United States government is also incentivizing cool pavement programs and several cities have followed suit (Wiltshire-Gordon 2020; FHA 2021; Garcetti 2021; SmartCities Connect 2021). We test the hypotheses that roads contribute to urban heat and that wider roads amplify those contributions. We further hypothesize that the impact of streets will vary based on the local physical context; hotter, more arid conditions will suppress the contribution of road widths to urban heat as will more intensively developed areas.

#### **4.2 Mitigating Urban Heat on Roads: Vegetation, Impervious Surfaces, and Land Morphology**

As conventionally described, a vegetation disparity across the urban environment creates a SUHI by producing hotter conditions in urban areas, especially developed downtown sectors, than surrounding undeveloped areas. The temperature disparity is largely driven by impervious surfaces like roads and buildings that absorb and slowly release heat throughout the day (Oke 1982; Rizwan et al. 2008) and, depending on regional conditions, usually peaks during the early afternoon due to dependence on shortwave radiation (Shastri et al. 2017; Lai et al. 2018). In hot desert climates, however, the typical urban heat pattern can be inverted: urbanized areas are often

cooler than the background reference desert during the daytime, but warm up at night (Lazzarini et al. 2015). Desert cities have substantially less dense vegetation and higher LST than temperate or forested cities, and a shallower diurnal heat cycle (Imhoff et al. 2010). The inverse urban heat island is largely attributable to differences in vegetation and canopy cover: bare soil or sand in undeveloped desert areas is warmer than shaded or irrigated landscape in city centers (Shastri et al. 2017; Mohamed et al. 2021). These studies demonstrate that the direction and characteristics of the SUHI depend on the background land and climate conditions of the reference system.

Vegetation is also a primary mechanism for cooling spaces within cities: impervious surfaces and bare land are significantly warmer than vegetated areas, particularly in hot areas (He et al. 2018). Shaded surfaces, and the air above those surfaces, are cooler than nearby unshaded impervious surfaces (Taleghani et al. 2016). Tree cover, in particular, is effective in reducing surface temperature, but the mere presence of vegetation is sufficient to reduce localized surface and air temperature in comparison to a paved surface (Adams and Smith 2014; Susca 2011). In addition to shade, vegetation provides heat reduction through transpiration: as water is released into the atmosphere, sensible heat is converted to latent heat, reducing overall air temperature (Ballinas and Barradas 2016). This effect is heightened in arid climates with a high vapor pressure deficit that increases transpiration.

Urban heat varies with race and income as well as physical characteristics, in ways that exacerbate environmental injustices. For example, historically redlined neighborhoods show elevated surface temperatures of  $\sim 2.6^{\circ}\text{C}$  across the U.S. (Hoffman et al. 2019; Wilson 2020). This trend holds for predominantly Black or Latino neighborhoods, primarily due to a lack of vegetation (Harlan et al. 2006; Dialesandro 2021).

Many cities have considered street trees as a strategy to mitigate urban heat given their large impacts on LST and their other benefits such as visual amenity and improved air quality (Mullaney et al. 2015). Though tree planting is shown to be effective in reducing LST, many urban trees in Southern California are non-native and require constant irrigation, increasing water imports (Roman et al. 2021). Indeed, angiosperm (broad-leaf) species comprise only 71% of trees in Los Angeles but contribute over 90% of tree transpiration (Litvak et al. 2017). Landscaping comprises ~54% of residential water use in Southern California, and irrigation is both more prevalent and less responsive to mandatory drought-related water rationing in wealthy neighborhoods, which are shadier and cooler than low-income areas (Mini et al. 2014; Clarke et al. 2013). Because trees – particularly leafy, traditionally “shady” trees – come with a cost, planners seek out alternate strategies for reducing LST.

Given these challenges, planners have also turned to road surface paint as a low-cost, easily-implemented method for mitigating LST. Roads, which are often constructed from dark asphalt, are logical targets for intervention: as continuous, often wide, impervious areas, they logically increase LST and radiant air temperature (Cheena et al. 2021; Pomerantz et al. 2003). Studies have tested potential reductions in LST from cool pavements, and found that higher-albedo surfaces are indeed cooler (Sodoudi et al. 2014; Sen et al. 2019). Citywide effects of cool pavement are mixed, however: as with any urban heat strategy that relies on increasing albedo, radiant temperature and midday temperature can increase even as incoming solar radiation decreases (Middell et al. 2020; Erell et al. 2013).

Cool pavements are often introduced inadvertently without regard to their albedo-increasing properties. For example, in Southern California, many of the widest roads are already concrete, which is classified as a cool pavement – studies have found that concrete with a higher

cement content increases albedo regardless of the remaining composition (Lee et al. 2002; Levinson and Akbari 2002; Sen et al. 2019). This practice is likely to continue: concrete sets rapidly and can include recycled tires at little extra cost, so it remains the primary surface used in newly-repaired freeways (Caltrans 2002; CalRecycle 2020). Concrete is less prone to cracking than painted asphalt, and its construction can incorporate reflective materials to increase albedo (Cheena et al. 2021).

While much has been made of the potential benefits and pitfalls of increasing cool pavement presence throughout cities, little research has evaluated the current effects of street abundance and width on LST. Microscale studies have compared road surfaces to one another, finding evidence of LST reduction with reflective pavements and shaded surfaces (Lee et al. 2018; Sadoudi et al. 2014). Others have evaluated the effects of building morphology, demonstrating that canyons and airflow can improve cooling at block and citywide scales (Giridharan et al. 2007; Johannson 2006). Hoehne et al. (2020) found increased sensible heat from combined car emissions and road surfaces across Phoenix. However, their LST readings seemed to correlate with imperviousness or bare ground, as opposed to irrigation. Yamazaki et al. (2009) used very high-resolution imagery (2 m) to examine LST, and found higher temperatures on impervious and road surfaces than in vegetated areas or water. However, they did not evaluate the effects of roads across a neighborhood or city scale, or in areas that are either highly vegetated or impervious.

There is substantial literature examining possible LST mitigation strategies across particular cities or neighborhoods (Mohammed et al. 2020; Deilami et al. 2018). However, few studies examine the relative impacts of vegetation or cool pavement strategies in distinct neighborhoods, rather than as a citywide panacea. Urban morphology can change at a



neighborhood, or even a block scale within a city, affecting localized and citywide temperatures (Yuan et al. 2020). Sodoudi et al. (2014) examined a hybrid cool pavement and vegetation cooling model in Tehran, and found it to be more effective than either strategy in isolation. Middel et al. (2020) found that cool pavement was not appropriate as a one-size-fits-all model, and should be applied with consideration of local context. To our knowledge, no studies have considered which areas might benefit from varying forms of LST mitigation.

In the Los Angeles area, the potential for neighborhood-scale heterogeneity is high: the urban environment is very different from native vegetation, which is primarily coastal or chaparral scrubland, with mountainous or desert regions in the more inland areas (Rashed et al. 2003). As a result, developed areas, irrigated landscaping, and indigenous vegetation have distinct diurnal and annual NDVI, heat, and evapotranspiration cycles (Mini et al. 2014; Hall et al. 2015). Notably, Los Angeles has a summertime marine layer, providing an overall cooling effect in many coastal areas (Edinger 1959).

These diverse physical conditions combine with some of the most diverse built urban landscape in the country: Los Angeles County alone is home to over 10 million people in 114 distinct neighborhoods, with a substantial range of income disparity and a legacy of environmental injustice (Rashed et al. 2003; Mini et al. 2014; Su et al. 2018). Los Angeles also enforces a highway dedication ordinance requiring developers to physically widen streets to accommodate more traffic in exchange for building permits (Manville 2017). At the same time, the city considers streets to be a primary avenue for mitigating LST; in 2021 the Mayor's office announced an initiative to bring 200 blocks of cool pavement and 2,000 new trees to eight residential areas (Garcetti 2021).

## 4.3 Data and Methods

### 4.3.1 Study Area and Sample Selection

We examined the urbanized portion of Los Angeles and southwest San Bernardino Counties, California. We choose these counties because of their size, variety of climatic conditions and urban forms, and growing urban heat island (Dialesandro et al. 2019; Ladochy et al. 2021). Together, the counties are home to ~12 million people and contain over 100 incorporated cities (US Census 2020). Our study area spans an east-west transect of California, covers elevation from sea level to >1000 m, and encompasses mediterranean and desert Koppen climate zones (Kesseli 1942). The built form encompasses single-family homes, apartments, high-rise residential and office buildings, and industrial uses, and streets that range from large arterials to narrower streets built before the private car became dominant. The primary urban area in our study region is the City of Los Angeles, which is classified as a global megacity and contains a dense urban core, sprawling residential areas, and low-rise industrial zones.

In Southern California, we examine areas with both traditional and inverted SUHI. In coastal Los Angeles, heavily impervious urban areas (e.g. South and East LA) are warmer than the more vegetated mountainous or coastal neighborhoods (Hulley et al. 2019; Dousset 1989). However, the eastern part of the state shows a reverse urban heat effect consistent with other hot desert cities (Shifflett et al. 2017).

### 4.3.2 Data Sources and Calculations

We calculated LST at 30 m resolution using Landsat 8, parameterized with water vapor and emissivity from NCEP/NCAR reanalysis and ASTER imagery (Ermida 2020). To check our calculations, we validated our LST data using an alternative algorithm (Landsat Provisional LST) and data source (NASA ECOSTRESS LST readings). All three approaches are widely used

in the literature, and we found agreement among the datasets. Thus, the remainder of the analysis uses the Landsat 8 imagery, so as to use a standard Landsat base for all variables and because of the ease of calculation in Google Earth Engine. Because we observed thermal LST, we were in effect observing the radiant temperature of tree canopy, shrubs, and grass in vegetated areas, rather than the temperature of the shaded pavement. Studies show, however, that shaded surfaces are significantly cooler than those in direct sunlight (Barbierato et al. 2019, Middel et al. 2020).

Our data on street area, width, and class (highway, arterial, and residential street) use a novel method derived by Millard-Ball (2022), which derives street area and width from the voids between tax assessment parcels, and matches each void to OpenStreetMap (OSM) ways.

We integrated additional data sources on urban form, vegetation, and demographics in order to incorporate other factors that prior studies show to have a strong influence on LST. We used building footprint polygons (Microsoft 2021) to calculate the largest building footprint within each 30 m pixel.

We also examined Local Climate Zones (LCZ), a product created to show categories of land use, vegetation, and development for urban temperature studies (Stewart and Oke 2012). To explore questions of environmental justice, we classified pixels as a Disadvantaged Community or not according to the California EPA's designation, which considers pollution burden, health outcomes, and vulnerability (CalEPA 2015).

To assess vegetation and land use, we examined Soil Adjusted Vegetation Index (SAVI) and Albedo at 30 m using Landsat 8 data in Google Earth Engine (Roy et al. 2014). A higher SAVI value indicates more greenness, with middling values corresponding to low vegetation and high values corresponding to forest. For each pixel's centroid, we calculated latitude, longitude, elevation, and distance from the Pacific Ocean (IHO 1953; Farr et al. 2007).

For more specific information on data sources and calculations, see Appendix C.

#### *4.3.3 Regression*

We use a linear regression model to test the association between LST (our dependent variable) and street area, while controlling for other predictors that may confound the relationship. Our primary control variables are largest building footprint; SAVI; and albedo (each which we standardize to a mean of zero and a standard deviation of one in order to be able to compare the magnitudes of the coefficients). We also include disadvantaged community status (as a binary variable) and Local Climate Zone, as well as elevation and distance from the Pacific Ocean (each of which we discretize into 10 bins in order to allow for nonlinear relationships).

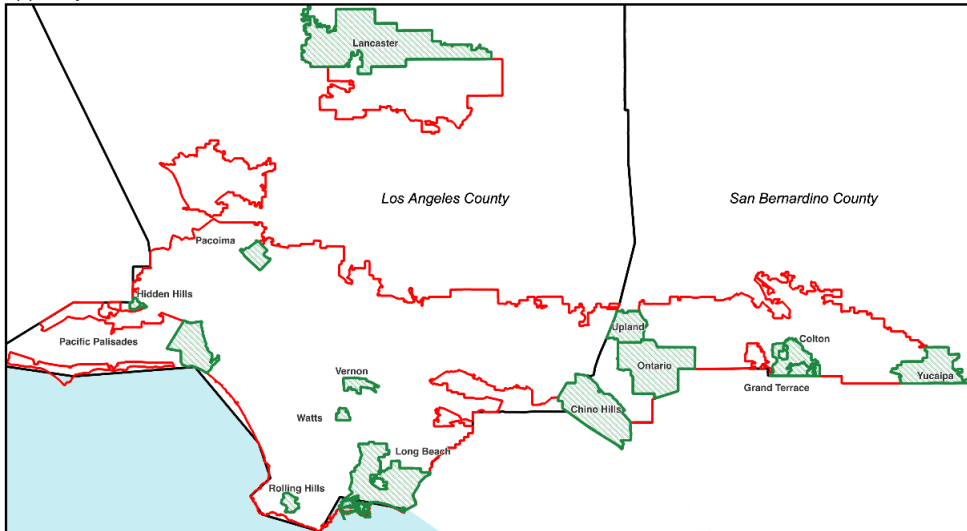
#### *4.3.4 Samples*

Our primary results are based on the urbanized areas of the two counties in our dataset. We complemented these results with a more focused analysis of 14 sample communities (Table 4.1; Figure 4.1) in order to better understand the mechanisms that link street widths with urban heat. To do so, we compiled total street area and median LST, albedo, and SAVI in each neighborhood. We then selected a sample based on an extreme value strategy, choosing the areas with the maximum and minimum values for each variable. There was some overlap: the Pacific Palisades had the lowest median albedo and LST; Vernon had the lowest SAVI and highest LST; Colton had the highest albedo and lowest SAVI; and Grand Terrace had the least street area and lowest LST (Figure 4.2).

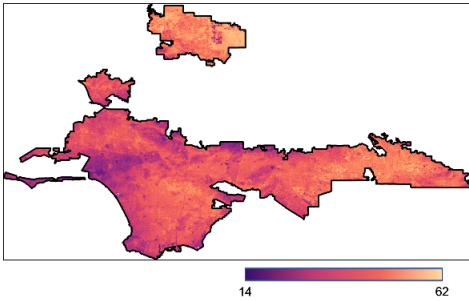
**Table 4.1:** Sample neighborhoods.

<b>Neighborhood</b>	<b>County</b>	<b>Median LST</b>	<b>Median Albedo</b>	<b>Median SAVI</b>	<b>Percent Street Area</b>	<b>Primary LCZ</b>	<b>Median Family Income</b>
Chino Hills	SB	45.28	0.159	0.160	0.52	open lowrise	117,452
Colton	SB	45.56	0.194	0.125	0.60	open lowrise	60,372
Grand Terrace	SB	43.07	0.184	0.163	0.70	open lowrise	75,378
Hidden Hills	LA	33.33	0.183	0.275	0.91	large lowrise	165,336
Lancaster	LA	38.64	0.218	0.160	11.44	bush, scrub	60,799
Long Beach	LA	34.34	0.166	0.146	26.41	large lowrise	64,813
Ontario	SB	47.65	0.189	0.146	0.69	open lowrise	71,374
Pacific Palisades	LA	28.95	0.129	0.288	6.54	bush, scrub	220,362
Pacoima	LA	37.66	0.171	0.119	28.48	large lowrise	64,688
Rolling Hills	LA	29.75	0.158	0.297	4.00	large lowrise	186,818
Upland	SB	44.14	0.180	0.179	0.74	open lowrise	85,235
Vernon	LA	38.82	0.190	0.031	14.98	large lowrise	45,647
Watts	LA	36.16	0.164	0.136	30.03	large lowrise	44,470
Yucaipa	SB	46.90	0.176	0.170	12.30	open lowrise	84,654

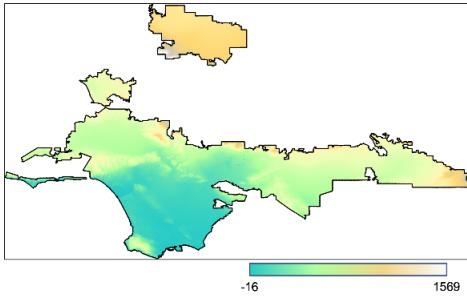
(a) Study Areas



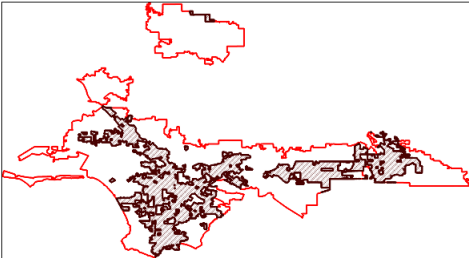
(b) LST (°C)



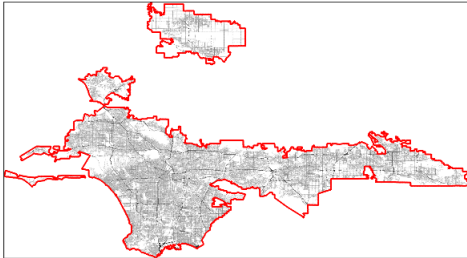
(c) Elevation (m)



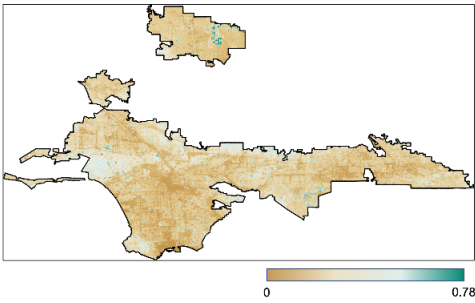
(d) Disadvantaged



(e) Streets



(f) SAVI



(g) LCZ

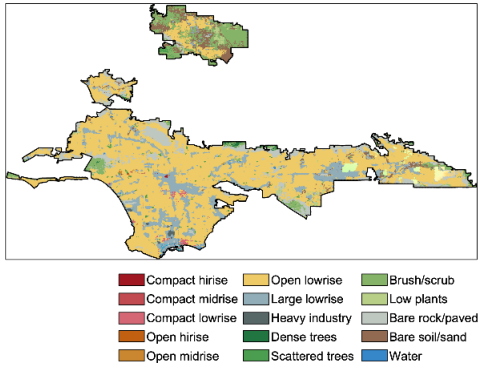


**Figure 4.1:** Spatial distribution of sample neighborhoods (a), LST (b) and selected contributing variables within the study area: Elevation (c), CalEPA Environmentally Disadvantaged Communities (d), Street networks (e), SAVI (f), and LCZs (g). Cooler areas are more mountainous and less developed, and often are coastal. Warmer areas are farther inland, and often are within large lowrise developments. Disadvantaged neighborhoods are, on average, hotter than non-disadvantaged neighborhoods.

We also included in our sample selection the three California Transformative Climate Communities (TCCs) within our study area: Ontario, Watts, and the San Fernando Valley (Transformative Climate Communities 2021). For the purposes of this study, the San Fernando Valley area is called Pacoima, as almost all of the TCC zone is within that neighborhood. The TCCs are part of a California State initiative to reduce the legacy of redlining and environmental racism on underserved communities throughout the state via community-led action plans (Transformative Climate Communities 2021). We include the three TCCs because they represent long-marginalized areas with substantial environmental disadvantages.

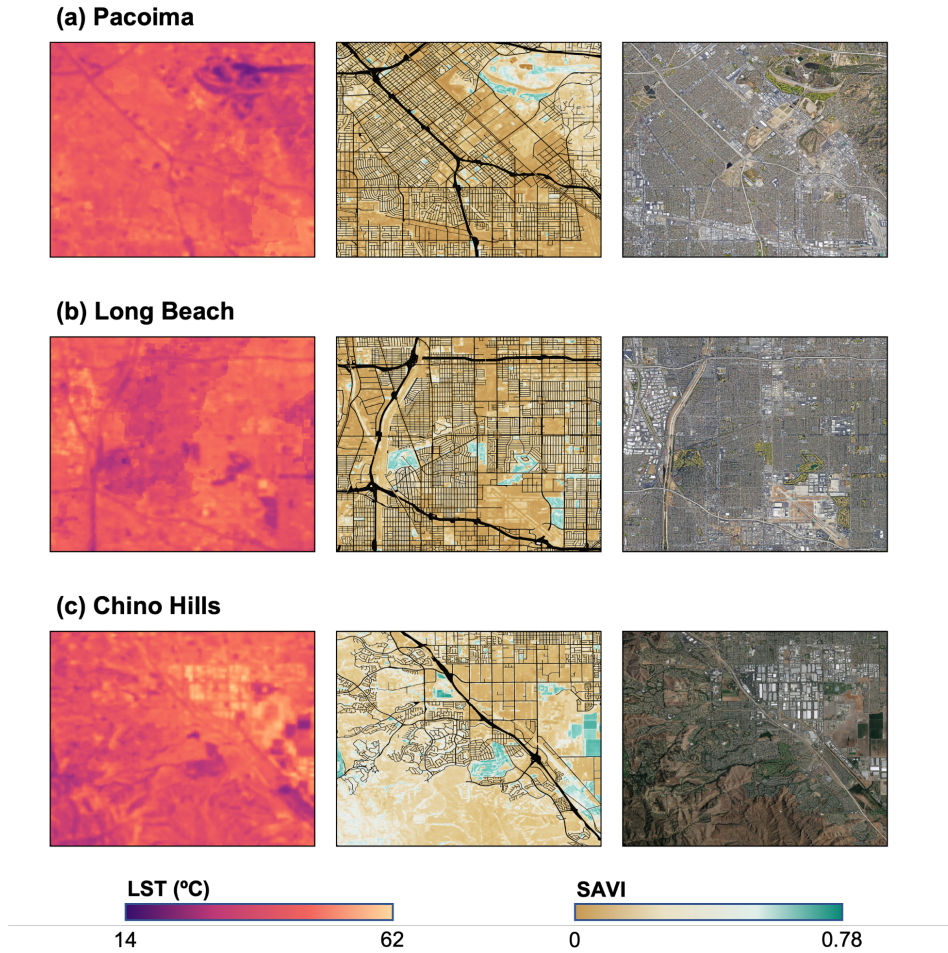


**Figure 4.2:** Temperature; SAVI and streets; and satellite imagery (Google 2021) for three sample neighborhoods. Pacoima is largely impervious and sits inland, in the San Fernando Valley. Highways are the coolest surfaces in the neighborhood. Long Beach is a diverse, coastal area, and generally cooler than other neighborhoods because of the summertime marine layer. Chino Hills is wealthier and more vegetated, though it sits inland, in San Bernardino County. Several large warehouses, technically just outside the neighborhood, show the higher LST commonly visible in heavily industrial areas.

## 4.4 Results

### 4.4.1 Effects of Vegetation

We found that more vegetation, as expressed by higher SAVI, is universally correlated with lower LST. Notably, SAVI was the only tested variable without a sign change across all sample areas – that is, in each case, the regression coefficient is negative (Table 2). Across the study area, SAVI also showed the strongest scaled correlations of any variable. We examined the



signless magnitude of scaled correlations for street area, SAVI, albedo, and large building footprints, and found that SAVI’s mean correlation was 1.8% higher than the correlation of the next largest variable.

**Table 4.2:** Scaled regression coefficients for study area and all samples from model including normalized street area, SAVI, albedo, and building footprint as well as bins for elevation and ocean proximity ( $R^2 = 0.767$ ). Variables are normalized so as to be directly comparable with one another. Coefficients between street area and LST tend to be small, and they do not demonstrate a particular pattern. SAVI is the most noticeable predictor of LST, with cooling effects across all areas.

Scaled Correlations vs Temperature					
Neighborhood	County	Street Area	SAVI	Albedo	Largest Building Footprint
All Urbanized Areas		-0.05	-1.83	0.36	0.18
Ontario	SB	-0.19	-0.86	-0.06	0.44
Yucaipa	SB	-0.60	-2.10	0.07	-0.93
Colton	SB	-0.09	-0.51	-0.13	0.29
Chino Hills	SB	-0.15	-1.03	0.05	0.09
Upland	SB	0.10	-2.23	0.10	0.57
Grand Terrace	SB	-0.06	-1.05	0.19	-0.11
Vernon	LA	-0.12	-0.82	-0.22	0.70
Lancaster	LA	0.13	-0.98	-0.04	0.44
Pacoima	LA	0.34	-0.96	0.67	-2.96
Watts	LA	-0.11	-0.72	0.59	0.06
Long Beach	LA	0.09	-1.18	1.07	-0.23
Hidden Hills	LA	0.37	-1.69	2.01	1.07
Rolling Hills	LA	-0.14	-1.40	0.82	-2.05
Pacific Palisades	LA	0.05	-1.53	1.48	-0.38

In examinations of specific areas, we found that higher SAVI correlated strongly with lower LST, but lower SAVI did not necessarily imply higher LST. Rather, areas with lower SAVI were more diverse, with a wider range of LST (Figure 4.3). In some coastal areas (e.g. Long Beach) the effect of SAVI on LST was less visible, likely because of the 10:30 am

collection time: Los Angeles experiences a summertime morning marine layer in coastal areas that can reduce LST (Edinger 1959).

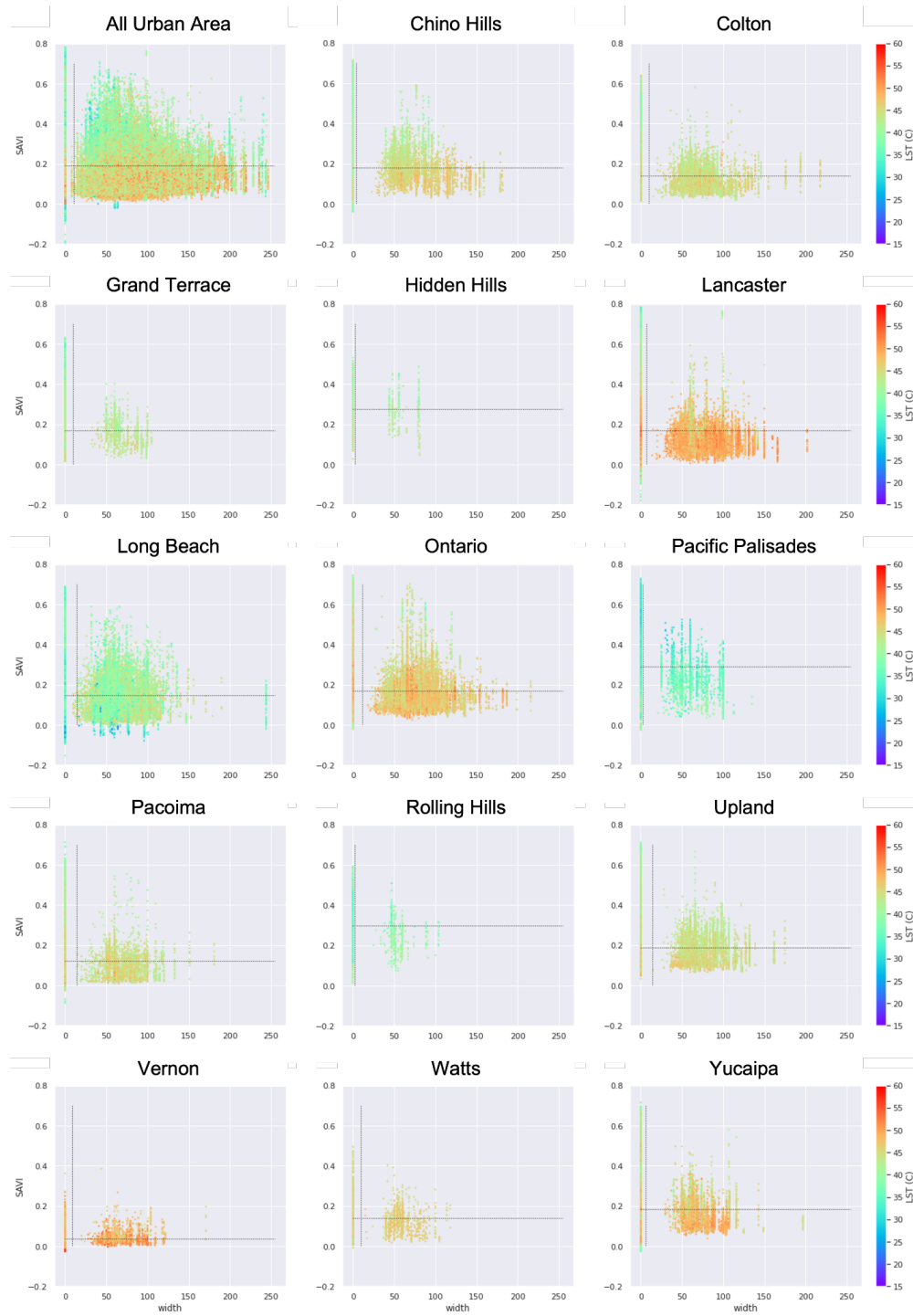


**Figure 4.3:** Most common street width (m) within each pixel and SAVI for each sample neighborhood. Colors represent summertime LST within a given pixel, and dashed lines are

mean values for width and SAVI. Points for “all urban area” plot come from a random selection of pixels to show a clear distribution without overcrowding. In both the study area as a whole and individual neighborhoods, SAVI is the primary moderator for LST: temperatures change along a vegetation gradient, but do not substantially differ in areas with narrow or wide streets. Areas with more vegetation (higher SAVI) are cooler, but areas with less vegetation (lower SAVI) are more diverse; low-SAVI areas are not universally warmer. In coastal neighborhoods (e.g. Hidden Hills, Long Beach, Pacific Palisades, and Rolling Hills) LST is lower across the board, a result of the summertime marine layer.

#### *4.4.2 Effects of roads*

As a whole, roads had no effect on LST in either the full sample or our 14 neighborhoods. The null effect is apparent in both our regression results, where correlations between street area and LST were minimal and demonstrated no overall pattern or trend, and graphically, where the plots in Figures 4.2 and 4.3 show no relationship between street width and LST.

Within residential neighborhoods, vegetation was the dominant signature, and road area was a negligible factor in affecting LST (Table 2). In highly impervious neighborhoods, road surface was often dwarfed by the presence of large buildings, which had a much more substantial impact on LST, with stronger correlations visible in Table 2.

Highways were consistently the coolest road class, with lower LST values than arterials or residential streets. Across the study area, the median LST of highways was  $>1^{\circ}\text{C}$  cooler than other road surfaces (Figure 4.4). In highly impervious areas with low SAVI, this effect is heightened; in Vernon, highways were  $2.5^{\circ}\text{C}$  cooler than other road surfaces. In more highly vegetated areas such as the Pacific Palisades or Chino Hills, the effect is flattened, and most road surfaces have similar LST values.

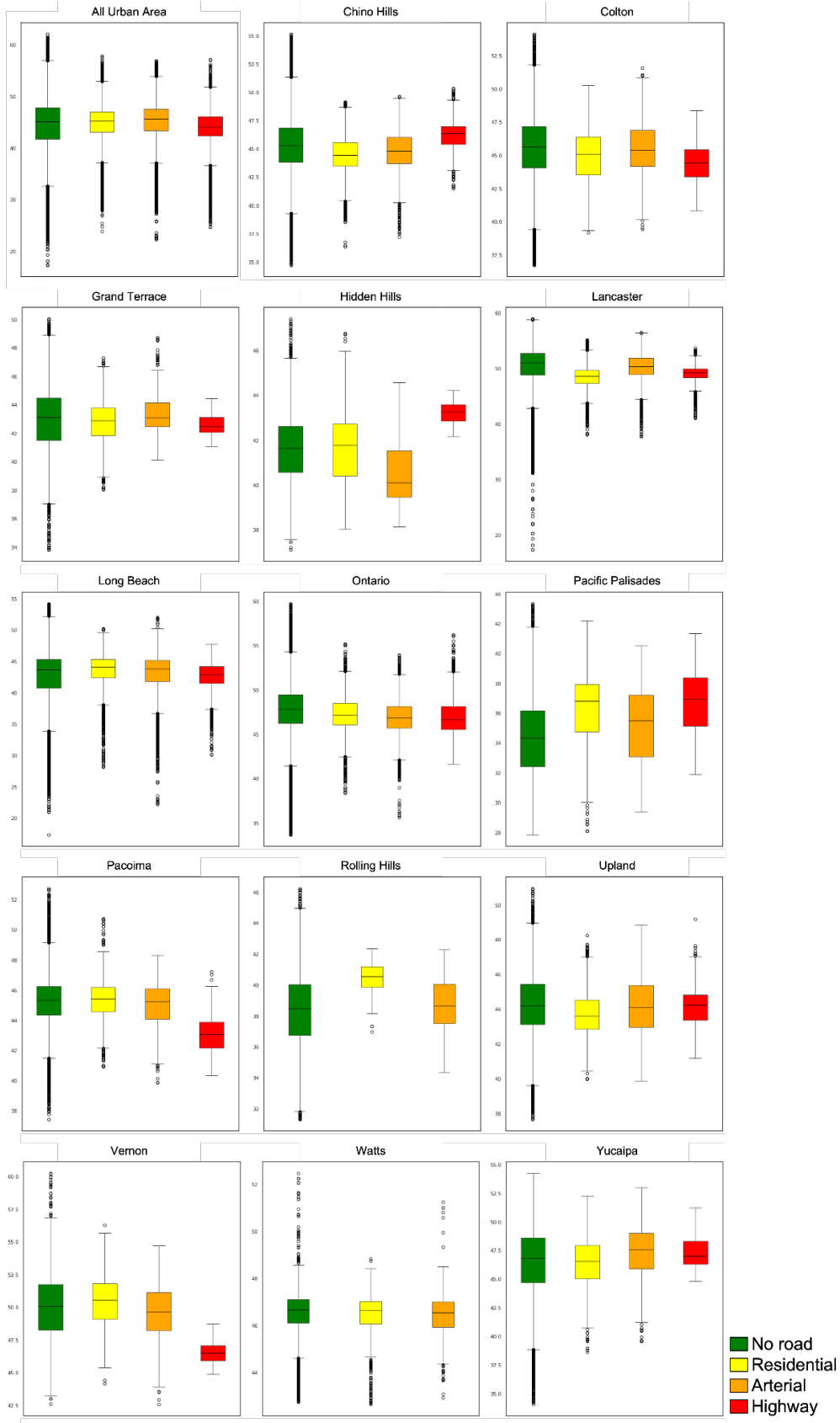


**Figure 4.4:** Distribution of LST (°C) of pixels with no roads (green), residential streets (yellow), arterials (orange), and highways (red) in each sample neighborhood. Rolling Hills and Watts have no highways. In wealthier neighborhoods with substantial vegetation (e.g. Chino Hills, Hidden Hills, Lancaster, and Pacific Palisades) the residential, high-SAVI areas are cooler than streets, and arterials with tree-lined medians can be especially cool. However, highways are the coolest streets in neighborhoods with diverse ground cover. In particularly impervious areas (e.g. Colton, Pacoima, and Vernon) highways are often the coolest areas overall.

In desertified or impervious sample areas, highways were often cooler than all other surrounding surfaces. Median highway temperature was 0.94° C cooler than areas without roads across the study area, though this effect is skewed by the highly desertified San Bernardino areas: in the greener LA County, highways were 0.3° C warmer than non-road surfaces. In extremely unvegetated areas, though, the effect is especially pronounced; Vernon's highways were 2.4° C cooler than surrounding areas. In the sample area, the (concrete) highways showed a lower albedo than buildings (predominantly large warehouses) but a higher albedo than other roads. Most vegetated regions (e.g. Pacific Palisades, Rolling Hills) showed lower non-road LST than highway LST, but industrial or desertified regions (e.g. Pacoima, Colton) had lower highway LST (Figure 4.4).

#### *4.4.3 Hotspots*

The primary cooling factor in most sample areas was vegetation. Most LST patterns, and correlations with albedo or road area, were visible in areas that lacked the overwhelming effects of vegetation. Without vegetation, albedo can become a strong factor. This pattern was visible on road surfaces, where higher-albedo concretized highways showed lower LST than arterials and residential streets.

In some areas, large hotspots – specific locations with strong SAVI or albedo signatures – skewed neighborhood effects. In homogeneous residential areas without major parks or barren sites (e.g. Upland, Watts, Pacoima), the relationship between albedo and LST was negative, as logic dictates. Lighter, more reflective surfaces had lower temperatures. In sample areas with

hotspots, some lower-albedo vegetation reduced overall LST (as in parks) or higher-albedo warehouses increased LST (Figure 4.2).

#### **4.5 Discussion**

Across urban regions and within individual neighborhoods, road area was not a contributing factor to LST. Rather, our finding that SAVI predicted lower LST at pixel and neighborhood scales supports findings pointing to the dominant role of vegetation in mitigating urban heat (Ballinas and Barradas 2016; Deilami et al. 2018). Our results support studies showing that increased urban vegetation, even in highly developed areas, mitigate SUHI across large cities (Deilami et al. 2016; Feng et al. 2021). Future studies should examine if this relationship is a function of scale, shade, evapotranspiration, vegetation's albedo, or other factors.

In Southern California's mediterranean and desert climates, a universal increase in urban forest is not a simple proposition: factors like irrigation and species suitability are necessary considerations (Mini et al. 2014). Many neighborhoods in our study area are dry and hot; grass and tree cover would not be feasible without a heavy investment in watering systems (Gober et al. 2010). In Los Angeles, only 14% of the city's water is sourced locally, and sustainability plans at both the city and county levels aim for reductions in water imports (LADWP 2018). A locally-driven LST mitigation program in Los Angeles could look similar to the model currently being piloted in Athens, Greece, using large, open, impervious spaces to improve "microclimates" (C40 2022). Strategies for SUHI mitigation rely on a highly targeted approach; planners and scientists alike are identifying areas of high LST or low heat resilience and addressing local conditions (Skoulika et al. 2014; Mavrakou et al. 2018; Mavrakou and Polydoros 2021). In diverse cities where regional changes might be expensive or impractical, a

suite of small-scale approaches can provide an achievable strategy. Future research could examine investments in native plant cover and in the efficiency of green and grey shade as options for reducing LST in different parts of the urban area.

To the extent that increasing vegetation is infeasible, would narrowing streets or introducing cool pavements be a useful urban heat strategy? Here our results are more surprising: we found no evidence that road surfaces in the study area increased LST relative to their surroundings. Large unbroken areas, such as warehouses or parking lots, played a bigger role in determining neighborhood-scale LST, echoing locally a result shown in citywide SUHI across other urban areas (Liu et al. 2021). In homogeneous residential neighborhoods with no parks, malls, or industrial sites, higher albedo was associated with lower LST. This effect was consistent regardless of climatic conditions. The presence of large warehouses, transportation centers, parks, or forested areas in many greener neighborhoods, however, led to a positive relationship between albedo and LST. The mechanism was imperviousness or building material rather than albedo: large white warehouses and bare ground are LST hotspots, while parks and green spaces are cooler than their surroundings. Although we did not measure the effect of shade, we hypothesize that shade from nearby structures like buildings contributed to lower LST on some surfaces like warehouse roofs. Future research might consider LiDAR or 3D building datasets to further investigate the role of shade in moderating LST. While mitigation strategies on road surfaces can be effective, addressing LST hotspots might also create change across a neighborhood or city.

In many neighborhoods, there was not a single dominant factor (e.g. vegetation, albedo) affecting LST. Rather, individual vegetated or industrial hotspots skewed variables like SAVI or albedo heavily, suggesting that a context-specific approach to mitigating LST might prove

beneficial for neighborhoods with mixed composition (Sodoudi et al. 2014; Feng et al. 2021). In considering mitigation strategies for LST in areas with very little vegetation, lighter pavement surfaces could help break up these large hotspots. We found that highways consistently had the lowest LST of all road surfaces, a result that confirms materials studies (Cheela et al. 2021; Sen et al. 2019). In impervious or desert neighborhoods, they had the lowest LST of all surfaces. Efforts to increase concrete or cool pavements in non-vegetated areas could be more effective at reducing LST than implementation in shadier neighborhoods.

Local climatic and socioeconomic conditions also varied among neighborhoods. Across Los Angeles County, we found that coastal areas had below-average LST and a weaker relationship between LST and SAVI due to a morning marine layer (Figure 4.3). Local changes in vegetation and land use were equally important. Although the Pacific Palisades and Lancaster are both primarily classified within the “brush, scrub” LCZ, the wealthy Palisades is heavily irrigated, while Lancaster has almost no irrigated urban canopy (Nowack et al. 1996; Galvin et al. 2019). LST mitigation strategies reflecting urban heterogeneity have been examined most notably in Hong Kong, where studies show that hotspots driving high LST are heterogeneously distributed throughout the city. Proposed mitigation strategies are aimed at reducing LST in the areas of highest contribution or social vulnerability, rather than seeking to improve conditions citywide (Wong et al. 2016; Hua et al. 2021). Greening high-rise developments, providing shade for the elderly, and strategic additions of pocket parks in coastal areas are all potential means of addressing a regional problem with targeted, local solutions (Giridhran et al. 2008; Peng and Jim 2013; Peng and Maing 2021). Additionally, Hong Kong’s varied topography and unique climate have led researchers to develop locally-determined “seasons” for examination based on highly



local conditions (Giridhran et al. 2007; Chan 2011). In desert climates, strong seasonal effects might also be considered in constructing neighborhood-based LST mitigation strategies.

#### **4.6 Conclusions**

We examined LST across urban areas in Los Angeles and San Bernardino Counties with respect to mitigation potential along road surfaces, but found no consistent statistical relationship between road area and LST suggesting that wide streets are a major contributor to urban heat. Rather, we observed that vegetated areas are universally cooler than unvegetated areas, and that concrete highways can be cooler than other impervious surfaces. Our findings suggest that policies may be based on assumptions and results that ignore the social, material, and land use context of areas in which they are being implemented. In particular, streets are often overemphasized. In comparison to large features – parking lots, warehouses, or parks – streets do not show a statistical relationship with LST at either a neighborhood or a citywide level.

A more thoughtful approach might consider microclimates and local conditions, including shade, coastal effects, and dominant neighborhood land use. While streets comprise a large share of land use, they are often dwarfed by green spaces, parking lots, or buildings. There may be marginal gains from moving to cooler pavements, but the bigger drivers of high LST are often large, unbroken areas (e.g. parking lots or large buildings). Our local sample areas show a diverse view of LST, with various neighborhoods affected by climate, urban morphology, and land cover. As LST and SUHI mitigation become higher policy priorities, cities should avoid focusing on publicly-owned streets without considering neighborhood context.

## References

- Adams, M. P., & Smith, P. L. (2014). A systematic approach to model the influence of the type and density of vegetation cover on urban heat using remote sensing. *Landscape and Urban Planning, 132*, 47–54. <https://doi.org/10.1016/j.landurbplan.2014.08.008>
- Ballinas, M., & Barradas, V. L. (2016). Transpiration and stomatal conductance as potential mechanisms to mitigate the heat load in Mexico City. *Urban Forestry & Urban Greening, 20*, 152–159. <https://doi.org/10.1016/j.ufug.2016.08.004>
- Barbierato, E., Bernetti, I., Capecchi, I., & Saragosa, C. (2019). Quantifying the impact of trees on land surface temperature: A downscaling algorithm at city-scale. *European Journal of Remote Sensing, 52*(sup4), 74–83. <https://doi.org/10.1080/22797254.2019.1646104>
- C40. (2017). *A Hot Topic: Cities tackle rising temperatures*. C40 Cities. <https://www.c40.org/news/cool-cities-august/>
- C40. (2022). *Athens – C40 City Solutions Platform*. <https://c40citysolutionsplatform.org/solutions/athens/>
- CalEPA. (2015, November 20). *SB 535 Disadvantaged Communities* [Text]. OEHHA. <https://oehha.ca.gov/calenviroscreen/sb535>
- CalRecycle. (2020). *Rubberized Asphalt Concrete (RAC)*. <https://www.calrecycle.ca.gov/tires/rac>
- Caltrans. (2002). *CA Use of Fast-Setting Hydraulic Cement Concrete for Interstate Concrete Pavement Rehabilitation 9902—MCL Project Reports—Resources—MCTC - Concrete—Materials & Construction Technology—Pavements—Federal Highway Administration*. <https://www.fhwa.dot.gov/pavement/concrete/mcl9902.cfm>
- Chan, A. L. S. (2011). Developing a modified typical meteorological year weather file for Hong Kong taking into account the urban heat island effect. *Building and Environment, 46*(12), 2434–2441. <https://doi.org/10.1016/j.buildenv.2011.04.038>
- Cheela, V. R. S., John, M., Biswas, W., & Sarker, P. (2021). Combating Urban Heat Island Effect—A Review of Reflective Pavements and Tree Shading Strategies. *Buildings, 11*(3), 93. <https://doi.org/10.3390/buildings11030093>
- Clarke, L. W., Jenerette, G. D., & Davila, A. (2013). The luxury of vegetation and the legacy of tree biodiversity in Los Angeles, CA. *Landscape and Urban Planning, 116*, 48–59. <https://doi.org/10.1016/j.landurbplan.2013.04.006>
- Deilami, K., Kamruzzaman, Md., & Liu, Y. (2018). Urban heat island effect: A systematic review of spatio-temporal factors, data, methods, and mitigation measures. *International Journal of Applied Earth Observation and Geoinformation, 67*, 30–42. <https://doi.org/10.1016/j.jag.2017.12.009>

- Dialesandro, J., Brazil, N., Wheeler, S., & Abunnasr, Y. (2021). Dimensions of Thermal Inequity: Neighborhood Social Demographics and Urban Heat in the Southwestern U.S. *International Journal of Environmental Research and Public Health*, 18(3), 941. <https://doi.org/10.3390/ijerph18030941>
- Dialesandro, J. M., Wheeler, S. M., & Abunnasr, Y. (2019). Urban heat island behaviors in dryland regions. *Environmental Research Communications*, 1(8), 081005. <https://doi.org/10.1088/2515-7620/ab37d0>
- Dousset, B. (1989). *AVHRR-derived cloudiness and surface temperature patterns over the Los Angeles area and their relationships to land use*. 2132–2137. <https://doi.org/10.1109/IGARSS.1989.577798>
- Edinger, J. G. (1959). Changes in the depth of the marine layer over the Los Angeles Basin. *Journal of Meteorology*, 16(3), 219–226.
- Erell, E., Pearlmutter, D., Boneh, D., & Kutiel, P. B. (2014). Effect of high-albedo materials on pedestrian heat stress in urban street canyons. *Urban Climate*, 10, 367–386. <https://doi.org/10.1016/j.uclim.2013.10.005>
- Ermida, S. L., Soares, P., Mantas, V., Göttsche, F.-M., & Trigo, I. F. (2020). Google Earth Engine Open-Source Code for Land Surface Temperature Estimation from the Landsat Series. *Remote Sensing*, 12(9), 1471. <https://doi.org/10.3390/rs12091471>
- Farr, T. G., Rosen, P. A., Caro, E., Crippen, R., Duren, R., Hensley, S., Kobrick, M., Paller, M., Rodriguez, E., Roth, L., Seal, D., Shaffer, S., Shimada, J., Umland, J., Werner, M., Oskin, M., Burbank, D., & Alsdorf, D. (2007). The Shuttle Radar Topography Mission. *Reviews of Geophysics*, 45(2). <https://doi.org/10.1029/2005RG000183>
- Feng, R., Wang, F., Wang, K., Wang, H., & Li, L. (2021). Urban ecological land and natural-anthropogenic environment interactively drive surface urban heat island: An urban agglomeration-level study in China. *Environment International*, 157, 106857. <https://doi.org/10.1016/j.envint.2021.106857>
- FHA. (2021). *Pavement Thermal Performance And Contribution To Urban And Global Climate—References—Sustainable Pavement Program—Sustainability—Pavements—Federal Highway Administration*. [https://www.fhwa.dot.gov/pavement/sustainability/articles/pavement\\_thermal.cfm](https://www.fhwa.dot.gov/pavement/sustainability/articles/pavement_thermal.cfm)
- Founda, D., & Santamouris, M. (2017). Synergies between Urban Heat Island and Heat Waves in Athens (Greece), during an extremely hot summer (2012). *Scientific Reports*, 7(1), 10973. <https://doi.org/10.1038/s41598-017-11407-6>

- Gago, E. J., Roldan, J., Pacheco-Torres, R., & Ordóñez, J. (2013). The city and urban heat islands: A review of strategies to mitigate adverse effects. *Renewable and Sustainable Energy Reviews*, 25, 749–758. <https://doi.org/10.1016/j.rser.2013.05.057>
- Galvin, M., & Oâ, J. (n.d.). *Los Angeles County Tree Canopy Assessment*. 10.
- Garcetti, E. (2021). *Mayor Garcetti kicks off second phase of 'Cool Streets L.A.' program*. Office of Los Angeles Mayor Eric Garcetti. <https://www.lamayor.org/mayor-garcetti-kicks-second-phase-cool-streets-la-program>
- Giridharan, R., Lau, S. S. Y., Ganesan, S., & Givoni, B. (2007). Urban design factors influencing heat island intensity in high-rise high-density environments of Hong Kong. *Building and Environment*, 42(10), 3669–3684. <https://doi.org/10.1016/j.buildenv.2006.09.011>
- Giridharan, R., Lau, S. S. Y., Ganesan, S., & Givoni, B. (2008). Lowering the outdoor temperature in high-rise high-density residential developments of coastal Hong Kong: The vegetation influence. *Building and Environment*, 43(10), 1583–1595. <https://doi.org/10.1016/j.buildenv.2007.10.003>
- Gober, P., Brazel, A., Quay, R., Myint, S., Grossman-Clarke, S., Miller, A., & Rossi, S. (2009). Using Watered Landscapes to Manipulate Urban Heat Island Effects: How Much Water Will It Take to Cool Phoenix? *Journal of the American Planning Association*, 76(1), 109–121. <https://doi.org/10.1080/01944360903433113>
- Hall, S. J., Learned, J., Ruddell, B., Larson, K. L., Cavender-Bares, J., Bettez, N., Groffman, P. M., Grove, J. M., Heffernan, J. B., Hobbie, S. E., Morse, J. L., Neill, C., Nelson, K. C., O'Neil-Dunne, J. P. M., Ogden, L., Pataki, D. E., Pearse, W. D., Polsky, C., Chowdhury, R. R., ... Trammell, T. L. E. (2016). Convergence of microclimate in residential landscapes across diverse cities in the United States. *Landscape Ecology*, 31(1), 101–117. <https://doi.org/10.1007/s10980-015-0297-y>
- Harlan, S. L., Brazel, A. J., Prashad, L., Stefanov, W. L., & Larsen, L. (2006). Neighborhood microclimates and vulnerability to heat stress. *Social Science & Medicine*, 63(11), 2847–2863. <https://doi.org/10.1016/j.socscimed.2006.07.030>
- He, B.-J., Zhao, Z.-Q., Shen, L.-D., Wang, H.-B., & Li, L.-G. (2019). An approach to examining performances of cool/hot sources in mitigating/enhancing land surface temperature under different temperature backgrounds based on landsat 8 image. *Sustainable Cities and Society*, 44, 416–427. <https://doi.org/10.1016/j.scs.2018.10.049>
- Hoehne, C. G., Chester, M. V., Sailor, D. J., & King, D. A. (2020). Urban Heat Implications from Parking, Roads, and Cars: A Case Study of Metro Phoenix. *Sustainable and Resilient Infrastructure*, 0(0), 1–19. <https://doi.org/10.1080/23789689.2020.1773013>

- Hoffman, J. S., Shandas, V., & Pendleton, N. (2020). The Effects of Historical Housing Policies on Resident Exposure to Intra-Urban Heat: A Study of 108 US Urban Areas. *Climate*, 8(1), 12. <https://doi.org/10.3390/cli8010012>
- Horowitz, J. (2021, August 21). Athens Is Only Getting Hotter. Its New ‘Chief Heat Officer’ Hopes to Cool It Down. *The New York Times*.  
<https://www.nytimes.com/2021/08/21/world/europe/athens-is-only-getting-hotter-its-new-chief-heat-officer-hopes-to-cool-it-down.html>
- Hua, J., Zhang, X., Ren, C., Shi, Y., & Lee, T.-C. (2021). Spatiotemporal assessment of extreme heat risk for high-density cities: A case study of Hong Kong from 2006 to 2016. *Sustainable Cities and Society*, 64, 102507. <https://doi.org/10.1016/j.scs.2020.102507>
- Hulley, G., Shivers, S., Wetherley, E., & Cudd, R. (2019). New ECOSTRESS and MODIS Land Surface Temperature Data Reveal Fine-Scale Heat Vulnerability in Cities: A Case Study for Los Angeles County, California. *Remote Sensing*, 11(18), 2136.  
<https://doi.org/10.3390/rs11182136>
- IHO. (1953). Limits of oceans and seas. *IHO Special Publication*, 3(23), 1–38.
- Imhoff, M. L., Zhang, P., Wolfe, R. E., & Bounoua, L. (2010). Remote sensing of the urban heat island effect across biomes in the continental USA. *Remote Sensing of Environment*, 114(3), 504–513. <https://doi.org/10.1016/j.rse.2009.10.008>
- Johansson, E. (2006). Influence of urban geometry on outdoor thermal comfort in a hot dry climate: A study in Fez, Morocco. *Building and Environment*, 41(10), 1326–1338.  
<https://doi.org/10.1016/j.buildenv.2005.05.022>
- Kesseli, J. E. (1942). The Climates of California According to the Köppen Classification. *Geographical Review*, 32(3), 476–480. <https://doi.org/10.2307/210390>
- Ko, J., Schlaerth, H., Bruce, A., Sanders, K. T., & Ban-Weiss, G. A. (2022). Measuring the impacts of a real-world neighborhood-scale cool pavement deployment on albedo and temperatures in Los Angeles. *Environmental Research Letters*.  
<https://iopscience.iop.org/article/10.1088/1748-9326/ac58a8/meta>
- Ladochy, S., Torres, T., & Hsu, Y. (2021). LOS ANGELES’ URBAN HEAT ISLAND CONTINUES TO GROW: URBANIZATION, LAND USE CHANGE INFLUENCES. *Journal of Urban and Environmental Engineering*, 15, 103–116.  
<https://doi.org/10.4090/juee.2021.v15n2.103116>
- Lai, J., Zhan, W., Huang, F., Voogt, J., Bechtel, B., Allen, M., Peng, S., Hong, F., Liu, Y., & Du, P. (2018). Identification of typical diurnal patterns for clear-sky climatology of surface urban heat islands. *Remote Sensing of Environment*, 217, 203–220.  
<https://doi.org/10.1016/j.rse.2018.08.021>

- Lazzarini, M., Molini, A., Marpu, P. R., Ouarda, T. B. M. J., & Ghedira, H. (2015). Urban climate modifications in hot desert cities: The role of land cover, local climate, and seasonality. *Geophysical Research Letters*, *42*(22), 9980–9989. <https://doi.org/10.1002/2015GL066534>
- Lee, E.-B., Roesler, J., Harvey, J. T., & Ibbs, C. W. (2002). Case Study of Urban Concrete Pavement Reconstruction on Interstate 10. *Journal of Construction Engineering and Management*, *128*(1), 49–56. [https://doi.org/10.1061/\(ASCE\)0733-9364\(2002\)128:1\(49\)](https://doi.org/10.1061/(ASCE)0733-9364(2002)128:1(49))
- Lee, S., Moon, H., Choi, Y., & Yoon, D. K. (2018). Analyzing Thermal Characteristics of Urban Streets Using a Thermal Imaging Camera: A Case Study on Commercial Streets in Seoul, Korea. *Sustainability*, *10*(2), 519. <https://doi.org/10.3390/su10020519>
- Levinson, R., & Akbari, H. (2002). Effects of composition and exposure on the solar reflectance of portland cement concrete. *Cement and Concrete Research*, *32*(11), 1679–1698. [https://doi.org/10.1016/S0008-8846\(02\)00835-9](https://doi.org/10.1016/S0008-8846(02)00835-9)
- Liao, W., Hong, T., & Heo, Y. (2021). The effect of spatial heterogeneity in urban morphology on surface urban heat islands. *Energy and Buildings*, *244*, 111027. <https://doi.org/10.1016/j.enbuild.2021.111027>
- Litvak, E., Manago, K. F., Hogue, T. S., & Pataki, D. E. (2017). Evapotranspiration of urban landscapes in Los Angeles, California at the municipal scale. *Water Resources Research*, *53*(5), 4236–4252. <https://doi.org/10.1002/2016WR020254>
- Liu, L., & Zhang, Y. (2011). Urban Heat Island Analysis Using the Landsat TM Data and ASTER Data: A Case Study in Hong Kong. *Remote Sensing*, *3*(7), 1535–1552. <https://doi.org/10.3390/rs3071535>
- Ma, Y., Zhang, S., Yang, K., & Li, M. (2021). Influence of spatiotemporal pattern changes of impervious surface of urban megaregion on thermal environment: A case study of the Guangdong – Hong Kong – Macao Greater Bay Area of China. *Ecological Indicators*, *121*, 107106. <https://doi.org/10.1016/j.ecolind.2020.107106>
- Manville, M. (2017). Automatic street widening: Evidence from a highway dedication law. *Journal of Transport and Land Use*, *10*(1), 375–393.
- Mavrakou, T., & Polydoros, A. (2021). Assessing Urban Resilience to Thermal Risk: An Application for Athens, Greece. *International Journal of Environmental Sciences & Natural Resources*, *29*(1), 1–3. <https://doi.org/10.19080/IJESNR.2021.29.556256>
- Mavrakou, T., Polydoros, A., Cartalis, C., & Santamouris, M. (2018). Recognition of Thermal Hot and Cold Spots in Urban Areas in Support of Mitigation Plans to Counteract Overheating: Application for Athens. *Climate*, *6*(1), 16. <https://doi.org/10.3390/cli6010016>

- Maxwell, K., Grambsch, A., Kosmal, A., Larson, L., & Sonti, N. (2018). Built Environment, Urban Systems, and Cities. *Impacts, Risks, and Adaptation in the United States: Fourth National Climate Assessment*, 2, 438–478.
- Meyer, J. R., & Gómez-Ibáñez, J. A. (2013). Autos, Transit, and Cities. In *Autos, Transit, and Cities*. Harvard University Press. <https://doi.org/10.4159/harvard.9780674421103>
- Microsoft. (2021). *Building Footprints*. Microsoft. <https://github.com/microsoft/USBuildingFootprints> (Original work published 2018)
- Middel, A., Turner, V. K., Schneider, F. A., Zhang, Y., & Stiller, M. (2020). *Solar reflective pavements—A policy panacea to heat mitigation?* 15(6), 064016. <https://doi.org/10.1088/1748-9326/ab87d4>
- Millard-Ball, A. (2022). The Width and Value of Residential Streets. *Journal of the American Planning Association*, 88(1), 30–43. <https://doi.org/10.1080/01944363.2021.1903973>
- Mini, C., Hogue, T. S., & Pincetl, S. (2014). Estimation of residential outdoor water use in Los Angeles, California. *Landscape and Urban Planning*, 127, 124–135. <https://doi.org/10.1016/j.landurbplan.2014.04.007>
- Mohamed, M., Othman, A., Abotalib, A. Z., & Majrashi, A. (2021). Urban Heat Island Effects on Megacities in Desert Environments Using Spatial Network Analysis and Remote Sensing Data: A Case Study from Western Saudi Arabia. *Remote Sensing*, 13(10), 1941. <https://doi.org/10.3390/rs13101941>
- Mohammed, A., Pignatta, G., Topriska, E., & Santamouris, M. (2020). Canopy Urban Heat Island and Its Association with Climate Conditions in Dubai, UAE. *Climate*, 8(6), 81. <https://doi.org/10.3390/cli8060081>
- Moretti, L., Cantisani, G., Carpiceci, M., D'Andrea, A., Del Serrone, G., Di Mascio, P., & Loprencipe, G. (2021). Effect of Sampietrini Pavers on Urban Heat Islands. *International Journal of Environmental Research and Public Health*, 18(24), 13108. <https://doi.org/10.3390/ijerph182413108>
- Mullaney, J., Lucke, T., & Trueman, S. J. (2015). A review of benefits and challenges in growing street trees in paved urban environments. *Landscape and Urban Planning*, 134, 157–166. <https://doi.org/10.1016/j.landurbplan.2014.10.013>
- Municipality of Athens. (2017). *Athens Resilience Strategy*.
- Nowak, D. J., Rowntree, R. A., McPherson, E. G., Sisinni, S. M., Kerkmann, E. R., & Stevens, J. C. (1996). Measuring and analyzing urban tree cover. *Landscape and Urban Planning*, 36(1), 49–57. [https://doi.org/10.1016/S0169-2046\(96\)00324-6](https://doi.org/10.1016/S0169-2046(96)00324-6)

- Oke, T. R. (1982). The energetic basis of the urban heat island. *Quarterly Journal of the Royal Meteorological Society*, 108(455), 1–24. <https://doi.org/10.1002/qj.49710845502>
- Peng, L. L. H., & Jim, C. Y. (2013). Green-Roof Effects on Neighborhood Microclimate and Human Thermal Sensation. *Energies*, 6(2), 598–618. <https://doi.org/10.3390/en6020598>
- Peng, S., & Maing, M. (2021). Influential factors of age-friendly neighborhood open space under high-density high-rise housing context in hot weather: A case study of public housing in Hong Kong. *Cities*, 115, 103231. <https://doi.org/10.1016/j.cities.2021.103231>
- Peng, S., Piao, S., Ciais, P., Friedlingstein, P., Otle, C., Bréon, F.-M., Nan, H., Zhou, L., & Myneni, R. B. (2012). Surface Urban Heat Island Across 419 Global Big Cities. *Environmental Science & Technology*, 46(2), 696–703. <https://doi.org/10.1021/es2030438>
- Pomerantz, M., Akbari, H., Chang, S.-C., Levinson, R., & Pon, B. (2003). *Examples of cooler reflective streets for urban heat-island mitigation: Portland cement concrete and chip seals* (LBNL--49283, 816205; p. LBNL--49283, 816205). <https://doi.org/10.2172/816205>
- Rashed, T., Weeks, J. R., Roberts, D., Rogan, J., & Powell, R. (2003). Measuring the Physical Composition of Urban Morphology Using Multiple Endmember Spectral Mixture Models. *Photogrammetric Engineering & Remote Sensing*, 69(9), 1011–1020. <https://doi.org/10.14358/PERS.69.9.1011>
- Rizwan, A. M., Dennis, L. Y. C., & Liu, C. (2008). A review on the generation, determination and mitigation of Urban Heat Island. *Journal of Environmental Sciences*, 20(1), 120–128. [https://doi.org/10.1016/S1001-0742\(08\)60019-4](https://doi.org/10.1016/S1001-0742(08)60019-4)
- Roman, L. A., Conway, T. M., Eisenman, T. S., Koeser, A. K., Ordóñez Barona, C., Locke, D. H., Jenerette, G. D., Östberg, J., & Vogt, J. (2021). Beyond ‘trees are good’: Disservices, management costs, and tradeoffs in urban forestry. *Ambio*, 50(3), 615–630. <https://doi.org/10.1007/s13280-020-01396-8>
- Roy, D. P., Wulder, M. A., Loveland, T. R., C.e., W., Allen, R. G., Anderson, M. C., Helder, D., Irons, J. R., Johnson, D. M., Kennedy, R., Scambos, T. A., Schaaf, C. B., Schott, J. R., Sheng, Y., Vermote, E. F., Belward, A. S., Bindshadler, R., Cohen, W. B., Gao, F., ... Zhu, Z. (2014). Landsat-8: Science and product vision for terrestrial global change research. *Remote Sensing of Environment*, 145, 154–172. <https://doi.org/10.1016/j.rse.2014.02.001>
- Santamouris, M. (2013). Using cool pavements as a mitigation strategy to fight urban heat island—A review of the actual developments. *Renewable and Sustainable Energy Reviews*, 26, 224–240. <https://doi.org/10.1016/j.rser.2013.05.047>
- SB County. (2020). *City Limits*. <https://open.sbcounty.gov/datasets/sbcounty::city-limits-1/about>



- Sen, S., Roesler, J., Ruddell, B., & Middel, A. (2019). Cool Pavement Strategies for Urban Heat Island Mitigation in Suburban Phoenix, Arizona. *Sustainability*, *11*(16), 4452. <https://doi.org/10.3390/su11164452>
- Shastri, H., Barik, B., Ghosh, S., Venkataraman, C., & Sadavarte, P. (2017). Flip flop of Day-night and Summer-Winter Surface Urban Heat Island Intensity in India. *Scientific Reports*, *7*(1), 40178. <https://doi.org/10.1038/srep40178>
- Shiflett, S. A., Liang, L. L., Crum, S. M., Feyisa, G. L., Wang, J., & Jenerette, G. D. (2017). Variation in the urban vegetation, surface temperature, air temperature nexus. *Science of The Total Environment*, *579*, 495–505. <https://doi.org/10.1016/j.scitotenv.2016.11.069>
- Skoulika, F., Santamouris, M., Kolokotsa, D., & Boemi, N. (2014). On the thermal characteristics and the mitigation potential of a medium size urban park in Athens, Greece. *Landscape and Urban Planning*, *123*, 73–86. <https://doi.org/10.1016/j.landurbplan.2013.11.002>
- Smart Cities Connect. (2021). *Phoenix Releases Cool Pavement Pilot Program Results – Smart Cities Connect*. <https://smartcitiesconnect.org/phoenix-releases-cool-pavement-pilot-program-results/>
- Soudoudi, S., Shahmohamadi, P., Vollack, K., Cubasch, U., & Che-Ani, A. I. (2014). Mitigating the Urban Heat Island Effect in Megacity Tehran. *Advances in Meteorology*, *2014*, e547974. <https://doi.org/10.1155/2014/547974>
- Stewart, I. D., & Oke, T. R. (2012, December 1). *Local Climate Zones for Urban Temperature Studies in: Bulletin of the American Meteorological Society Volume 93 Issue 12 (2012)*. <https://journals.ametsoc.org/view/journals/bams/93/12/bams-d-11-00019.1.xml>
- Su, J. G., Morello-Frosch, R., Jesdale, B. M., Kyle, A. D., Shamasunder, B., & Jerrett, M. (2009). An Index for Assessing Demographic Inequalities in Cumulative Environmental Hazards with Application to Los Angeles, California. *Environmental Science & Technology*, *43*(20), 7626–7634. <https://doi.org/10.1021/es901041p>
- Susca, T., Gaffin, S. R., & Dell’Osso, G. R. (2011). Positive effects of vegetation: Urban heat island and green roofs. *Environmental Pollution*, *159*(8), 2119–2126. <https://doi.org/10.1016/j.envpol.2011.03.007>
- Taleghani, M., Sailor, D., & Ban-Weiss, G. A. (2016). Micrometeorological simulations to predict the impacts of heat mitigation strategies on pedestrian thermal comfort in a Los Angeles neighborhood. *Environmental Research Letters*, *11*(2), 024003. <https://doi.org/10.1088/1748-9326/11/2/024003>
- Transformative Climate Communities. (2021). *Transformative Climate Communities*. <https://greenlining.org/our-work/environmental-equity/transformative-climate-communities-2/>

- Tsou, J., Zhuang, J., Li, Y., & Zhang, Y. (2017). Urban Heat Island Assessment Using the Landsat 8 Data: A Case Study in Shenzhen and Hong Kong. *Urban Science*, 1(1), 10. <https://doi.org/10.3390/urbansci1010010>
- Turner, K., M. French, E., & Hondula, D. (2021). *How are U.S. Cities Planning for Heat?* [Data set]. DesignSafe-CI. <https://www.designsafe-ci.org/data/browser/public/designsafe.storage.published//PRJ-3180>
- US EPA. (2012). Reducing Urban Heat Islands: Compendium of Strategies, Cool Pavements. *Reducing Urban Heat Islands: Compendium of Strategies*.
- USC. (2017). *Los Angeles Neighborhood Map | Open Data*. USC Price Center. <https://usc.data.socrata.com/dataset/Los-Angeles-Neighborhood-Map/r8qd-yxsr>
- Wilson, B. (2020). Urban Heat Management and the Legacy of Redlining. *Journal of the American Planning Association*, 86(4), 443–457. <https://doi.org/10.1080/01944363.2020.1759127>
- Wiltshire-Gordon, S. (2020). *New federal bill supports heat island mitigation | U.S. Green Building Council*. <https://www.usgbc.org/articles/new-federal-bill-supports-heat-island-mitigation>
- Wong, M. S., Peng, F., Zou, B., Shi, W. Z., & Wilson, G. J. (2016). Spatially Analyzing the Inequity of the Hong Kong Urban Heat Island by Socio-Demographic Characteristics. *International Journal of Environmental Research and Public Health*, 13(3), E317. <https://doi.org/10.3390/ijerph13030317>
- Yamazaki, F., Murakoshi, A., & Sekiya, N. (2009). Observation of urban heat island using airborne thermal sensors. *2009 Joint Urban Remote Sensing Event*, 1–5. <https://doi.org/10.1109/URS.2009.5137723>
- Yuan, C., Adelia, A. S., Mei, S., He, W., Li, X.-X., & Norford, L. (2020). Mitigating intensity of urban heat island by better understanding on urban morphology and anthropogenic heat dispersion. *Building and Environment*, 176, 106876. <https://doi.org/10.1016/j.buildenv.2020.106876>

## Chapter 5. Conclusions and recommendations for further work

I assessed urban dynamics and their impacts on one another in different parts of the greater Los Angeles area. The science questions I addressed were:

1. How have urban land cover and irrigation in Los Angeles changed over the last 35 years (1984-2019)?
2. What are the cumulative effects of small-scale land use changes on evapotranspiration (ET) and water balance, both across Los Angeles and within distinct neighborhoods?
3. Is there a relationship between street area and Land Surface Temperature (LST), either regionally or at a local scale, and is that relationship affected by urban form?

Each chapter included analyses encompassing both a regional view of the Los Angeles area and conditions within individual neighborhoods. In assessing changes to land cover, hydrology, and LST, I considered a wide range of physical processes across and within a megacity.

In Chapter 2, **Examining urban land cover change using a deep encoder-decoder convolutional neural network**, results showed that land cover changes across the Los Angeles Sedimentary Basin were moderate, with little new development over between 1984-2019. A deep learning approach to mixed pixel disaggregation demonstrated 91% accuracy when compared to classifications derived from contemporary 10 cm composite imagery. Relative to moderate-resolution datasets, the new land cover time series identified more small minority-pixel urban green spaces and how they changed over time.

The results can be used to support further studies in regional hydrology, carbon cycles, or urban land use (Thanapakpawin et al. 2007; Churkina 2008; Pataki et al. 2013). In particular, this new land cover dataset can facilitate more localized modeling studies, providing detail about small features that matter more within a small area than across a region. As research moves

toward understanding ecosystem services at the neighborhood scale, these land use classifications could play a role. Additionally, this approach contributes to the growing body of literature on deep learning for segmentation of remotely sensed data (Mitraka et al. 2016; Shao et al. 2019; Sultana et al. 2020). Considering the increasing availability of high-resolution training data, similar approaches can be readily applied to a variety of datasets.

Chapter 3, **The role of urban vegetation change in the basin-scale hydrology of Los Angeles**, demonstrated that changes to land cover have a small regional effect, and instead primarily impact individual neighborhoods. Increased vegetation modestly reduced runoff in >90% of modeled days, with larger reductions during precipitation events. These results were most dramatic in Long Beach, which is mostly impervious, and weaker in Woodland Hills, which is heavily irrigated. Long Beach also experienced higher changes in ET with variations in vegetation; summertime ET in particular was higher in years with increasing vegetation. Across all seasons and conditions, though, Woodland Hills saw higher ET than Long Beach due to irrigation.

In combination with data showing that over half of residential water use in Los Angeles goes to landscaping, my results indicate that irrigation varies substantially among neighborhoods, and that changes to minority-area land cover can have an outsize effect on local hydrology (Mini et al. 2014). Accordingly, small-scale land use changes in heavily impervious areas might increase aquifer recharge and disrupt stormwater runoff, but emphasis on locally driven solutions (e.g. indigenous vegetation or grey systems) could achieve similar ends without increasing ET and raising water use (McPhearson et al. 2014). Simultaneously, reductions in year-round irrigation in green neighborhoods make a smaller neighborhood-scale difference in ET due to the continued impact of the surrounding vegetation. Systemic measures (e.g. irrigation

limits and turf replacement programs) might be more effective in these areas, where larger changes would lead to more substantial water savings (Mini et al. 2014; Porse et al. 2017).

Because of variations in both neighborhood composition and local responses to land use change, ongoing research and solutions might be examined at smaller scales. Within Los Angeles, future work could extend neighborhood-scale modeling to assess opportunities for targeted land use change and water savings. These analyses could also integrate projections for both land cover and climate to understand how different parts of Los Angeles – particularly the Transformative Climate Communities and other environmentally disadvantaged areas – will respond to projected heat waves and increasing drought conditions (Transformative Climate Communities 2021; CalEPA 2022). Given the increasing abundance of high-resolution land cover data, these analyses could guide policies and plans for reducing ET and increasing aquifer recharge across the Los Angeles area.

Chapter 4, **Contributions of roads to surface temperature: evidence from Southern California**, showed that road area was not a driver of LST at either a regional or a neighborhood scale. Rather, the presence of vegetation – and, accordingly, shade and ET – was a factor in decreasing LST. In heavily impervious or desertified areas, highways were often the coolest surfaces: their concrete pavement was cooler than large warehouses or uninterrupted impervious spaces like parking lots. Responses to LST mitigation strategies varied across neighborhoods. The cooling effect of vegetation was tempered in cloudy or coastal neighborhoods, and individual large features (e.g. parks, shipping facilities, airports) often dominated neighborhood LST signatures.

The effects of vegetation and urban morphology on LST suggest a consideration of microclimates and local conditions, including coastal effects, shade, and building patterns. While

streets cover entire cities, their potential as a panacea for LST mitigation is minimal. Rather, individual large features in distinct neighborhoods offer provide more substantial cooling effects across neighborhoods. Similar strategies are proposed in other diverse megacities. In Hong Kong, researchers suggest highly targeted heat mitigation strategies in areas where they would have the greatest local effect or where the population is most vulnerable (Giridhran et al. 2008; Peng and Miang 2021). In Tehran, a “hybrid” style of green and grey cooling measures has been proposed to reduce regional heat through a combination of local changes (Sodoudi et al. 2014). These approaches, and others like them, demonstrate that individual neighborhood characteristics matter in regional planning.

Going forward, this chapter’s research suggests potential for increased investigation into the mechanisms of heat within individual neighborhoods. Building morphology, vegetation, and microclimates all play a role in determining LST, and understanding their interactions across Los Angeles could help guide a series of local mitigation strategies. The research could also be expanded to understand local air temperature or thermal comfort, which also vary substantially with local conditions.

This dissertation examines disparities in land use, hydrology, and surface temperature across the Los Angeles area. I highlight the effects of urban vegetation and irrigation in different neighborhoods and examine drivers of LST in varying conditions. Each chapter parses an aspect of heterogeneity in the urban form of Los Angeles, and explores ways in which spatial patterns might influence future research and planning efforts. My results demonstrate that differences in landscaping, urban morphology, and climate can change the outcomes of physical systems and ecosystem services at a local scale. As sustainable cities become ever-increasing policy priorities, researchers and managers should consider neighborhood context in proposing change.

## References

- CalEPA. (2015, November 20). SB 535 Disadvantaged Communities [Text]. OEHHA. <https://oehha.ca.gov/calenviroscreen/sb535>
- Churkina, G. (2008). Modeling the carbon cycle of urban systems. *Ecological Modelling*, 216(2), 107–113. <https://doi.org/10.1016/j.ecolmodel.2008.03.006>
- Giridharan, R., Lau, S. S. Y., Ganesan, S., & Givoni, B. (2007). Urban design factors influencing heat island intensity in high-rise high-density environments of Hong Kong. *Building and Environment*, 42(10), 3669–3684. <https://doi.org/10.1016/j.buildenv.2006.09.011>
- McPhearson, T., Hamstead, Z. A., & Kremer, P. (2014). Urban Ecosystem Services for Resilience Planning and Management in New York City. *AMBIO*, 43(4), 502–515. <https://doi.org/10.1007/s13280-014-0509-8>
- Mini, C., Hogue, T. S., & Pincetl, S. (2014). Estimation of residential outdoor water use in Los Angeles, California. *Landscape and Urban Planning*, 127, 124–135. <https://doi.org/10.1016/j.landurbplan.2014.04.007>
- Mitraka, Z., Frate, F. D., & Carbone, F. (2016). Nonlinear Spectral Unmixing of Landsat Imagery for Urban Surface Cover Mapping. *IEEE Journal of Selected Topics in Applied Earth Observations and Remote Sensing*, 9(7), 3340–3350. <https://doi.org/10.1109/JSTARS.2016.2522181>
- Pataki, D. E., McCarthy, H. R., Gillespie, T., Jenerette, G. D., & Pincetl, S. (2013). A trait-based ecology of the Los Angeles urban forest. *Ecosphere*, 4(6), art72. <https://doi.org/10.1890/ES13-00017.1>
- Peng, S., & Maing, M. (2021). Influential factors of age-friendly neighborhood open space under high-density high-rise housing context in hot weather: A case study of public housing in Hong Kong. *Cities*, 115, 103231. <https://doi.org/10.1016/j.cities.2021.103231>
- Porse, E., Mika, K. B., Litvak, E., Manago, K. F., Naik, K., Glickfeld, M., Hogue, T. S., Gold, M., Pataki, D. E., & Pincetl, S. (2017). Systems Analysis and Optimization of Local Water Supplies in Los Angeles. *Journal of Water Resources Planning and Management*, 143(9), 04017049. [https://doi.org/10.1061/\(ASCE\)WR.1943-5452.0000803](https://doi.org/10.1061/(ASCE)WR.1943-5452.0000803)
- Shao, Z., Cai, J., Fu, P., Hu, L., & Liu, T. (2019). Deep learning-based fusion of Landsat-8 and Sentinel-2 images for a harmonized surface reflectance product. *Remote Sensing of Environment*, 235, 111425. <https://doi.org/10.1016/j.rse.2019.111425>
- Sodoudi, S., Shahmohamadi, P., Vollack, K., Cubasch, U., & Che-Ani, A. I. (2014). Mitigating the Urban Heat Island Effect in Megacity Tehran. *Advances in Meteorology*, 2014, e547974. <https://doi.org/10.1155/2014/547974>

Sultana, F., Sufian, A., & Dutta, P. (2020). Evolution of Image Segmentation using Deep Convolutional Neural Network: A Survey. *Knowledge-Based Systems*, 201–202, 106062. <https://doi.org/10.1016/j.knosys.2020.106062>

Thanapakpawin, P., Richey, J., Thomas, D., Rodda, S., Campbell, B., & Logsdon, M. (2007). Effects of landuse change on the hydrologic regime of the Mae Chaem river basin, NW Thailand. *Journal of Hydrology*, 334(1), 215–230. <https://doi.org/10.1016/j.jhydrol.2006.10.012>

Transformative Climate Communities. (2021). *Transformative Climate Communities*. <https://greenlining.org/our-work/environmental-equity/transformative-climate-communities-2/>



## **Appendix A**

Examining urban land cover change using a deep encoder-decoder convolutional neural network

– Supplementary Material

### **A.1 Examination of water**

We used the Global Surface Water (GSW) dataset (1984-2019) because it shows natural water bodies in the Los Angeles Basin across our time period without selecting false positive water pixels (Pekel et al. 2016). To choose the water mask, we tried a supervised Random Forest Classifier, a Normalized Difference Water Index (NDWI) threshold, and the GSW analysis.

For the Random Forest Classification we used a training dataset of 243 swimming pools and 67 lakes across Southern California. The training polygons were manually selected from National Agriculture Imagery Program (NAIP) data from 2016 at 1m. We trained the Random Forest Classifier across 7 bands (Red, Green, Blue, Near Infrared, Shortwave Infrared 1 and 2). Ultimately, it selected most highways as water when applied to the 30 m data, and failed to recognize any of 20 manually selected test swimming pools. While the classification was effective when applied to 1 m data, it did not reproduce accuracy at a moderate resolution.

The NDWI threshold uses Near Infrared and Shortwave Infrared to identify water also failed to identify any of the test swimming pools, and also selected a number of false positive points (primarily shadows).

The GSW dataset can be selected for each year within our time period, though bodies of water do not change substantially within our study area. It does not include swimming pools, but it also does not classify downtown areas as water (Figure A1). Accordingly, we implemented a GSW mask in our preprocessing.

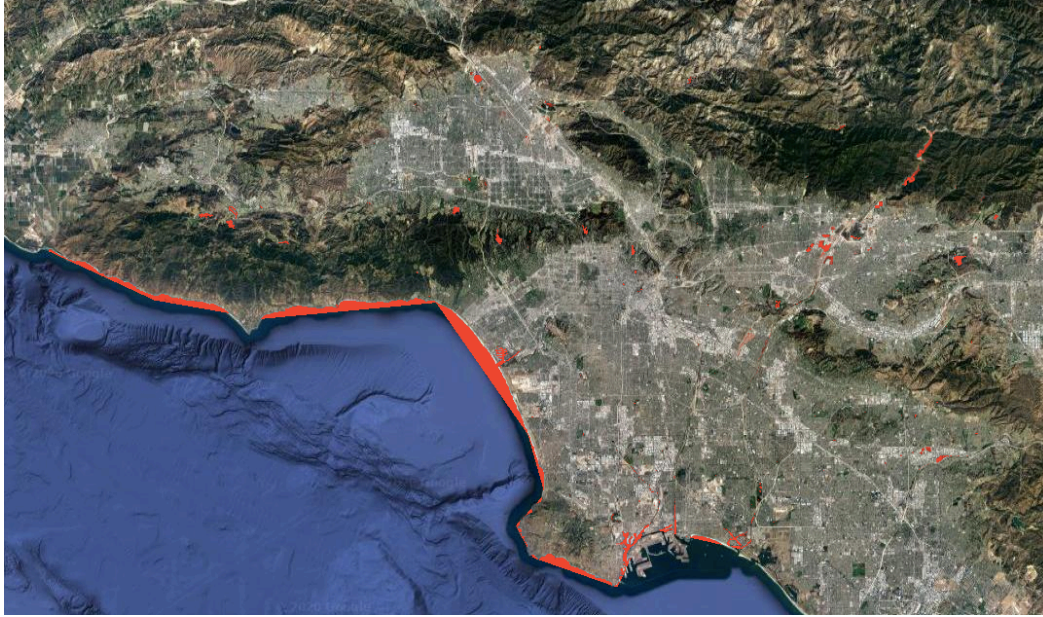


**Figure A1:** Water in the Los Angeles Basin (2019), shown in red (Pekel et al. 2016).

## **A.2 Distinguishing irrigated and non-irrigated vegetation**

To distinguish between irrigated and non-irrigated vegetation, we applied a binary mask to the summer-winter Normalized Difference Vegetation Index (NDVI) difference. In order to establish the threshold, we manually selected 16 polygons of irrigated and non-irrigated non-forested vegetation (grass, shrub/scrub). We examined Landsat 8 summer (June, July, August) and winter (December, January, February) NDVI across the regions using a cloud-free median value composite from 2013-2019. Because Los Angeles has a Mediterranean climate with very dry summers and winter-dominant precipitation, we tested to ensure that natural areas had higher wintertime NDVI (Gillespie et al. 2018).

We found that that NDVI is higher (greener) in irrigated areas than non-irrigated areas generally. In irrigated areas, winter NDVI is only slightly higher (greener) than summer NDVI (median difference 0.016). In natural areas, winter NDVI is much higher (greener) than summer (median difference 0.154). Accordingly, we set a non-irrigated vegetation threshold in urban areas at 0.069, the midpoint of the two numbers (Table A1).

**Table A1:** NDVI values.

	Irrigated	Non-Irrigated
Winter NDVI	0.666	0.532
Summer NDVI	0.650	0.378
Difference	0.016	0.154

We further masked non-irrigated vegetation by removing summertime NDVI regions between 0.3 and 0.6, which reflects both our survey and the time series of Gillespie et al. (2018) surveying the Santa Monica Mountains. The summertime mask eliminated areas of vegetation that were not being watered, but still were alive, during the warmest and driest part of the year.

### **A.3 Data validation**

To validate our data, we compared our land cover percentages to manually-classified data over both the urban parts of Los Angeles and two small-scale regions. We provide here an overview of those two validation datasets.

We primarily used the 2017 Los Angeles Region Image Acquisition Consortium (LARIAC) 10 cm composite orthogonal imagery dataset for citywide validation. The LARIAC data are categorized across 218 individual city areas within Los Angeles County (LARIAC 2015). The 10 cm pixels were cleaned and classified into 8 categories: tree canopy, grass, bare soil, water, buildings, roads/rail, other paved surfaces, and shrubs (Figure A2). We used these data to assess the accuracy of our land cover estimates across the entire urban area.

To additionally validate our land cover estimates regarding specific land cover, we chose two small-scale areas (1 km<sup>2</sup>) for comparison. We used one in a residential neighborhood, with houses and lawns, and one in Downtown LA, with almost 100% impervious surfaces (Appendix A.4). To acquire the data, we traced polygons using the ESRI Collector app. We first traced

polygons in a test area, around the UCLA campus, with field surveys (Figure A3). All 30 field test points computed as statistically significant (95% confidence interval).

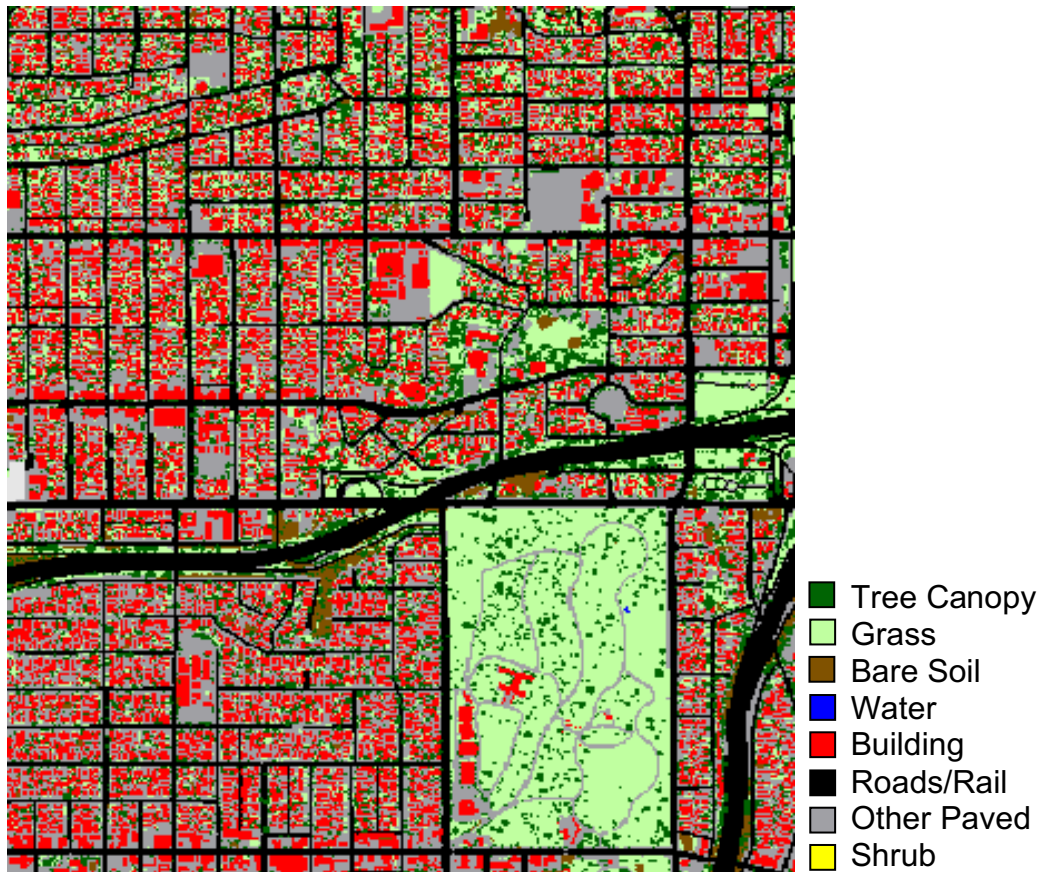


**Figure A2:** LARIAC land cover data (2017) in East Los Angeles. Data is classified orthogonal LiDAR imagery (10 cm).

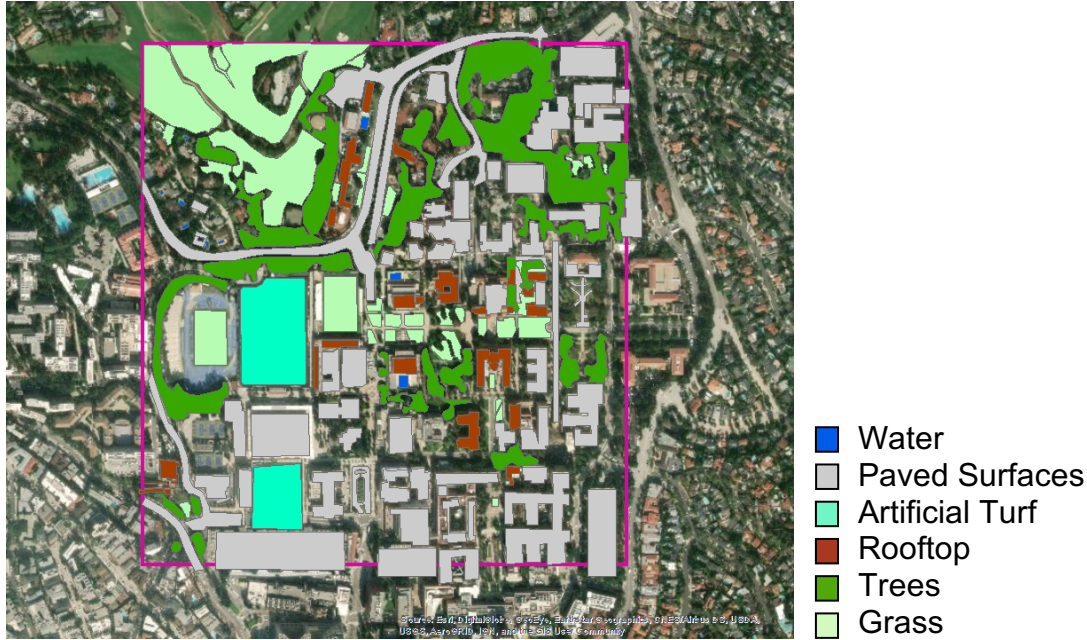


**Figure A3:** Ground truth polygons of land cover classes in the test area. The dataset comprises 165 polygons and was constructed from a combination of field survey and manual categorization of 0.5m October 2019 imagery (ESRI 2021).

#### A.4 Local validation

To examine the distribution of the calculated data over different regions within the urban area, we compared calculated and manually-collected land cover for two randomly-selected test areas of one square kilometer each. We selected area (a) at random from the dense urban downtown and area (b) at random from the more residential San Fernando Valley. We outlined features within each area using the ESRI collector app. For a locally-accessible test case we used the ESRI Collector app, which tracks the user’s location in the field and provides a basemap of 0.5 m DigitalGlobe imagery collected October 30, 2019 (ESRI 2021). To verify features traced on the imagery, 30 test points were visited, and the GPS accuracy was determined to be, on average,  $10.4 \pm 0.45$  m using an average of 11.7 satellites to compute location. All test points computed as statistically significant (95% confidence interval). For the inaccessible validation

areas, we digitized polygons using the same 2019 DigitalGlobe imagery, but with no physical validation.

In the dense downtown area (a), which we treated as an extreme case that nevertheless still included mixed pixels, the neural network accurately captured the complete lack of grass. Our results overestimated tree cover (62.88 percent error) but over an extremely small region (we reported that 0.54% of the area was trees compared to 0.33% in the ground truth data). In the more diverse, residential area with the classic mixed pixels of houses and yards, we assessed grass/shrubs with 14.46 percent error and trees with 21.80 percent error. Overall, we slightly overestimated grassy area and underestimated trees (Table A2).

**Table A2:** Accuracy for neural network derived land cover types within urban space in two validation areas of one square kilometer each. Each table shows calculated percent of area, actual percent of area, and percent accuracy for impervious surfaces, irrigated low vegetation, and urban trees. (a) Accuracy within a highly impervious commercial area. (b) Accuracy within a mixed-use residential area.

**(a)**

Land Cover	Calculated % Land Cover	Actual % Land Cover	Percent Error
Impervious	99.46	99.67	0.21
Irr. Low Veg	0	0	0
Urban Trees	0.54	0.33	62.88

**(b)**

Land Cover	Calculated % Land Cover	Actual % Land Cover	Percent Error
Impervious	95.05	94.99	0.061
Irr. Low Veg	3.27	2.85	14.46
Urban Trees	1.69	2.16	21.80

## A.5 References

- ESRI. (2021). World Imagery.  
<https://www.arcgis.com/home/item.html?id=10df2279f9684e4a9f6a7f08febac2a9>
- Gillespie, T. W., Ostermann-Kelm, S., Dong, C., Willis, K. S., Okin, G. S., & MacDonald, G. M. (2018). Monitoring changes of NDVI in protected areas of southern California. *Ecological Indicators*, 88, 485–494. <https://doi.org/10.1016/j.ecolind.2018.01.031>
- LARIAC. (2015). LARIAC Product Guide. Los Angeles County.  
[https://egis2.lacounty.gov/hub/lariac\\_documents/LARIAC4-Product-Guide-1.pdf](https://egis2.lacounty.gov/hub/lariac_documents/LARIAC4-Product-Guide-1.pdf)
- Pekel, J.-F., Cottam, A., Gorelick, N., & Belward, A. S. (2016). High-resolution mapping of global surface water and its long-term changes. *Nature*, 540(7633), 418–422.  
<https://doi.org/10.1038/nature20584>

## Appendix B

The role of urban vegetation change in the basin-scale hydrology of Los Angeles –  
Supplementary Material

The two Los Angeles Basin (LAB)-wide runs of the Distributed Hydrology Soil Vegetation Model (DHSVM) – one time-varying and one static – encompassed ~5.8 million pixels (30 m resolution over ~211,000 ha). This scale is more than 500 times larger than the next-largest instance of DHSVM we have anecdotally heard run. In order to facilitate future projects, we would like to include here some notes on the use of DHSVM at this scale.

### B.1 Parallelization

We ran identical versions of our static vegetation model in the sequential (traditional) and the parallel versions of DHSVM3.2 (Wigmosta et al. 1994; Perkins et al. 2019) on the UCLA Hoffman2 Cluster. The parallel implementation of the model was slower and used more memory than the sequential. The parallel documentation notes that speed is limited by large inputs; we found here that speed is reduced substantially as input size increases (Perkins et al. 2019). Table B1 shows the processing statistics for each model run.

**Table B1:** Processing time and memory demands for various implementations of DHSVM with identical size (~5.8 million pixels) and timespan (01/01/1980-12/31/2020)

Model	Parallelization	Vegetation Changes	CPU Time (hours)	Maximum Memory (GB)
DHSVM3.2	Parallel	Static	115.3	8.2
DHSVM3.2	Sequential	Time-Varying	65.72	6.4
DHSVM3.1.2	Sequential	Static	62.61	4.0

### B.2 Preprocessing

Data preparation for DHSVM is not overly affected by scale in its essentials: masking by hydrologic regions is an easily automated process, and the increasing ubiquity of physical and



remotely sensed datasets on cloud platforms (e.g. Google Earth Engine) further reduce the burden of preparing individual raster files.

However, a major step in the preprocessing workflow is the generation of stream network and stream map files. Currently, a series of Python scripts for ArcGIS Desktop (ArcPy) automate the process in theory. In practice, any large-scale dataset (>100,000 pixels) will cause these programs run slowly and to crash entirely at several points. Crashes occur consistently but not exclusively during:

- Generation of stream network
- Conversion of stream network to watershed
- Joining of row and column rasters (used to create grid)
- Conversion of large row column raster to polygon

For most datasets, crash points can be resolved by running the command manually within ArcGIS, saving the output, and modifying the ArcPy accordingly. For the joining of row and column rasters, we recommend running the tool in Model Builder, which by default uses foreground processing. We also recommend waiting to let the tool finish processing even though it might seem stuck at 99% complete.

The inability of the ArcPy scripts to handle large datasets is a function of ongoing shortcomings in ArcMap in dealing with large datasets (ESRI 2016). Given the availability and sophistication of GDAL, we recommend updating the stream network scripts if future projects continue to increase project scale.

### **B.3 Time-Varying Land Cover**

In large runs of DHSVM with land cover changes, segmentation faults are common. These usually occur when a new land cover dataset is being read, but sometimes they occur

without an obvious cause (e.g. on the 3<sup>rd</sup> day of the model run). Conservative land cover changes (proportional to overall land use change but across a smaller number of pixels) can resolve the issue; future versions of the model might address memory allocation for large-scale changes.

## B.4 References

ESRI. (2016). Bug: Spatial join with large datasets fails to complete.  
<https://support.esri.com/en/technical-article/000009130>

Perkins, W. A., Duan, Z., Sun, N., Wigmosta, M. S., Richmond, M. C., Chen, X., & Leung, L. R. (2019). Parallel Distributed Hydrology Soil Vegetation Model (DHSVM) using global arrays. *Environmental Modelling & Software*, 122, 104533.  
<https://doi.org/10.1016/j.envsoft.2019.104533>

Wigmosta, M. S., Vail, L. W., & Lettenmaier, D. P. (1994). A distributed hydrology-vegetation model for complex terrain. *Water Resources Research*, 30(6), 1665–1679.  
<https://doi.org/10.1029/94WR00436>

## **Appendix C**

Contributions of roads to surface temperature: evidence from Southern California –

Supplementary Material

### **C.1 LST**

Following Ermida (2020), we calculated thermal LST at 30 m in Google Earth Engine using a statistical mono-window algorithm. We derived a Normalized Difference Vegetation Index (NDVI) and fractional vegetation cover from Landsat 8 cloud-free mosaics (Roy et al. 2014). We obtained total column water vapor from 2.5 degree NCEP/NCAR reanalysis (Kalany et al. 1996) and bare ground emissivity from 100 m ASTER imagery (Hulley et al. 2015). We then calculated thermal infrared emissivity and LST at Landsat 8 resolution.

To validate our calculations, we compared our summer 2020 LST to Landsat Provisional LST (30 m) and ECOSTRESS LST (38 x 69 m) from similar times of day (~6pm UTC) (Cook et al. 2014; Hulley et al. 2019). Our data showed similar data distribution to both datasets.

### **C.2 Physical Data**

We calculated Soil Adjusted Vegetation Index (SAVI) and Albedo from Landsat 8 (30 m) using Google Earth Engine (Roy et al. 2014). Because we examined specific, localized examples – often highly arid ones – in addition to the area as a whole, we selected SAVI to provide the most accuracy within semi-arid or arid regions (Vani and Mandala 2017).

We derived elevation from a 30 m Shuttle Radar Topography Mission DEM (Farr et al. 2007) in Google Earth Engine. Using a polygon of the Pacific Ocean's boundaries, we calculated distance from the coast (IHO 1953). We calculated latitude and longitude for each pixel centroid in Google Earth Engine.

### **C.3 Street and Building Data**

We used street data from Millard-Ball (2022), obtained using GIS to derive road area from the spaces between plots of land. Each road segment corresponded to an OpenStreetMap (OSM) identifier, which was used to obtain street width and category. We aggregated OSM road categories into three: highway, arterial, and residential street. To calculate street area per 30 m pixel, we used Google Earth Engine to first rasterize the street polygons at 1m, and then to aggregate them within each 30 m pixel. We obtained building footprints from Microsoft (2021), and identified the area of the largest building that intersected each 30 m pixel.

#### **C.4 Land Use Data**

To define our study area, we selected neighborhoods within city limits in San Bernardino County's Southwest corner, adjacent to Los Angeles County (SB County 2020). The majority of San Bernardino County is not urbanized, and we excluded small, individual cities (e.g. Barstow, Needles) surrounded by desert so as to examine a cohesive urban area. Within Los Angeles County, we selected incorporated neighborhoods; most of the excluded area is in the Angeles National Forest (USC 2017).

To examine land use, we used Land Cover Zones (LCZs) classified at 30 m for urban temperature analyses (Stewart and Oke 2012). The LCZs break down urban form based on vegetation and building density. In our study area, many of the less-developed urban areas are either chaparral or desert environments.

We obtained polygon data for Environmentally Disadvantaged Areas from CalEPA (2015), and rasterized them at 30 m. Environmentally Disadvantaged Areas represent the top 25% of the CalEnviroScreen 3.0 Assessment, which scored census tracts based on their economic condition as well as their climatic and pollution burdens. Several areas with very low populations but high pollution burdens are also included as Disadvantaged.

## C.5 References

- CalEPA. (2015, November 20). *SB 535 Disadvantaged Communities* [Text]. OEHHA. <https://oehha.ca.gov/calenviroscreen/sb535>
- Cook, M., Schott, J. R., Mandel, J., & Raqueno, N. (2014). Development of an Operational Calibration Methodology for the Landsat Thermal Data Archive and Initial Testing of the Atmospheric Compensation Component of a Land Surface Temperature (LST) Product from the Archive. *Remote Sensing*, 6(11), 11244–11266. <https://doi.org/10.3390/rs6111244>
- Ermida, S. L., Soares, P., Mantas, V., Göttsche, F.-M., & Trigo, I. F. (2020). Google Earth Engine Open-Source Code for Land Surface Temperature Estimation from the Landsat Series. *Remote Sensing*, 12(9), 1471. <https://doi.org/10.3390/rs12091471>
- Farr, T. G., Rosen, P. A., Caro, E., Crippen, R., Duren, R., Hensley, S., Kobrick, M., Paller, M., Rodriguez, E., Roth, L., Seal, D., Shaffer, S., Shimada, J., Umland, J., Werner, M., Oskin, M., Burbank, D., & Alsdorf, D. (2007). The Shuttle Radar Topography Mission. *Reviews of Geophysics*, 45(2). <https://doi.org/10.1029/2005RG000183>
- Hulley, G. C., Hook, S. J., Abbott, E., Malakar, N., Islam, T., & Abrams, M. (2015). The ASTER Global Emissivity Dataset (ASTER GED): Mapping Earth’s emissivity at 100 meter spatial scale. *Geophysical Research Letters*, 42(19), 7966–7976. <https://doi.org/10.1002/2015GL065564>
- Hulley, G., Shivers, S., Wetherley, E., & Cudd, R. (2019). New ECOSTRESS and MODIS Land Surface Temperature Data Reveal Fine-Scale Heat Vulnerability in Cities: A Case Study for Los Angeles County, California. *Remote Sensing*, 11(18), 2136. <https://doi.org/10.3390/rs11182136>
- IHO. (1953). Limits of oceans and seas. *IHO Special Publication*, 3(23), 1–38.
- Kalnay, E., Kanamitsu, M., Kistler, R., Collins, W., Deaven, D., Gandin, L., Iredell, M., Saha, S., White, G., Woollen, J., Zhu, Y., Chelliah, M., Ebisuzaki, W., Higgins, W., Janowiak, J., Mo, K. C., Ropelewski, C., Wang, J., Leetmaa, A., ... Joseph, D. (1996). The NCEP/NCAR 40-Year Reanalysis Project. *Bulletin of the American Meteorological Society*, 77(3), 437–472. [https://doi.org/10.1175/1520-0477\(1996\)077<0437:TNYRP>2.0.CO;2](https://doi.org/10.1175/1520-0477(1996)077<0437:TNYRP>2.0.CO;2)
- Microsoft. (2021). *Building Footprints*. Microsoft. <https://github.com/microsoft/USBuildingFootprints> (Original work published 2018)
- Millard-Ball, A. (2022). The Width and Value of Residential Streets. *Journal of the American Planning Association*, 88(1), 30–43. <https://doi.org/10.1080/01944363.2021.1903973>

- Roy, D. P., Wulder, M. A., Loveland, T. R., C.e., W., Allen, R. G., Anderson, M. C., Helder, D., Irons, J. R., Johnson, D. M., Kennedy, R., Scambos, T. A., Schaaf, C. B., Schott, J. R., Sheng, Y., Vermote, E. F., Belward, A. S., Bindenschadler, R., Cohen, W. B., Gao, F., ... Zhu, Z. (2014). Landsat-8: Science and product vision for terrestrial global change research. *Remote Sensing of Environment*, 145, 154–172.  
<https://doi.org/10.1016/j.rse.2014.02.001>
- SB County. (2020). *City Limits*. <https://open.sbcounty.gov/datasets/sbcounty::city-limits-1/about>
- Stewart, I. D., & Oke, T. R. (2012, December 1). *Local Climate Zones for Urban Temperature Studies in: Bulletin of the American Meteorological Society Volume 93 Issue 12 (2012)*.  
<https://journals.ametsoc.org/view/journals/bams/93/12/bams-d-11-00019.1.xml>
- USC. (2017). *Los Angeles Neighborhood Map | Open Data*. USC Price Center.  
<https://usc.data.socrata.com/dataset/Los-Angeles-Neighborhood-Map/r8qd-yxsr>
- Vani, V., & Mandla, V. R. (2017). Comparative Study of NDVI and SAVI vegetation Indices in Anantapur district semi-arid areas. *International Journal of Civil Engineering Technology*, 8(4), 559–566.